EVALUATION OF PRESTRESS LOSSES IN AN INNOVATIVE PRESTRESSED PRECAST PAVEMENT SYSTEM

_____

A Thesis
presented to
the Faculty of the Graduate School
University of Missouri – Columbia

_____

In Partial Fulfillment
of the Requirements for the Degree

Master of Science

_____

by
BRENT M. DAVIS E.I.

Dr. Vellore S. Gopalaratnam P.E., Thesis Advisor

December 2006

The undersigned, appointed by the Dean of the Graduate School, have examined the thesis entitled

EVALUATION OF PRESTRESS LOSSES IN AN INNOVATIVE PRESTRESSED PRECAST PAVEMENT SYSTEM

presented by

Brent Davis E.I.

a candidate for the degree of

Master of Science

and hereby certify that in their opinion it is worthy of acceptance.

_____
Dr. Vellore S. Gopalaratnam, P.E.

_____
Dr. Glenn Washer, P.E.

_____
Dr. Sanjeenv K. Khanna

_____
John P. Donahue, P.E.

ACKNOWLEDGEMENTS

engineering professional. I will carry the many lessons and work standards you have instilled in me over the last few years throughout the rest of my career.

Family and friends have also aided in my success and I would like thank them as well. My parents, Bill and Marsha have always supported all my decisions, and I thank them for their guidance and great examples they have been throughout my life. I would also like to thank my future wife Katie McMan for her support and patience with me throughout the project.

TABLE OF CONTENTS

LIST OF TABLES

LIST OF FIGURES

NOMENCLATURE /LIST OF NOTATION

A_c — AREA OF CONCRETE CROSS-SECTION

A_{ps} — AREA OF PRESTRESSING STEEL

c — CEMENT CONTENT

C_{CU} — ULTIMATE CREEP COEFFICIENT

E_{ps} — MODULUS OF ELASTICITY OF PRESTRESSING STRANDS

$(f_{cgp})_{FJ}$ — STRESS IN CONCRETE AT THE CENTROID OF PRESTRESSING TENDONS DUE TO

PRESTRESSING FORCE

$(f_{cgp})_G$ — STRESS IN CONCRETE AT CENTROID DUE TO SELF-WEIGHT

f_{pi} — INITIAL PRESTRESSING FORCE

f_{py} — YIELD STRENGTH OF STEEL

f_{pJ2} — INITIAL STRESS IN PRESTRESSING TENDON AT END OF STRESSING

Δf_{pC} — CHANGE IN PRESTRESSING FORCE DUE TO CREEP

Δf_{pES} — CHANGE IN APPLIED FORCE DUE TO ELASTIC SHORTENING

Δf_{pR1} — STRAND RELAXATION AT ANY TIME AFTER STRESSING

Δf_{pS} — CHANGE IN PRESTRESSING FORCE DUE TO SHRINKAGE

Δf_{pR} — CHANGE IN PRESTRESSING FORCE DUE TO RELAXATION

Δf_{pT} — TOTAL CHANGE IN PRESTRESSING FORCE

$g(t)$ — TIME FUNCTION

h_o — MEMBER THICKNESS

I — MOMENT OF INERTIA

K — CORRECTION FACTOR FOR STRESS RELIEVED OR LOW RELAXATION STRANDS

K_{CA} — CORRECTION FACTOR FOR AGE AT LOADING

K_{CH} — CORRECTION FACTOR RELATIVE HUMIDITY

K_{CS} — CORRECTION FACTOR FOR SIZE AND SHAPE

K_{SH} — CORRECTION FACTOR FOR RELATIVE HUMIDITY

K_{SS} — CORRECTION FACTOR FOR SIZE AND SHAPE

N — NUMBER OF CYCLES

n_p — MODULAR RATIO

n_{pi} — INITIAL MODULAR RATIO

P — APPLIED LOAD

R — MODULUS OF RUPTURE

r — RADIUS OF GYRATION

s — CONCRETE SLUMP

t — TIME

T_c — INITIAL MOIST CURING TIME

v/s — VOLUME TO SURFACE RATIO

ε_{su} — ULTIMATE CONCRETE SHRINKAGE STRAIN

δ — DEFLECTION

ε_{sh} — SHRINKAGE STRAIN

ε_{sh}^{*} — SHRINKAGE STRAIN AT TIME INFINITY

λ — RELATIVE HUMIDITY

α — AIR CONTENT

ε — CREEP STRAIN

τ — TIME AT LOADING

σ — STRESS

$\phi(t,\tau)$ — CREEP-TIME RELATIONSHIP

$\phi^*(t)$ — FINAL CREEP COEFFICIENT

ψ — RATIO OF FINE AGGREGATE TO TOTAL AGGREGATE

$\gamma_1 - \gamma_7$ — CORRECTION FACTORS FOR RELATIVE HUMIDITY, MEMBER SIZE AND SHAPE, CONCRETE SLUMP, FINE AGGREGATE TO TOTAL AGGREGATE RATIO, AIR CONTENT, CEMENT CONTENT, AND INITIAL CURING PERIOD

EVALUATION OF PRESTRESS LOSSES IN AN INNOVATIVE PRESTRESSED PRECAST PAVEMENT SYSTEM

Brent Davis, E.I.

Dr. Vellore S. Gopalaratnam, Thesis Advisor

ABSTRACT

To date no streamlined user efficient concrete roadway rehabilitation method is in practice in the United States. However, the use precast pavement is being evaluated and successful projects in Georgetown, Texas, El Monte, California, and most recently Charleston, Missouri are paving the way for the use of prestressed precast concrete pavement. The use of prestressed precast concrete pavement for the replacement of damaged roadways gives contractors and designers significant advantage by decreasing construction time, improving pavement performance, and mitigating user cost.

The project in Charleston, Missouri, funded by the FHWA and MoDOT, is the focus of this thesis. A total of 101 panels were cast and seven were instrumented to monitor temperature and strain.

The objectives set forth were to understand important properties of the materials used, study losses due to creep and shrinkage of precast pavement panels, and develop pre and post-tension loss prediction models and compare them to actual values measured in the pavement. Concurrent works by Cody Dailey and Grant Luckenbill examine early age performance of the precast panels and analyze strains relating to daily thermal gradients, seasonal trends, and traffic.

1. INTRODUCTION

1.1. PRESTRESSED PRECAST ROADWAYS IN THE UNITED STATES

1.1.1. FHWA CONCRETE PAVEMENT TECHNOLOGY PROGRAM (CPCT) TASK 58

The Federal Highway Administration (FHWA) started a lead state program to promote advances in concrete pavement technology. Task 58, "The Use of Precast Concrete Panels to Expedite Highway Pavement Construction," is part of the Concrete Pavement Technology Program (CPTP) sponsored by the FHWA. The CPTP consists of research, development, and technology-delivery activities to foster innovation, improve the performance and cost effectiveness of concrete pavements, and ultimately reduce user delays (Tyson and Merritt 2005). Current states involved in the program include Texas, California, Missouri, Indiana, and Iowa. The first demonstration of precast pavement technology was completed on an outer road near Georgetown, TX in 2002.

1.1.2. PRESTRESSED PRECAST CONCRETE PAVEMENT IN MISSOURI

The state of Missouri demonstrated a commitment to developing precast prestressed concrete pavement (PPCP) technology by jointly funding a new test section in cooperation with the FHWA. The Missouri PPCP test section is located on the northbound lanes of I-57 near Charleston, MO. The project was completed in December, 2005 and opened to traffic in mid January, 2006.

The charge of the Missouri project was to advance technologies developed in recently completed projects near Georgetown, TX and El Monte, CA. During the developmental stages of the Missouri project, input from experienced parties was vital.

Several meetings were held to discuss the feasibility of using precast pavement to rehabilitate an existing highway. Upon reviewing contributions from the many parties involved, a project location was chosen, and goals were set forth to advance the new technology. The overall goal of the project was to demonstrate the feasibility of using PPCP to rehabilitate high volume roadways. The primary objective of the University of Missouri-Columbia was to evaluate the performance of the PPCP which would be subjected to severe weather and traffic conditions and ultimately develop data on performance. A main difference in the Missouri pilot project compared with recently completed projects is the incorporation of heavily instrumented sections to quantify pavement performance and verify design.

1.2. RESEARCH OBJECTIVES

1.2.1. NEED FOR EXPERIMENTAL INVESTIGATION

With new technology a need exists to verify assumptions made during design through methods of analysis and experimental programs. Precast pavement technology has only been around for a handful of years, and all design aspects are not yet fully understood. Much of what is known about precast pavement design is based off of the design of other prestressing applications such as bridge girders. Using embedded instrumentation to verify assumptions made during design will allow researchers to develop design standards and methods. Proving or disproving assumptions will give researchers and designers experience and confidence for future projects.

Hands-on experience for contractors is also important in developing new technology. In early stages of new construction methods contractors should be involved

in the process, because they will be the ones building or constructing the conceived technology. During construction, contractors develop the skills and processes necessary to complete new designs, and also demonstrate to other contractors the ability to complete the project.

Developing design standards, which is an inherent goal of the instrumentation and monitoring program, and demonstrating successful completion of the project will give MoDOT the confidence to utilize this new technology in future projects. The following sections will outline the entire scope of the research project, and look at the specific topics covered in this thesis.

1.2.2. GENERAL INFORMATION AND PROJECT SCOPE

Due to the broad scope of the research goals a companion thesis titled, "Instrumentation and Early Performance of an Innovative Prestressed Precast Pavement System" (Dailey 2006) by Cody Dailey was written to cover aspects of the project not discussed herein. It will be referenced throughout where overlapping topics are discussed. The following text outlines the entire scope of the research objectives followed by an overview of the topics covered in this report.

As stated earlier, the primary research objective of the project was to evaluate the performance of precast, prestressed pavements subjected to severe weather and traffic conditions and ultimately develop data on performance. Specific goals within the above objective include:

- Study early age behavior of prestressed panels. Parameters to investigate include; hydration and shrinkage effects, potential residual stresses, and transfer of pretensioning.

- Understand behavior of joint, anchor, and base panels at various stages of construction and service.

- Study stress losses during post-tensioning and under service conditions.

- Evaluate the overall performance of individual panels and the interaction of the panels within the system. Specifically curling at joints, chloride ingress, performance under traffic loads, and daily and seasonal thermal effects.

The topics covered in this thesis are limited to material studies, comparisons to theoretical values, and an in-depth analysis of predicted post-tension losses versus measured post-tension losses in the pavement. Laboratory experiments were carried out to quantify material properties. Theoretical studies were completed and comparisons to field measurements are ongoing. The thesis by Mr. Dailey covers early-age monitoring and in-service performance of the precast panels themselves. Also, an in-depth look at the instrumentation is covered as well. A future thesis will focus on long-term evaluation of the precast pavement system and also summarize the entire scope of the project objectives.

1.2.3. PREDICTION AND EXPERIMENTAL VERIFICATION OF PRESTRESS LOSSES

One of the main differences between PPCP and conventionally reinforced concrete pavements is the use of a pre-compressive force to economize the use and long-term performance of concrete; therefore, the major focus of this thesis will be to understand the mechanisms of pre and post-tension losses in the pavement. Results from the multiple laboratory studies are incorporated in the models used to predict losses. For example comparing predicted losses due to creep through experimental methods will

validate parameters input into the models used for pre and post-tension loss prediction in the concrete.

As stated earlier, optimizing the use of concrete by applying a pre-compressive force is advantageous with regards to long-term durability and economical use of concrete. However, it is important to understand the decrease or loss of this applied force over time. Multiple models exist to predict loss of stress in pre-tensioning or post-tensioning strands. A time-step model looking at creep and shrinkage independently was followed. Furthermore, coupled time-step models taking into account not only creep and shrinkage of the concrete but also relaxation and elastic shortening of the strand and friction between the strand and concrete was done to predict total prestress loss in the pavement. A comparison between predicted total post-tensioning loss and field measurement of total post-tensioning loss is done. Verifying prediction models with actual results will give future practitioners confidence in their final design.

1.2.4. LABORATORY RESEARCH OBJECTIVES

The main objective of the laboratory studies is to characterize concrete properties to more readily understand field results. Many experiments were done to achieve this objective. Concrete compressive strength and modulus were determined to ensure the mix design met specified requirements. Unrestrained creep and shrinkage was studied to quantify losses in both pre-tensioning and post-tensioning of the concrete. Deicing salts are readily used on pavements in Missouri; therefore baseline chloride permeability tests were performed to compare with in-service values in the future. Large temperature fluctuations are also commonplace in southeastern Missouri; as a result the concrete was

subjected to rapid freezing and thawing to test its long-term durability. Finally, flexure tests were done to determine the tensile strength and fracture toughness of the concrete.

1.3. PROJECT LOCATION AND INFORMATION

1.3.1. SPECIFICATIONS FOR PRECAST PAVEMENT TEST SECTION

The PPCP test section in Missouri replaced an existing 45 year old cast in-place roadway with distress dating back 9 years, and is the first of its kind in Missouri. The project was along I-57 in Mississippi County near Charleston, MO. This is the first time the University of Missouri - Columbia used instrumentation to monitor a precast roadway system. Previous projects at the University of Missouri - Columbia involving the successful instrumentation of High Performance Concrete bridge girders gave the researchers a model to follow (Eatherton 1999). PPCP is constructed using multiple panel types, each playing a vital role in the whole system.

The Missouri pilot project used three types of panels which were cast at a precasting yard: base panels, joint panels, and anchor panels. A typical overhead view of a joint panel is shown in Figure 1.1, and in Figure 1.2 typical base and anchor panels are depicted. A longitudinal cross section for both panel types is shown in Figure 1.3, and transverse cross sections for base and joint panels are depicted in Figure 1.4 and Figure 1.5 respectively.

Pretensioned Strands (3@ 0'-6" T&B)

38'-0"

10'-0"

Inside Shoulder

Blockout for Post-tensioning

Post-Tensioning Ducts (18@2'-0")

Outside Shoulder
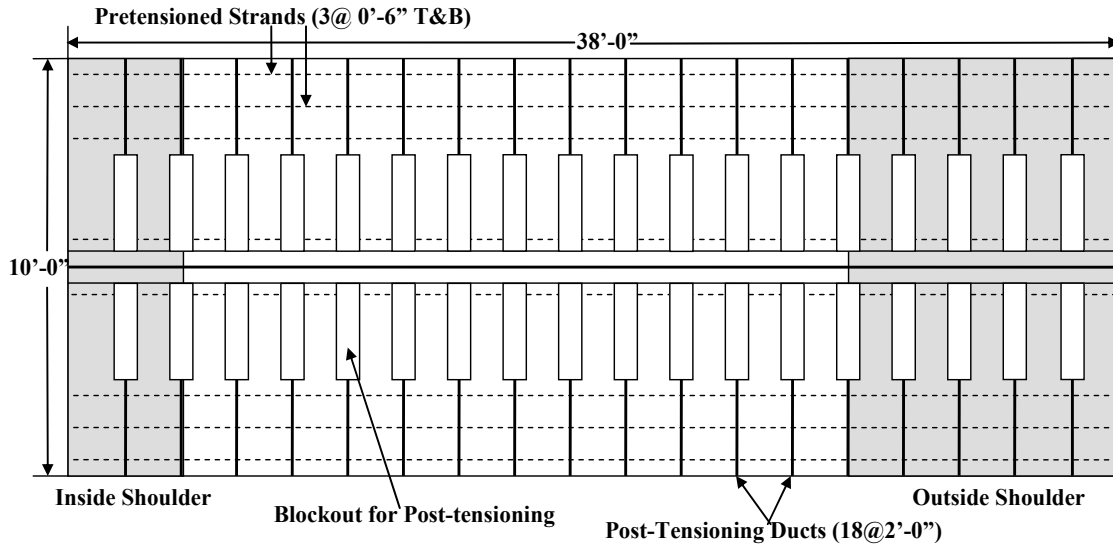
Figure 1.1 – Overhead view of a typical joint panel utilized for construction of precast pavement.

Pretensioned Strands (8@1'-3")

38'-0"

10'-0"

Inside Shoulder

Post-Tensioning Ducts (18@2'-0")

Outside Shoulder
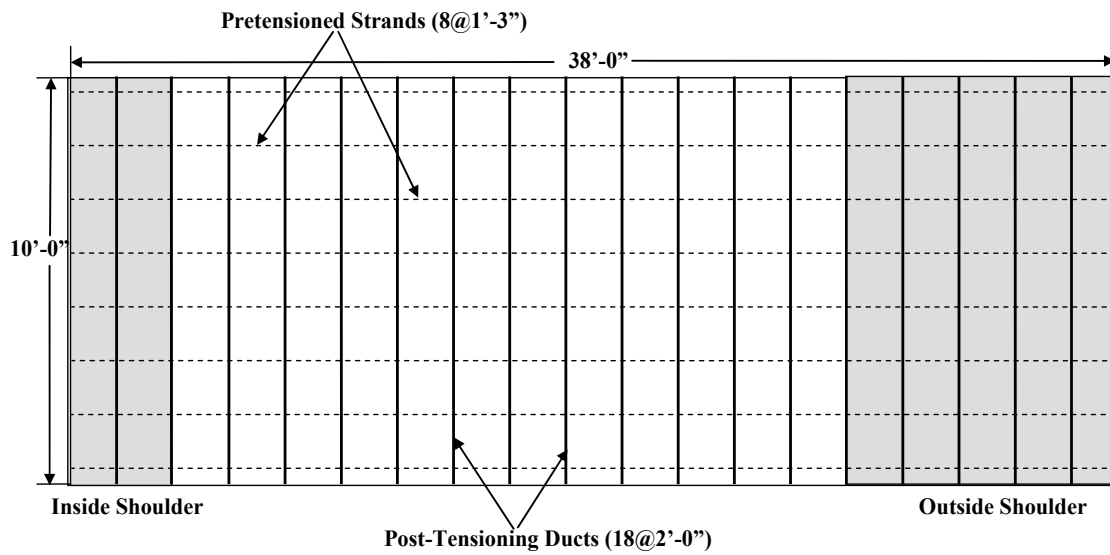
Figure 1.2 – Overhead view of typical base or anchor panel. Anchor panels are cast with full-depth blockouts to secure the panel to the sub-grade.

Shear Key

Post-tensioning Strands/Ducts

4' Inside Shoulder

12' Driving Lane

12' Driving Lane

10'Outside Shoulder
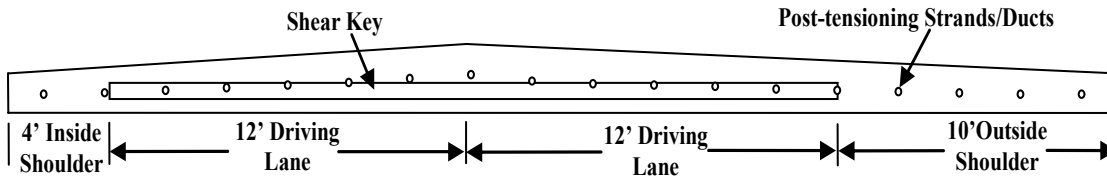
Figure 1.3 – Cross section view of panel longitudinal to the direction of traffic.

Prestressing Strands   **Post-tensioning Strand**

7"   10 7/8"

←————————— 10'-0" —————————→
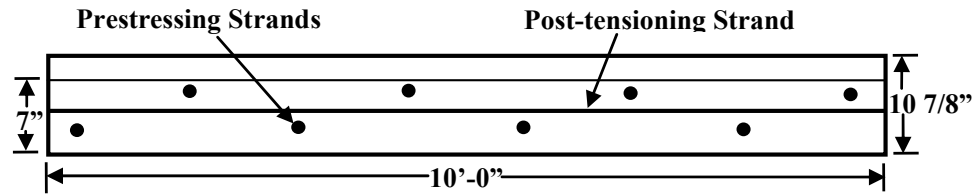
Figure 1.4 – **Cross section view of anchor/base panel transverse to the direction of traffic.**

Prestressing Strands Post-tensioning Blockouts

7"   10 7/8"

←————————— 10'-0" —————————→

Post-tensioning Strand
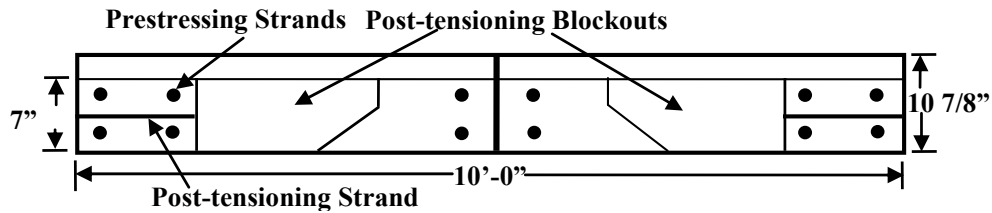
Figure 1.5 – **Cross section view of joint panel transverse to direction of traffic.**

Each 10'-0"x 38'-0" panel is pre-tensioned transversely (long dimension of the panel) and cast with post-tensioning ducts longitudinally (short dimension of the panel). The panels have a 4'-0" inside shoulder, two 12'-0" driving lanes, and a 10'-0" outer shoulder with a crown between the driving lanes and a 2% grade on either side to facilitate drainage. A typical pavement section (between joint panels) consists of an anchor panel in the middle with eleven or twelve base panels extending on either side to joint panels at the section ends. Base panels act as filler panels, with the number depending upon the design length of each section. The anchor panels contain full depth holes to accommodate dowel bars which are driven into the sub-grade to provide anchorage. Joint panels have expansion joints to allow for thermal movement. Stressing pockets straddle the expansion joint allowing post-tensioning on adjacent sections. Male and female shear keys cast into the side of the panels help with load transfer and to align the panels during placement and post-tensioning (shear keys extend only to limits of the driving lanes). Once in place, post-tensioning strands were fed through the ducts (cast

into the panels) and stressed at the joint panels. The ducts were then grouted to seal and protect the strands and block-outs were filled. Diamond grinding was performed for smoothness in ride quality and mitigation of impact/fatigue effects.

A total of 101 panels were cast by Concrete Products Incorporated (CPI) in Memphis, TN. Dimensional and material specifications were developed before casting, and it was imperative they were followed throughout the construction process. Visual inspection and formwork measurements were completed by MoDOT personnel before each panel casting to ensure proper alignment of the panels when placed and post-tensioned. The concrete strength was specified to be 5,000 psi at 28 days and 3,500 psi at pre-tension transfer. Pre-tensioned strands were seven-wire, 0.5" diameter with a 270 ksi ultimate strength (ASTM A 416). Individual panels contained 8 or 12 strands depending on whether they were base panels or joint panels, respectively. The post-tensioning strands were seven wire, 0.6" diameter with a 270 ksi ultimate strength (ASTM A 416). Job specifications required stressing to be 80% (216 ksi) of the ultimate strength.

The panels fabricated by CPI were cast during the months of October through December 2005. The panels were individually transported on flatbed trailers and placed during the week of December 12, 2005 by Gaines Construction out of St. Louis, MO. Post-tensioning operations were completed on December 22, 2005 and the roadway was reopened to traffic during the week of January 16, 2006.

1.4. ORGANIZATION OF THE THESIS

A brief overview of the thesis chapters are described in the following paragraphs.

Chapters 1 and 2 introduce the reader to the subject matter of the thesis. In chapter 1 research goals are presented along with specific information on the Missouri PPCP

pilot project. Chapter 2 reviews the state of the industry regarding pavement technology. Also, in depth discussion on the various material properties such as time dependent losses due to creep and shrinkage are presented.

The experimental program is outlined in detail within chapter 3. Instrumentation and monitoring plans are presented along with an in depth look at the laboratory procedures carried out to obtain material properties.

Results of the laboratory investigations are presented in chapter 4. The focus of this chapter is to give the reader a baseline for the materials used in the construction of PPCP in Missouri.

Chapter 5 investigates theoretical pre-tension and post-tensioning losses due to creep and shrinkage individually, and total losses. The results from the prediction models are then compared to values observed in the field. Finally, chapter 6 overviews the entire thesis and recommendations for future work are discussed

2. BACKGROUND INFORMATION (LITERATURE REVIEW)

2.1. PRESTRESSED PRECAST CONCRETE PAVEMENT

2.1.1. GENERAL

Currently, only 7% of our nation's roadway corridors are constructed using rigid pavement (Muench 2004). However, the heaviest traffic volumes are seen on rigid pavements because of its durability. Major arterial highways connecting suburbs to central business districts and the roads in between are very important to users who rely on them everyday to commute to and from work. These larger arterials are normally constructed using rigid pavement design, which allow for heavy truck traffic and a higher volume of traffic. However, the increasing volume of traffic utilizing our nation's major highways and their age is causing roadways to deteriorate beyond repair. Current design practices can cause roadways to be shutdown for long periods of time due to construction, causing huge user delays and therefore increased costs (Merrrit, McCullough et al. 2000). Realizing more efficient methods to help curb user costs during construction is a key issue in replacement of the many busy highways that are beyond repair in large cities (Merrrit, McCullough et al. 2000). A possible solution to alleviate user costs during construction practices is the use of prestressed, precast panels for the replacement of damaged or un-repairable roadways. The use of precast panels in building construction and precast girders in bridge construction has helped minimize construction time, and therefore the use of precast panels in roadway construction is currently being investigated to minimize replacement time of roadways (Merrrit, McCullough et al. 2000).

Pavement design and construction technologies are always evolving to meet user demands. Rigid pavements are utilized each day by hundreds of millions of people throughout the United States for travel, commute, and distribution of goods. Much of the nation's high volume roadway infrastructure was built using rigid pavement construction practices(Gopalaratnam, Donahue et al. 2006). The advantages of rigid pavement construction include over a thirty year expected life span, the requirement of only two main layers (base course and surface course) for construction, and an ability to sustain a high number of Equivalent Single Axle Loads (ESAL's). Having only two main layers in construction of rigid pavements minimizes preparation time for the surface course, and therefore decreases construction time. Maximizing the time between replacement and repair of roadways decreases costs to taxpayers for construction purposes and also to users with regards to delays from construction. Also, with heavy truck traffic increasing on highways, the largest contributor to the number of ESAL's, being able to withstand them over a long period of time is important in the design of a roadway.

The efficiency of load transfer in rigid pavements between slabs allows rigid pavement to support millions of ESAL's throughout its expected life. Heavy truck traffic is the single largest concern with regard to performance of pavements. Non-rigid pavements may deform easily under repeated ESAL's, which increases the frequency of repairs. However, rigid pavements deform and deflect minimally under loading due to the high modulus of elasticity of their surface course, therefore allowing for more efficient load distribution. The high number of sustained ESAL's and thirty year expected life of rigid pavements puts these types of pavements at an advantage over non-rigid pavements. Rigid pavements play an important role in the U.S. infrastructure

system, and must be further developed to ensure users are obtaining the highest benefit possible.

2.1.2. CURRENT DESIGN PRACTICES

Three main techniques exist for rigid pavement construction; Jointed Concrete Pavement (JCP), Jointed Reinforced Concrete Pavement (JRCP), and Continuously Reinforced Concrete Pavement (CRCP).

2.1.2.1. JOINTED CONCRETE PAVEMENT (JCP)

JCP contains no reinforcing steel and contains enough joints to control the location of natural cracks (ACPA 2004). To help in load transfer dowel bars are often used between joints. Figure 2.1 shows an overhead and side view of typical JCP construction. Dowel bars embedded in the surface course are important to transfer load between joints.
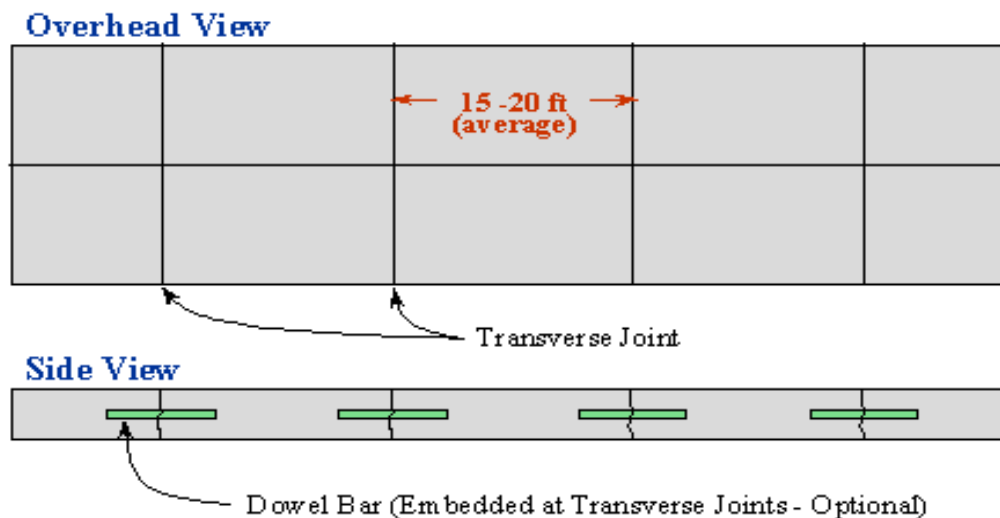
Figure 2.1 –   Overhead and side view of Jointed Concrete Pavement (ACPA 2004).

2.1.2.2. JOINTED REINFORCED CONCRETE PAVEMENT

JRCP is somewhat similar to JCP; however a reinforcing wire mesh is used to hold cracks together between joints. Normally the joints are spaced at 30 feet or more (ACPA 2004). Figure 2.2 shows cracks that have formed between joints, but because of the wire mesh reinforcement the cracks are held together. JRCP also uses dowel bars between joints for load transfer efficiency (ACPA 2004).
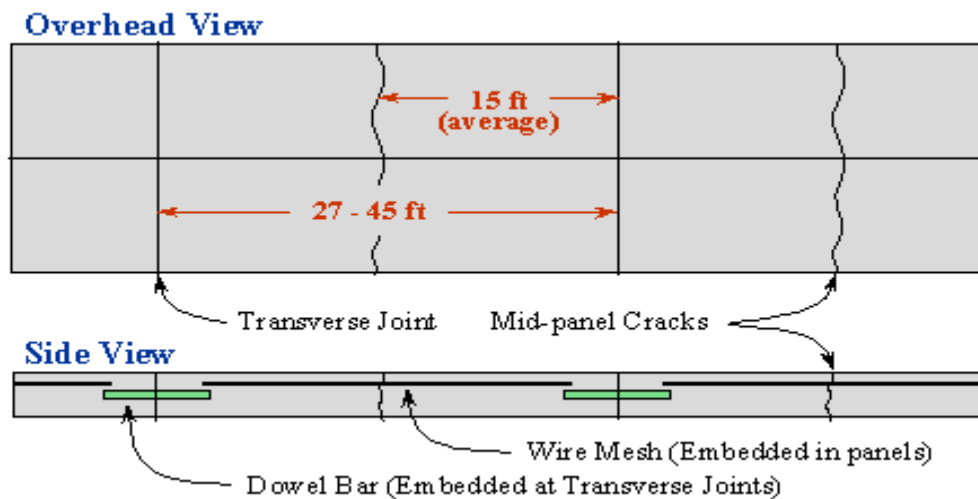
Figure 2.2 – Overhead and side-view of Jointed Reinforced Concrete Pavement (ACPA 2004).

2.1.2.3. CONTINUOUSLY REINFORCED CONCRETE PAVEMENTS (CRCP)

CRCP, unlike JCP and JRCP, requires no transverse joints. Cracks are expected in the slab, but are held together tightly through the use of reinforcing steel (ACPA 2004). When designing, the crack spacing is normally predicted. The cost of CRCP is more than that of JCP and JRCP, but is justified by its long-term effectiveness (ACPA 2004). Figure 2.3 shows typical CRCP construction and typical cracking patterns.
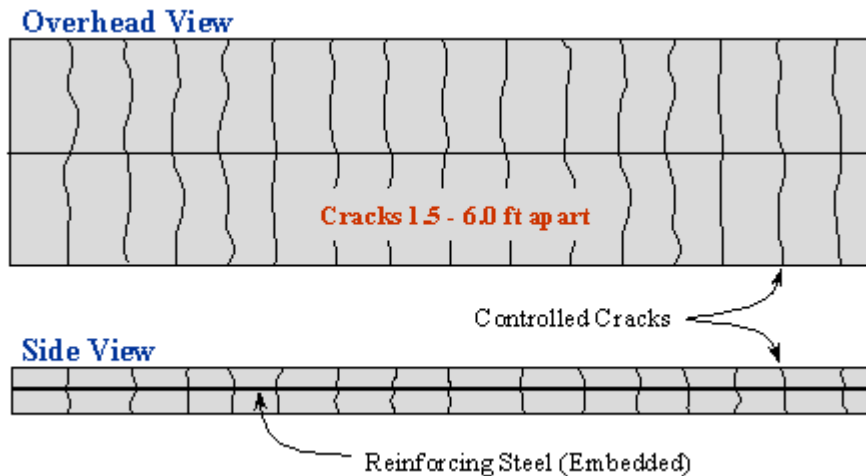
Figure 2.3 – **Overhead and side-view of Continuously Reinforced Concrete Pavement (ACPA 2004).**

2.1.3. ISSUES RELATED TO RIGID PAVEMENT CONSTRUCTION

Current rigid pavement replacement practices, although reliable, are the cause of high user costs. As with any innovative method of construction, there is always room for improvements or modifications. In the past few years research has been done to identify more efficient methods of rigid pavement construction practices. This research has brought to light key issues related to rigid pavement construction.

Optimizing material use is a large component in curbing costs associated with any construction venture. If it were possible to make an 8" thick pavement perform like a 14" thick pavement then material costs would be cut in half. Concrete, used in rigid pavement construction, is inherently weak in tension, but very strong in compression. One reason why current pavements are so thick is due to this weakness in tension. Figure 2.4 illustrates how a pavement acts under tire loadings. A possible way to overcome concretes weakness in tension is to place pre-compression forces where tensile stresses occur. Placing compression or prestressing forces in concrete has been successfully used in bridge girder construction, foundation mats, parking structures, and floor systems.

Taking lessons learned in these varying applications and applying them to roadway construction may be a viable option for future rigid pavement rehabilitation.
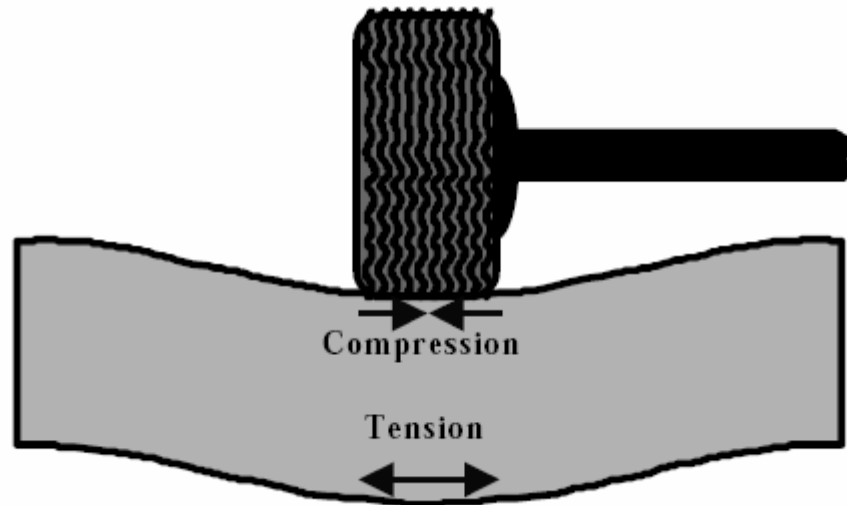
Figure 2.4 –   **Slab stresses generated from wheel loads (Merrrit, McCullough et al. 2000).**

A related aspect to the long-term performance of concrete is the curing process. When environmental conditions permit, curing may have no affect on the performance of a roadway. However, in many locations across the U.S. environmental conditions can change rapidly, thus having an effect on the curing of concrete. Concrete poured on a base course will tend to have a rough underside, because it takes the shape of the base course. This causes an increase in the coefficient of friction between the base and surface course, thus when the concrete cures, and shrinks, residual stresses are built up in the concrete. The placement of polyethylene sheeting is sometimes used to help limit the friction coefficient, but more often then not some residual stresses are developed in the concrete. The residual stresses resulting often cause the roadway to deteriorate much faster than normal. By curing concrete in a controlled environment, such as a casting yard, curing is normally not an issue (Merrrit, McCullough et al. 2000).

The largest issue related to rigid pavements is the rerouting of traffic in order to repair sections of highways. Any individual traveling on interstate highways or other arterials, knows first hand the effects a detour can have on travel time. Currently, there exists no streamline method for roadway replacement that allows roadways to stay open during peak traffic periods. The process of removing the existing roadway, preparing a sub base, placing reinforcement, pouring concrete, and allowing curing time can add up to months. Developing a more efficient method of placement is necessary to limit user costs, especially in heavily traversed urban highways.

Based on these three issues it may seem as though rigid pavements have no value. However, the many highways and roadways seen today would not be around had they not been constructed using rigid paving techniques. Rigid pavements provide smooth and reliable transportation corridors, with expected lives of over thirty years. The main goal of discussing these issues is to develop new technologies for replacing and constructing rigid pavements mainly in urban areas. Advancing rigid pavement design will result in decreased costs to users of the many great highways and roadways across the U.S.

2.1.4. USE OF PRESTRESSED PRECAST CONCRETE PAVEMENT

2.1.4.1. GENERAL

Realizing the issues related to rigid pavements discussed above, a possible design alternative is in the developing stages. Traffic congestion due to the presence of construction activities results in, among many other variables, increased fuel consumption and lost work time, or user costs and safety issues related to construction (Merritt 2001). The issues discussed in the previous section can all be resolved using precast panels and post tensioning them. Projects in the mid 1980's, utilizing prestressed

cast in place concrete, in Texas and South Dakota have proven very effective. More recently, in Georgetown, Texas a frontage road along Interstate 35 was replaced using precast prestressed concrete panels. Currently, in Michigan, California, and Missouri pilot projects using techniques developed in the Georgetown, Texas project are either underway or completed. Building on the concepts from the more recent Texas project will allow transportation officials to realize the benefits of precast construction, and hopefully demonstrate the niche precast panels will serve in urban pavement replacement projects.

The main advantage of using a prestressing force in any construction using concrete is the optimization of material use. When a PPCP is constructed, there will inevitably be voids beneath the panels. These voids reduce the support given to the pavement, thereby reducing the life of the pavement under repetitive wheel loading. A prestressed concrete pavement however has the ability to "span" these voids, because of the pre-compressive stress in the pavement. Simply increasing the prestressing force will help the panel act like a thicker pavement (Merrrit, McCullough et al. 2000).

The curing process with respect to precast panels will not be an issue, because the panels are cast at a precasting yard. Casting at a curing yard allows for control of the curing process. The panels can be cured in a number of ways to help minimize shrinkage affects, and the development of residual stresses.

Another advantage of precast panels is the ability to repair or replace roads without affecting traffic during peak hours. Panels constructed offsite can be placed and post-tensioned at night allowing traffic on the newly placed panels the very next morning. The linear feet of roadway replaced per day by using precast panels is much less than can

be placed using conventional construction practices, however traffic can be let back on

the new panels almost immediately after placement of panels. Figure 2.5 and Figure 2.6

show traffic flows on a roadway. With conventional construction the roadway is closed

24 hours a day and greatly affects traffic during peak hours. The use of precast panels

and placing them at night reduces the affect on users.
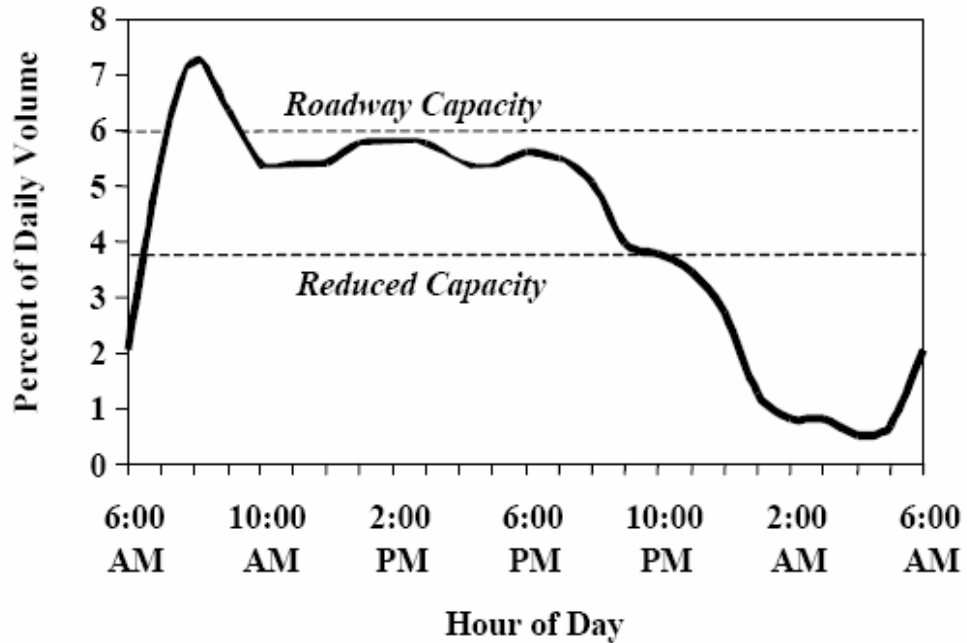
Figure 2.5 – **Over-capacity produced by conventional pavement construction (Merrrit, McCullough et al. 2000).**
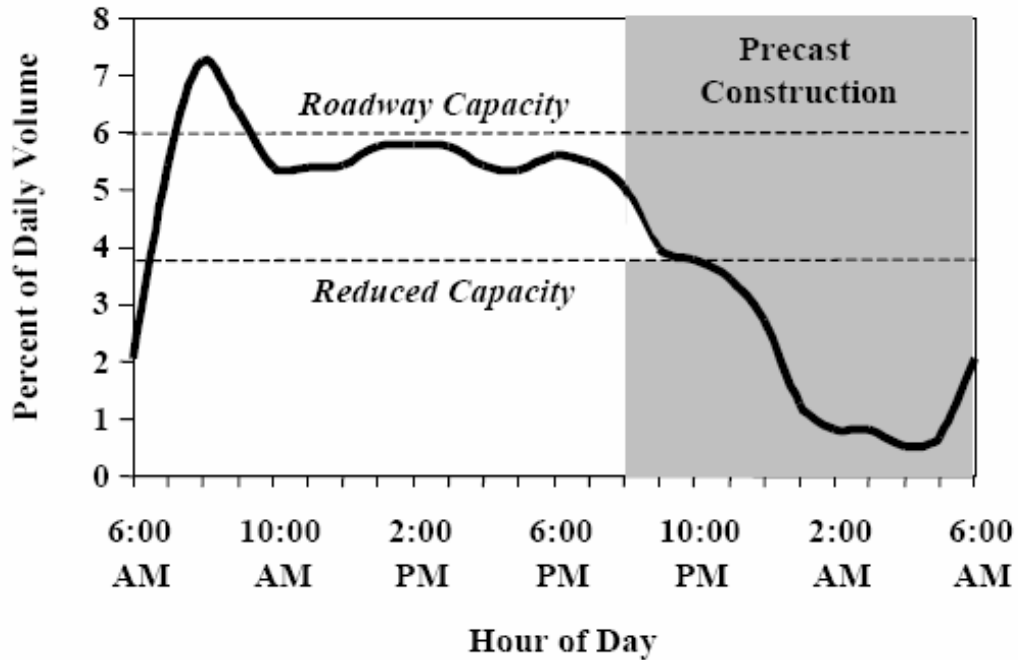
Figure 2.6 –   Over-capacity produced by overnight precast pavement construction (Merrrit, McCullough et al. 2000).

Load transfer efficiency is another issue in regards to precast panels. When cracks in concrete become larger than 0.03 – 0.04 inches, the pavement must rely on aggregate interlock to provide load transfer. This load transfer ability decreases as the cracks increase in size. The reinforcement placed in pavement is to help limit the opening up of these cracks. The use of prestressed reinforcement further helps by pulling the cracks back together. The shear friction alone, provided by the pre-compression in a prestressed pavement, provides optimal load transfer across joints and cracks (Merrrit, McCullough et al. 2000).

The benefit of using precast panels for the replacement of rigid pavements has a high upside. In rural areas where traffic congestion is minimal the user costs would not outweigh the cost of construction using precast panels. However, the use of precast panels is well suited in urban roadway replacement projects.

2.1.4.2.   GEORGETOWN, TEXAS

A prestressed precast roadway project in Texas was the first of many planned joint FHWA and state DOT projects involving this new technology. The location for the Texas project was a frontage road along IH-35 just north of Georgetown, TX. The Texas project incorporated both full width and partial width panels. The full width panels were post-tensioned longitudinally, and the partial width panels were post-tensioned both longitudinally and horizontally. A total of 339 panels were fabricated, of which 123 were full width and 216 were partial width.   The full width panels were wide enough to accommodate two twelve foot lanes an eight foot outside shoulder and a four foot inside shoulder.   The partial width panels were 16 feet and 20 feet in width respectively. When placed, the centerline of the roadway matched with the joint between the two panels. The length of the panels was ten feet, which was controlled by weight restrictions for transportation to the sight (Tyson and Merritt 2005).

The pavement in Texas has been in service since March 2002 and has shown no signs of deterioration.   Careful planning and the overall success of the project in Georgetown, Texas opened doors for pilot projects in California and Missouri.

2.1.4.3.   CALIFORNIA

In April 2004 the California Department of Transportation (Caltrans) completed a project on Interstate 10 near El Monte, CA.   This project involved a little more complexity compared with the Texas project by requiring varying cross-slopes cast into the panels, and nighttime construction operation (Tyson and Merritt 2005).   The total length of roadway replaced was 250' and consisted of two driving lanes and a 10' shoulder. A total of 31 panels were fabricated and placed over a two night period. The

panels were prestressed transverse to the direction of traffic and post-tensioned in two 124' sections longitudinal to traffic (Tyson and Merritt 2005).

2.1.4.4. OTHERS

More projects at various stages of completion are part of the advancement in precast prestressed pavement technology. A project in Indiana will utilize precast pavement to replace an existing jointed pavement and improve clearance of an underpass on Route 13 under I-69 (Tyson and Merritt 2006). A challenging Iowa project will incorporate the use precast prestressed pavements for bridge approach slabs, and another Texas project will utilize this technology in conjunction with weigh-in-motion (WIM) scales.

2.1.4.5. SIGNIFICANCE OF MISSOURI PILOT PROJECT

The pilot project in Missouri using PPCP is significant for many reasons. The completed projects in Texas and California are located in climates that do not have large seasonal temperature variations and deicing salts are seldom used. The Missouri project will be subject to significant seasonal as well as daily temperature variations. Furthermore, deicing salts are commonly used due to winter precipitation events.

The research completed to date for precast pavements is purely based on knowledge gained through other applications of prestressed and precast concrete. Although it is very helpful to use this knowledge, the same assumptions cannot always be made for new technological advancements. Instrumentation of the Missouri project will enable researchers to understand and verify the many assumptions made from knowledge

gained through similar applications. Validating design through instrumentation will also hopefully give future practitioners the confidence to apply this new technology.

2.2. MATERIAL TESTING

2.2.1. GENERAL

The following sections present background information on the various experiments carried out on the concrete used in the precast pavement project. Literature was reviewed for background information on each test standard and is presented along with applicable theoretical prediction models.

2.2.2. COMPRESSIVE STRENGTH TESTS

2.2.2.1. GENERAL

The compressive strength test is the most common test carried out to validate concrete mix designs (Mindess, Young et al. 2003). According to Mindess four reasons exist for this; it is assumed to be directly related to the compressive strength, the compressive strength is the most important property of concrete since it is inherently weak in tension, structural design codes are based on the compressive strength, and it is easy and relatively inexpensive. Cylinders are easily cast offering practitioners a viable means of confirming concrete mix designs, determining when forms can be removed, and making sure structures are put into service at the right time (Mindess, Young et al. 2003).

2.2.2.2. ISSUES WITH COMPRESSIVE STRENGTH TESTS

Correctly determining the compressive strength of concrete is only possible under a state of uniaxial loading. Due to friction between a cylinder and the supports of a

testing apparatus, confinement normally occurs causing a conical shaped failure. To limit the effect of confinement, literature suggests l/d ratios be greater than 2.0. With l/d ratios less than 2.0 the apparent compressive strength of concrete will increase due to confinement (Mindess, Young et al. 2003). An l/d ratio of 3.0 is said to subject the middle portion of specimens to pure uniaxial compression. The actual supports or platens used can have an affect on results as well. The platens should not cause any confinement, and a spherically seated platen should be used to account for small deviations from parallelism (Mindess, Young et al. 2003).

Other factors affecting results from strength tests include specimen geometry (cubes or cylinders), loading rate, moisture content of the specimen, and temperature. The many factors related to correctly determining compressive strengths of concrete using ASTM standards may cause some to question the standards usefulness. However, the main goal of a standard is to provide uniformity and comparability of results. Being able to compare results that are tested in the same manner gives a basis for following standards.

2.2.3. CREEP AND SHRINKAGE OF CONCRETE

2.2.3.1. GENERAL

Time dependent phenomena such as creep, shrinkage, and relaxation will be important to predict, measure in the laboratory under controlled environments, and compare with actual values measured in the field. Determining losses from creep and shrinkage and comparing to theoretical models will ensure proper design in the future. Quantifying these losses will ensure proper prestressing forces are applied to the pavement. The following sections provide an overview of creep, shrinkage, and an in-

depth summary of ACI 209, "Prediction of Creep, Shrinkage and Temperature Effects in Concrete Structures."

2.2.3.2.   SHRINKAGE STRAINS

Shrinkage, defined by ACI, is the decrease of concrete volume with time after hardening. Shrinkage is due to changes in moisture content and physico-chemical changes which occur without stress (ACI 1997). Two types of shrinkage exist; plastic shrinkage and drying shrinkage. Plastic shrinkage is the loss of water from fresh concrete (Mindess, Young et al. 2003). Drying shrinkage (of hardened concrete) is due to loss of moisture in concrete. Due to the scope of the project only drying shrinkage will be studied. Plastic shrinkage occurs at very early ages before the prestressing strands were cut. Therefore prestress losses due to plastic shrinkage are negligible. Figure 2.7 shows a typical strain history of drying shrinkage and subsequent rewetting.

Many variables influence the magnitudes of shrinkage strains. Water cement ratios directly affect shrinkage of the concrete paste. However, many variables within the makeup of the concrete structure and the environment will affect shrinkage strains. Some of the variables affecting shrinkage include; aggregate content, size of the concrete element (specimen geometry), temperature and humidity, admixtures, and restraint due to reinforcement (Bazant and Wittmann 1982; Eatherton 1999; Mindess, Young et al. 2003).
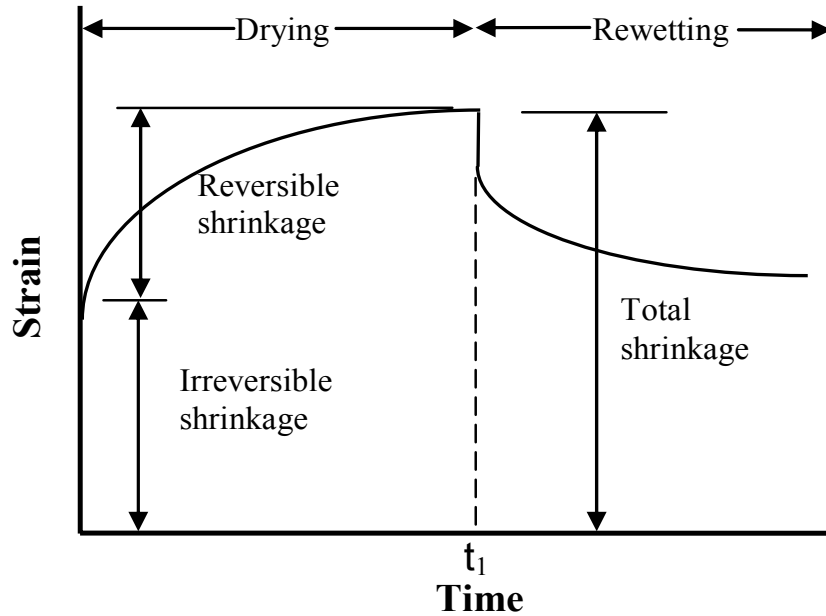
Figure 2.7 – **Typical strain histories due to drying shrinkage and subsequent rewetting (Mindess, Young et al. 2003).**

2.2.3.3. SHRINKAGE PREDICTION MODELS

There are several models for the prediction of shrinkage in concrete. The method outlined describes ACI 209. It should be noted this method should be used for isothermal conditions. When the concrete panels are placed a temperature gradient will exist. In the lab specimens were tested in a hermetically sealed chamber with constant humidity and temperature. The equations for predicting shrinkage are as follows:

- For moist cured concrete:

$$\varepsilon_{sh}(t) = \frac{t}{35+t} \varepsilon_{sh}^* \qquad \textbf{2.1}$$

- For steam cured concrete:

$$\varepsilon_{sh}(t) = \frac{t}{55+t} \varepsilon_{sh}^* \qquad \textbf{2.2}$$

Where the terms in the above are defined by:

t = time after initial curing (days)

ε_{sh}^* = the final shrinkage at time infinity

$$\varepsilon_{sh}^* = 780\gamma_1\gamma_2\gamma_3\gamma_4\gamma_5\gamma_6\gamma_7 10^{-6} \text{ in/in, (mm/mm)} \qquad \textbf{2.3}$$

Where:

γ_1 = Correction for the effect of variations in the relative humidity, λ (in percent):

$$\gamma_1 = 1.40 - 0.0102\lambda \qquad \text{for } 40 \le \lambda \le 80 \qquad \textbf{2.3a}$$

$$\gamma_1 = 3.00 - 0.030\lambda \qquad \text{for } 80 < \lambda \le 100 \qquad \textbf{2.3b}$$

γ_2 = Correction for the size and shape of the member based on the average thickness h_o

(= 4 $^V/_S$) or the volume to surface area ratio ($^V/_S$):

When 50 mm $\le h_o \le$ 150 mm:

h_o (mm)	50	75	100	125	150
γ_2	1.35	1.25	1.17	1.08	1.00

- When 150 mm < $h_o \le$ 380 mm:

$$\gamma_2 = 1.23 - 0.00015h_0 \qquad \text{when } t \le 365 \text{ days} \qquad \textbf{2.3c}$$

$$\gamma_2 = 1.17 - 0.00114h_0 \qquad \text{when } t > 365 \text{ days} \qquad \textbf{2.3d}$$

- When h_o > 380 mm:

$$\gamma_2 = 1.2e^{-0.00472\,v/s} \qquad \textbf{2.3e}$$

γ_3 = Correction for the composition of the concrete based on the slump of the fresh

concrete, s, in mm:

$$\gamma_3 = 0.89 + 0.00161s \qquad\qquad \textbf{2.3f}$$

γ_4 = Correction for the composition of the concrete based on the ratio of the fine

aggregate to total aggregate by weight, ψ (in percent):

$$\gamma_4 = 0.30 + 0.014\Psi \qquad \text{for } \psi \leq 50\% \qquad \textbf{2.3g}$$

$$\gamma_4 = 0.90 + 0.002\Psi \qquad \text{for } \psi > 50\% \qquad \textbf{2.3h}$$

γ_5 = Correction for the composition of the concrete based on the air content of the

concrete, α (in percent):

$$\gamma_5 = 0.95 + 0.008\alpha \qquad\qquad \textbf{2.3i}$$

γ_6 = Correction for the cement content, c (kg/m^3):

$$\gamma_6 = 0.75 + 0.00061c \qquad\qquad \textbf{2.3j}$$

γ_7 = Correction for the variation in the period of initial moist curing T_c (in days):

T_c (days	1.0	3.0	7.0	14.0	28.0	90.0
γ_7	1.2	1.1	1.0	0.93	0.86	0.75

The Prestressed Concrete Institute (PCI) stipulates for standard conditions an

average value of nominal ultimate shrinkage strain, $\varepsilon_{sh}* = 820 \times 10^{-6}$ in/in. Other models

not used for shrinkage prediction include the CEB-FIP and the AFREM models.

2.2.3.4.   CREEP STRAINS

Creep is the increase in strain due to sustained loading. Creep strains are

determined by subtracting the total measured strain in a loaded specimen, the

instantaneous strain due to sustained stress (elastic deformation), the shrinkage, and the

eventual thermal strain in an identical load free specimen which is subject to the same

relative humidity and temperature conditions (ACI 1997). Total creep is the result of two components; basic creep and drying creep. Basic creep occurs under uniform moisture conditions. Drying creep occurs as concrete dries.

Figure 2.8 shows a typical strain versus time history for concrete creep. An initial elastic deformation occurs due to loading, followed by creep strain. When concrete is unloaded, elastic deformations are fully recovered, but creep strains are only partially recovered. Creep strain magnitudes are dependent on many parameters. The following factors affect creep; level of sustained stress, humidity and temperature, water – cement ratio, aggregate modulus, aggregate/ paste ratio, age at loading, specimen size, and reinforcement (Bazant and Wittmann 1982; Eatherton 1999; Mindess, Young et al. 2003).
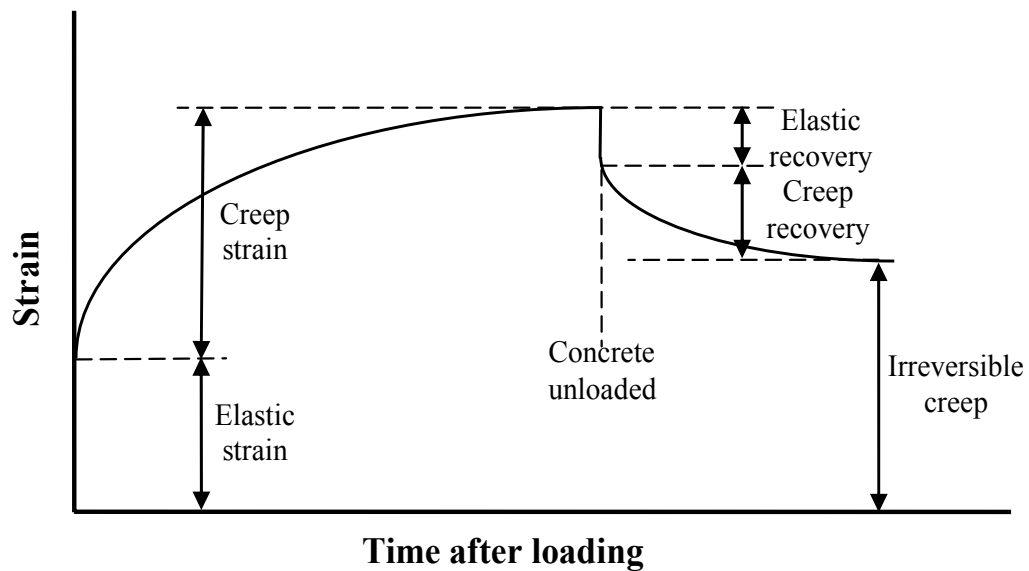
Figure 2.8 –   Schematic of the various types of creep (Mindess, Young et al. 2003).

2.2.3.5. CREEP PREDICTION MODELS

There are several models to predict creep in concrete. The model that is presented here is the ACI 209 method which is based on a hyperbolic function to represent the creep-time relationship (ACI 1997).

$$\varepsilon(t) = \frac{\sigma_0}{E_c(\tau)} + \phi(t,\tau)\frac{\sigma_0}{E_c(\tau)} \qquad \textbf{2.4}$$

$$\phi(t,\tau) = \frac{(t-\tau)^{0.6}}{10 + (t-\tau)^{0.6}}\phi^*(\tau) \qquad \textbf{2.5}$$

Where the terms are defined as:

σ_0 = Applied stress

$E_c(\tau)$ = Modulus of elasticity at the time of loading

τ = Time at loading (days)

$t - \tau$ = The duration of loading (days)

$\phi(t,\tau)$ = Creep – time relationship

$\phi^*(\tau)$ = Final creep coefficient:

$$\phi^*(\tau) = 2.35\gamma_1\gamma_2\gamma_3\gamma_4\gamma_5\gamma_6 \qquad \textbf{2.6}$$

Where:

γ_1 = Correction for loading age

        For moist cured concrete: $\gamma_1 = 1.23\tau^{-0.118}$ **2.6a**

        For steam cured concrete: $\gamma_1 = 1.13\tau^{-0.094}$ **2.6b**

γ_2 = Correction for the effect of variations in the relative humidity, λ (in percent):

         $\gamma_2 = 1.27 - 0.0067\lambda$ for $\lambda > 40$ **2.6c**

γ_3 = Correction for the size and shape of the member based on the average thickness h_o

(= 4 $^V/_S$) or the volume to surface area ratio ($^V/_S$):

When $h_o \le 150$ mm:

h_o (mm)	50	75	100	125	150
γ_3	1.30	1.17	1.11	1.04	1.00

- When 150 mm < h_o < 380 mm:

$$\gamma_3 = 1.14 - 0.00092\, h_0 \qquad \text{when t-τ} \le 365 \text{ days} \qquad \textbf{2.6d}$$

$$\gamma_3 = 1.10 - 0.00067\, h_0 \qquad \text{when t-τ} > 365 \text{ days} \qquad \textbf{2.6e}$$

- When $h_o \ge 380$ mm:

$$\gamma_3 = \frac{2}{3}\left[1 + 1.13e^{-0.54 v/s}\right] \qquad \textbf{2.6f}$$

γ_4 = Correction for the composition of the concrete based on the slump of the fresh

concrete, s, in mm:

$$\gamma_4 = 0.82 + 0.00264 s \qquad \textbf{2.6g}$$

γ_5 = Correction for the composition of the concrete based on the ratio of the fine

aggregate to total aggregate by weight, ψ (in percent):

$$\gamma_5 = 0.88 + 0.0024 \Psi \qquad \textbf{2.6h}$$

γ_6 = Correction for the composition of the concrete based on the air content of the

concrete, a (in percent):

$$\gamma_6 = 0.46 + 0.09\alpha < 1.0 \qquad \textbf{2.6i}$$

2.2.4. **CHLORIDE PERMEABILITY TESTS**

2.2.4.1. **GENERAL**

Determining the permeability of concrete is important because of its relation to the durability. Limiting the movement of water and harsh chemicals such as chlorides will help in the long-term performance of concrete. The water – cement ratio is the single parameter that has the largest influence on concrete durability (Mindess, Young et al. 2003). Lower water-cement ratios (below 0.42) limit capillary volume, thus providing a more durable concrete.

2.2.4.2. **ISSUES OF RAPID CHLORIDE PERMEABILITY TEST**

The permeability of concrete is normally measured by the movement of water or the movement of electrical charge. The movement of electrical charge is studied herein, because the tests run at the University of Missouri – Columbia followed ASTM C 1202, "Standard Test Method for the Electrical Indication of Concrete's Ability to Resist Chloride Ion Penetration."

The six hour test involves a concrete specimen sandwiched between solutions of sodium hydroxide and sodium chloride solutions. A voltage is passed through the specimen and current or electron flow is subsequently measured. Concrete with water – cement ratios between 0.4 and 0.75 provide good correlations between the ASTM standard test and more conventional pressure methods (Mindess, Young et al. 2003). A problem with the test stems from the measurement of current. A high initial current will result in heating, which leads to an increase in conductivity. A more objective method of utilizing the ion penetration test is to use the charge passed in the first half-hour for

comparisons rather than the full six-hour test (Mindess, Young et al. 2003). Other problems of the test are the current passed is related to all ions in the pore solution not just chloride ions and the measurements are made before steady-state migration is achieved (Kropp and Hilsdorf 1995; Hooton and Stanish 1997).

2.2.5. FREEZE-THAW TESTS

2.2.5.1. GENERAL

Concrete durability is also related to freezing and thawing cycles under saturated moisture conditions. As water present in the concrete matrix freezes it expands causing tensile stresses. Concrete structures in close proximity to the water line, such as pavements, are subjected to saturated freeze-thaw cycles which can result in durability problems (Pigeon and Pleau 1995).

2.2.5.2. ISSUES OF FREEZE – THAW TESTS

The tests performed at the University of Missouri – Columbia were in accordance with Procedure A of ASTM 666. The test subjects concrete prisms to rapid freeze-thaw cycles in the presence of water. Some concerns of the test are the variability of the test from laboratory to laboratory and how representative the test conditions are to actual field conditions (Pigeon and Pleau 1995).

For example, the rate of cooling is an important parameter affecting frost durability. Generally, increased cooling rates result in larger decreases in concrete durability (Pigeon and Pleau 1995). The ASTM standard specifies a cooling rate between 6 and 15° C/h, whereas in nature the cooling rate rarely exceeds 2° C/h. Therefore, concrete that shows a low durability in the lab may actually be able to resist natural

freezing and thawing cycles without any damage (Pigeon and Pleau 1995). Other variations between natural conditions and the actual test is the length of time the specimen remains frozen, and the moisture conditions during freezing and thawing. In the field concrete is exposed to long periods of below freezing temperatures. Also, variations in moisture conditions in the field during freezing and thawing cycles are different from the fully saturated conditions of the test (Pigeon and Pleau 1995).

2.2.6. FLEXURE TESTS

2.2.6.1. GENERAL

Concrete flexural strength is determined using ASTM C 78. This standard specifies a 3-point bending of a prism turned on its side. The tensile strength of the concrete can be overestimated by nearly 50% because the formula used assumes the stress varies linearly across the cross section (Mindess, Young et al. 2003). Due to the non-linearity of concretes stress versus strain response the stress distribution more closely resembles a parabola. However, the standard is very useful because concrete is normally loaded in bending.

2.3. PRESTRESS LOSSES

2.3.1. GENERAL

Determining losses is imperative in the design of any structure utilizing pre-tension or post-tension tendons. Losses or decreases in the pre-compressive force due to time dependent or instantaneous affects are the result of many different factors, which include; elastic shortening of tendons, strand relaxation, creep and shrinkage of concrete,

friction, and anchorage set. Figure 2.9 is a diagram of the various factors contributing to prestress losses. The total prestress loss in a structure is the addition of all the factors listed above. Two basic methods exist for the prediction of prestress losses; a lump sum method or time-step model (Namaan 2004). For comparative reasons a time-step model was used to predict the creep and shrinkage losses in the PPCP test section. Also, a coupled model taking into account all factors contributing to prestress losses was performed.
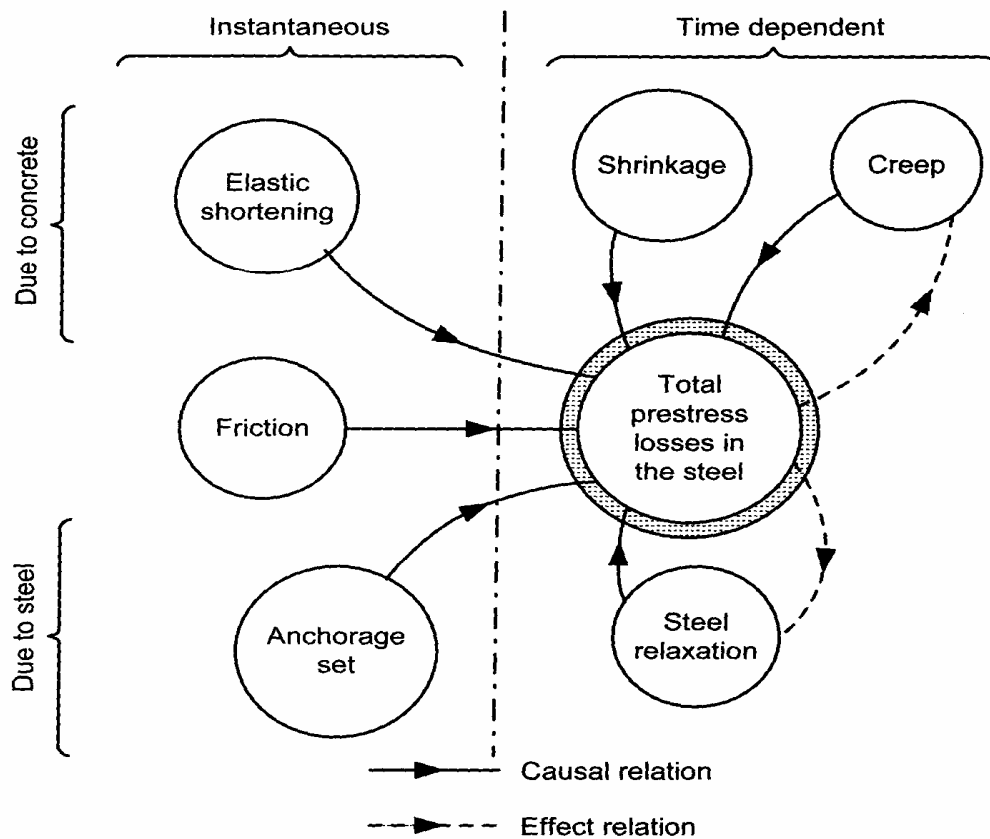
Figure 2.9 –   Schematic of prestress loss sources (Namaan 2004).

2.3.2.   TIME STEP MODEL FOR PREDICTION OF PRESTRESS LOSSES

The time step model used was adapted from Naaman et al. A flow chart of the procedure is shown in Figure 2.10. Since pre and post-tensioning was used both sides of the flow chart were followed. In calculating losses it should be noted there are

interdependencies that exist (Namaan 2004). For example as the concrete shrinks the force applied to the concrete decreases, thus decreasing the amount of creep. To account for these interdependencies a repetitive computational procedure was used using successive time intervals. At each of the time steps the applied force on the concrete is updated to account for losses in the preceding time-step.

The following is a detailed step by step method used for the prediction of total prestress losses for prestressing strands. The method is similar for post-stressing strands.

- Estimate f_{pJ2};

f_{pJ2} = initial stress in tendon at the end of stressing or jacking (ksi or MPa)

- Compute total relaxation loss at any time after jacking, Δf_{pR1};

$$\Delta f_{pR1} = \frac{\log(24t)}{K}\left[\frac{f_{pJ2}}{f_{py}} - 0.55\right]f_{pJ2} \qquad \textbf{2.7}$$

K = 10 for stress relieved strands and 40 for low-relaxation strands

t = time in days from stressing to transfer (days)

f_{py} = yield strength of steel (ksi or MPa)

- Calculate initial prestressing force f_{pi};

$$f_{pi} = f_{pJ2} - \Delta f_{pR1} \qquad \textbf{2.8}$$

- Compute change in force due to elastic shortening Δf_{pES};

$$\Delta f_{pES} = \frac{(f_{cgp})_{F_J}\left[f_{pJ2} - \Delta f_{pR}(t_o, t_t)\right] + (f_{cgp})_G f_{pJ2}}{f_{pJ2}/n_{pi} + (f_{cgp})_{F_J}} \qquad \textbf{2.9}$$

$(f_{cgp})_{FJ}$ = stress in concrete at the centroid of prestressing tendons due to prestressing force F_J

$(f_{cgp})_G$ = stress in concrete at the centroid due to self weight of member

n_{pi} = initial modular ratio

- Calculate prestressing force at time t_j;

$$\left[f_p(t_j) \right]_1 = f_{pJ2} - \Delta f_{pR1} - \Delta f_{pES}$$

2.10

The equations above calculate the initial losses in the prestressing force. The following assume a time step approach. Certain time intervals are chosen and the prestressing force is updated after subsequent iterations.

- When m is equal to m+1 select a time interval from t_i to t_j;

$$\left[f_p(t_i) \right]_m = \left[f_p(t_j) \right]_{m-1}$$

2.11

- Compute the force applied from the prestressing strands at the center of gravity;

$$f_{cgp}(t_i) = \frac{f_p(t_i)A_{ps}}{A_c} \left(1 + \frac{e_o^2}{r^2} \right) - \frac{M_D e_o}{I}$$

2.12

A_{ps} = area of prestressing steel

A_c = area of concrete cross section

e_o = eccentricity

r = radius of gyration of the section

I = moment of inertia of the cross section

- Compute the change in prestressing force due to shrinkage, creep, and relaxation over time-step

$$\Delta f_{pS}(t_i, t_j) = E_{ps}\varepsilon_{SU}K_{SH}K_{SS}\left[g(t_j) - g(t_i) \right]$$

2.13

E_{ps} = modulus of the prestressing strands

ε_{su} = ultimate shrinkage strain of concrete material

K_{SH} = correction factor for relative humidity

K_{SS} = correction factor for shape and size of the member

g(t) = time function recommended by ACI 209

$$\Delta f_{pC}(t_i, t_j) = n_p C_{CU} K_{CH} K_{CA} K_{CS} f_{cgp}(t_i)[g(t_j) - g(t_i)]$$ **2.14**

n_p = modular ratio

C_{CU} = ultimate creep coefficient

K_{CH} = correction factor for relative humidity

K_{CA} = correction factor for age at loading

K_{CS} = correction factor for size and shape

$$\Delta f_{pR}(t_i, t_j) = \frac{f_p(t_i)}{K} \left(\frac{f_p(t_i)}{f_{py}} - 0.55 \right) \log\left(\frac{t_j}{t_i}\right)$$ **2.15**

- Calculate the total change in the prestressing force;

$$\Delta f_{pT}(t_i, t_j) = [f_p(t_i)]_m - \Delta f_{pS}(t_i, t_j) - \Delta f_{pC}(t_i, t_j) - \Delta f_{pR}(t_i, t_j)$$ **2.16**

- Update the prestressing force;

$$[f_p(t_j)]_m = [f_p(t_i)]_m - \Delta f_{pT}(t_i, t_j)$$ **2.17**

After the change in prestressing force has been calculated over all time intervals the final effective prestressing force is equal to the value calculated in the final step above. The total change in prestressing force or total loss can be calculated with the following.

$$\Delta f_{pT} = f_{pe} - f_{pJ2}$$ **2.18**

Pretensioned

Estimate f_{pJ2}

Compute Δf_{pR1}

$f_{pi} = f_{pJ2} - \Delta f_{pR1}$

Compute Δf_{pES}

$[f_p(t_j)]_1 = f_{pJ2} - \Delta f_{pR1} - \Delta f_{pES}$

Select section x. Divide life time into a number of time intervals: n

$m = 1$

Posttensioned

Estimate f_{pJ}

Compute Δf_{pF}

Compute Δf_{pES}

Compute Δf_{pA}

$[f_p(t_j)]_1 = f_{pJ} - \Delta f_{pF} - \Delta f_{pES} - \Delta f_{pA}$

$m = m + 1$; Select: (t_i, t_j) for $m + 1$

$[f_p(t_i)]_m = [f_p(t_j)]_{m-1}$

Compute $f_{cgp}(t_i)$

Compute: $\Delta f_{pS}(t_i, t_j)$; $\Delta f_{pC}(t_i, t_j)$; $\Delta f_{pR}(t_i, t_j)$

$\Delta f_{pT}(t_i, t_j) = [f_p(t_i)]_m - \Delta f_{pS}(t_i, t_j) - \Delta f_{pC}(t_i, t_j) - \Delta f_{pR}(t_i, t_j)$

$[f_p(t_j)]_m = [f_p(t_i)]_m - \Delta f_{pT}(t_i, t_j)$

NO

$m = n$?

YES

$f_{pe} = [f_p(t_j)]_n$; $\Delta f_{pT} = f_{pe} - f_{pJ}$ or $\Delta f_{pT} = f_{pe} - f_{pJ2}$

Figure 2.10 – Flow chart for the prediction of prestress losses using the time step method (Namaan 2004).

3. EXPERIMENTAL PROGRAM

3.1. FIELD INSTRUMENTATION

3.1.1. GENERAL INFORMATION ON INSTRUMENTATION

Due to the scope of this research report only a brief overview of details regarding field instrumentation are discussed. The overall test section logistics are presented, followed by specific instrumentation locations within the instrumented panels. A look at the five strain and temperature measuring devices used for observation and their function, and an overview of the data acquisition system will conclude this section. A more in depth and detailed background on instrumentation is discussed in the companion thesis, "Instrumentation and Early Performance of an Innovative Prestressed Precast Pavement System," referenced in chapter 1.

3.1.1.1. TEST SECTION LAYOUT

The pilot project encompassed 1,000 feet of roadway rehabilitation and consisted of four 250' sections or slab lengths. A goal of the research program was to study the three different panel types and understand their behavior. To accomplish this, the research team decided to focus on a single 250' slab length and instrument panels within this section. The section chosen was the third in line from the beginning extents of the PPCP project limits. It was selected based on its proximity to an AC power source and to limit possible transition effects from conventional concrete pavements adjacent to the PPCP. Four base panels, two joint panels, and one anchor panel were instrumented to understand the characteristics of the individual panels and how they perform under

service loads. Figure 3.1 shows the location of the instrumented panels within the chosen

section. The panel marked B4 in Figure 3.1 lies outside the third section and was

instrumented for redundancy purposes.
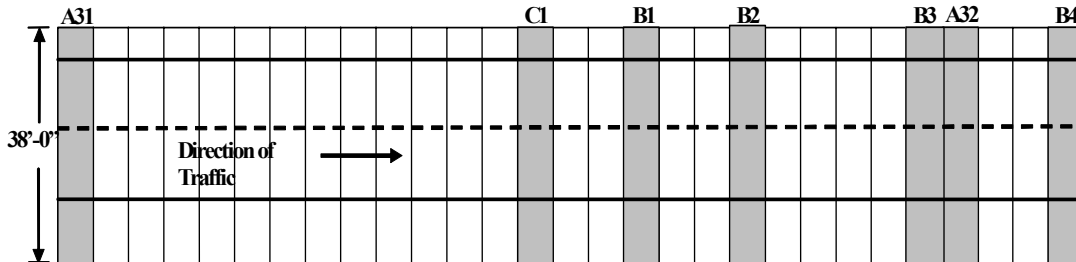
Figure 3.1 – **Overall view of test-section and location of instrumented panels. (A refers to a joint panel, B refers to a base panel, and C refers to a anchor panel)**

3.1.1.2. INSTRUMENTED PANELS

The seven instrumented panels incorporated five different devices to measure

strain and temperature of the concrete along with strain in the post-tensioning strands.

Figure 3.2 depicts typical instrumentation in a base or anchor panel and Figure 3.3 shows

the instrumentation locations in joint panel A32. Concrete strain was measured using

instrumented rebar and vibrating wire gages and strain in the post-tensioning strands was

measured by vibrating wire strandmeters. Temperature measurements were observed by

thermocouples and iButtons imbedded in the concrete along with thermistors

incorporated in the vibrating wire gages.

3.1.1.3. INSTRUMENTATION LABELING

The precast panels used in the project are identified by two different methods.

The identification system used by CPI and Gaines Construction used letters and numbers

to signify the different panel types. An "A" panel was a joint panel, a "B" panel was a

base panel, and a "C" panel was an anchor panel. Since three different types of joint panels were used, a number after the "A" differentiated the joint panels. Labels "A1" and "A2" represented the joint panels at the north and south limits of the overall pavement test section respectively. The symbol "A3" was used for the three intermediate joint panels in the project.

To differentiate the instrumented panels from the non-instrumented panels the MU research team added a number after the symbols used by the contractors. The panel numbering increased from south to north. For example the four base panels were labeled B1, B2, B3 and B4. The southern most base panel was B1 and the northern most was B4. The single instrumented anchor panel was marked C1, and the joint panels were marked A31 and A32 respectively.

The gages within the panels were further identified by their type and location. Vibrating wire gages were marked with a V, instrumented rebar with an R, thermocouples with a T, and strandmeters with an S. The location of the gage was identified by a number after the type of gage.
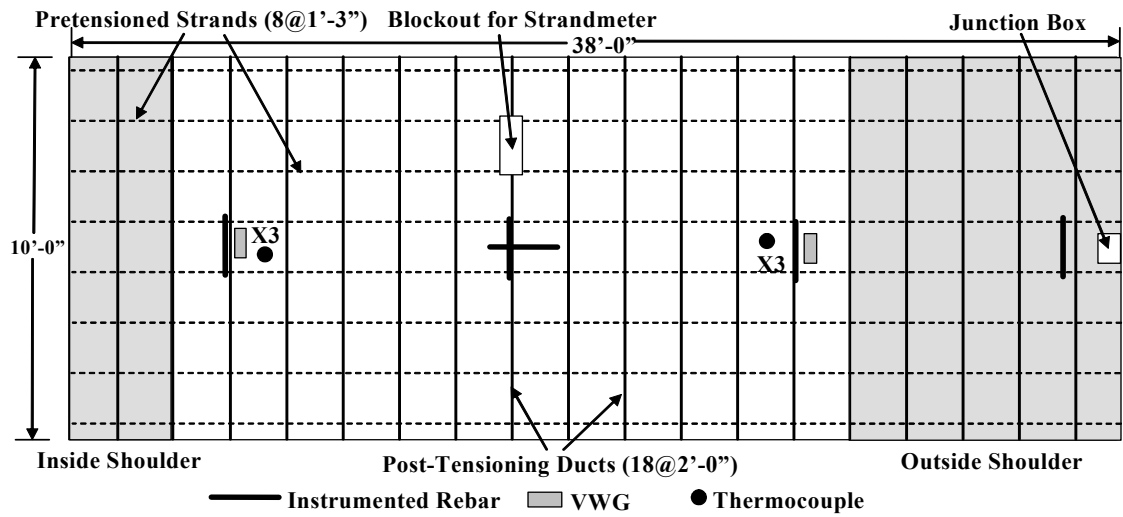
Figure 3.2 – Typical instrumented base or anchor panel.
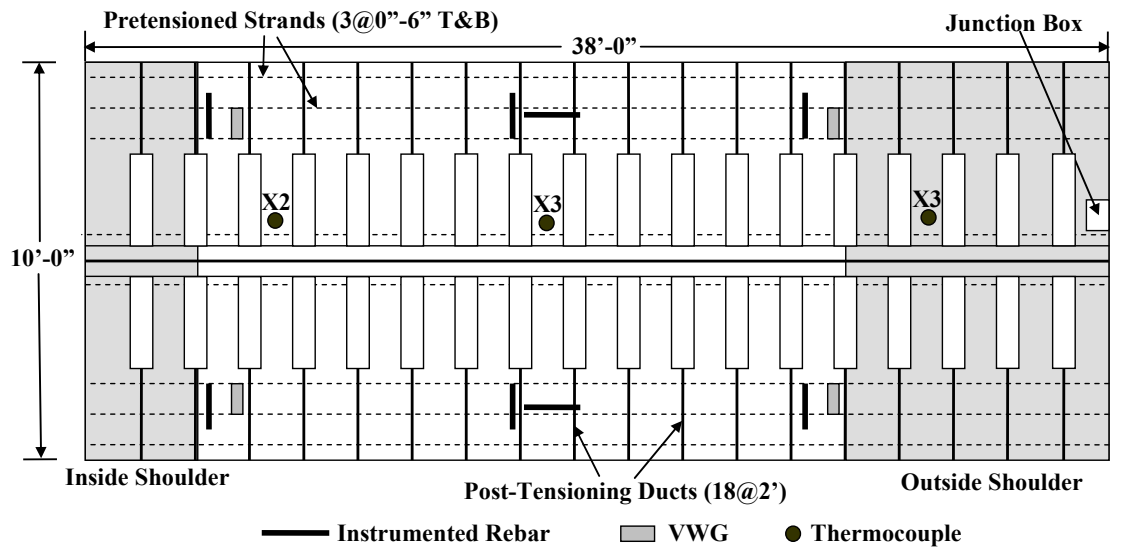
Figure 3.3 – Instrumented joint panel A32.

3.1.2. INTERNAL INSTRUMENTATION

3.1.2.1. STRAIN GAGE REBAR

Four standard 20', #4 (nominal diameter = 0.5"), Grade 60 rebar sections were

purchased from Ahren's Steel in Columbia, MO to fabricate the strain gage rebar for the

project.   The 20' rebar sections were chop sawed into ten equal sections measuring approximately 24" in length.   Either end of the 24" section was machined smooth and threaded to accommodate gripping during calibration.   The middle two inches were also machined smooth as preparation for strain gage application.   Gage application and subsequent calibration and waterproofing all were very involved processes.

A full strain gage bridge was installed on each 24 inch rebar section. A schematic of the strain gage configuration is shown in Figure 3.4 below. The two-inch machined section was degreased, sanded smooth, and cleansed before strain gage application. Two gages were installed transverse to the length of the rebar and the other two were installed along or longitudinal to the length of the rebar. The ribs on either side of the rebar were used to line up the gages consistently. After gage application wires were run to complete the bridge. By using a full bridge of active strain gages the effects of temperature on measured strains are eliminated

A completed strain gage rebar is shown in Figure 3.5. Strain gage rebar are capable of measuring very dynamic events such as stress transfer from strand cutting and traffic loads while in-service. The instruments are also very robust and have a good track record from previous projects completed here at the University of Missouri – Columbia.
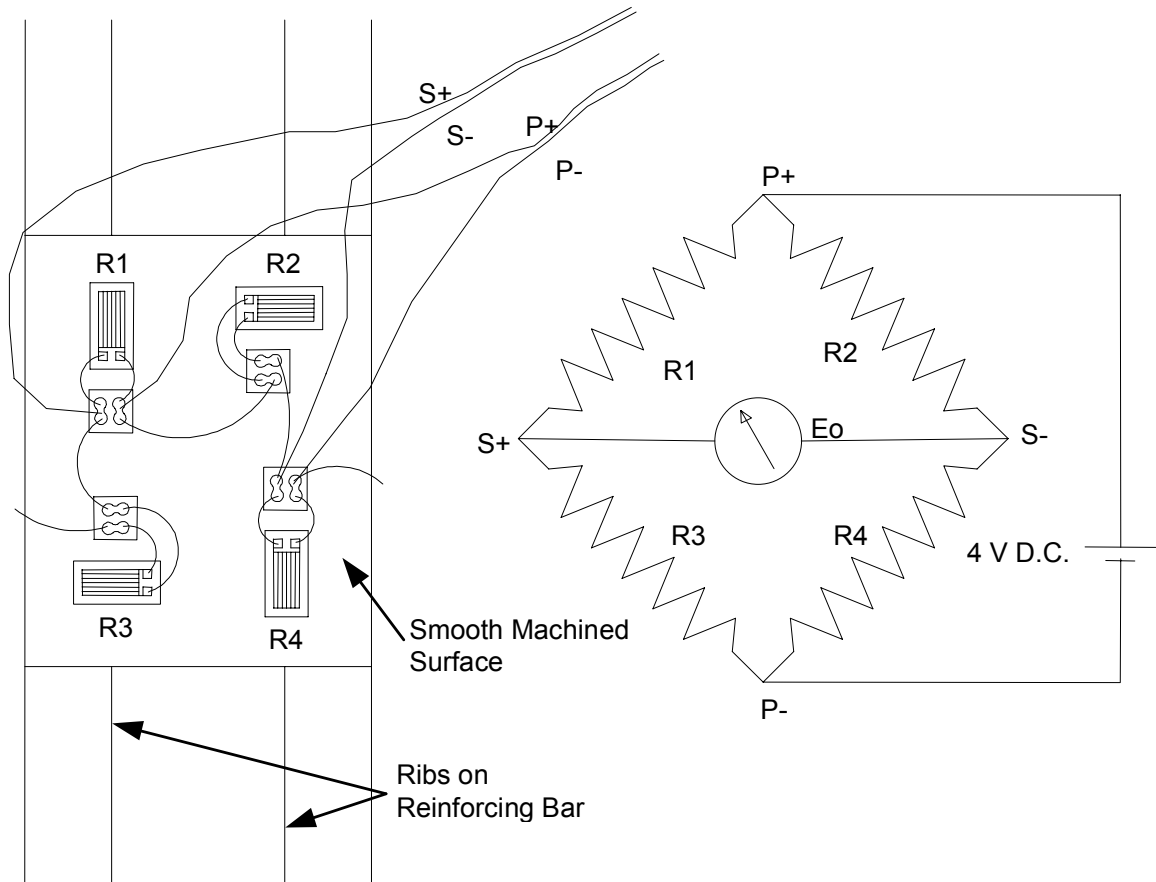
Figure 3.4 – **Schematic of the strain gage configuration on the strain gage rebar(Eatherton 1999).**

Figure 3.5 – **A completed strain-gage bar along with an instrumented bar yet to be waterproofed and sealed (Eatherton 1999)**

3.1.2.2.   VIBRATING WIRE STRAIN GAGES

Model 4200 Vibrating Wire embedment type strain gages were purchased from Geokon Incorporated. The 6" gage is depicted in Figure 3.6. The gage consists of a wire stretched between two flanges, an electromagnetic plucking device, and a thermistor used for temperature compensation. The gage operation relies on the change in resonant frequency of the wire based on its length. When one flange displaces relative to the other, the wire is elongated resulting in a change in resonant frequency. This change in resonant frequency can then be related to strain by simple mechanics.

The vibrating wire gages are very useful for long-term strain measurements; however, dynamic events cannot be measured due to settling time of the stretched wire. After imbedding the gage in concrete a zero reading can be taken. At any time the zero reading can be referenced and the state of strain of the concrete can be determined.
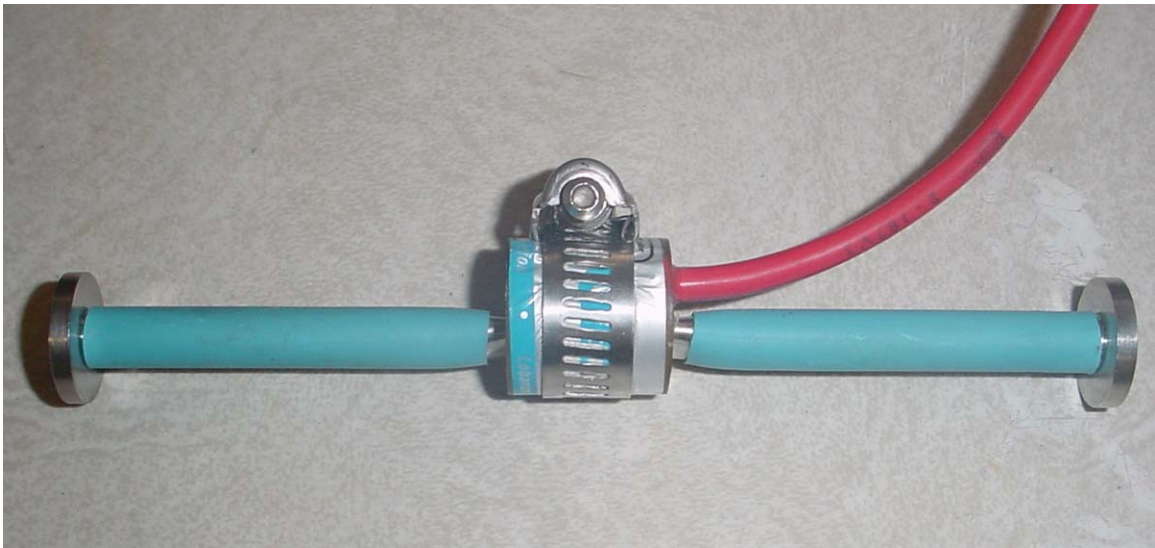
Figure 3.6 –   Model 4200 vibrating wire gage from Geokon Incorporated.

3.1.2.3.   VIBRATING WIRE STRANDMETERS

Model 4410 Vibrating Wire strandmeters were also purchased from Geokon Incorporated and one is depicted in Figure 3.7. The gage operates on the same principles

as the model 4200 discussed above. However, clamps at either end accommodate fixing to a pre or post-tensioning strand. Individual calibration information was supplied by Geokon. However, since the gages have never been used by research personnel at the University of Missouri – Columbia they were individually calibrated to ensure proper operation.

The main purpose of the gage was to measure strains during post-tensioning of the strands, understand frictional losses associated with strand stressing, and measure time-dependent prestress loss. The gages were encased in a PVC tube, and it was assumed the gages were isolated from the surrounding concrete and only measured strain in the post-tensioning strand.

Figure 3.7 –   Model 4410 vibrating wire strandmeter purchased from Geokon Incorporated.

3.1.2.4.   THERMOCOUPLES

Type T thermocouples utilizing a copper-constantan connection were used for concrete temperature measurement. The specified temperature range was -328° to 663° F ($-200°$ to $900°$ C). The thermocouples were cut to length, welded using thermocouple welders, and coated in epoxy at the University of Missouri – Columbia. This type of

temperature measuring device is very advantageous due to its robustness, ease of use, and accuracy (+/- 0.1^o C).

3.1.2.5. IBUTTONS

iButtons manufactured by Dallas Semiconductors were also used to measure temperature. Twelve Dallas Semiconductor model DS1922L iButtons were purchased from Embedded Data Systems. The DS1922L is capable of measuring temperatures in a range from -40° C to 85° C with a resolution of 0.0625^o C. The iButtons store time and temperature logs in self contained memory unit and only require a single lead wire to communicate with a computer or other datalogging device. Lead wires were soldered on the iButtons at the University of Missouri – Columbia, and the devices were coated in epoxy to protect them from contact with other ferrous materials.

3.1.2.6. GAGE INSTALLATION

All gages were tested at the University of Missouri before being installed in the precast panels. The gages were sorted according to the specific panel they were installed in and boxed in plastic tubs for transportation to the precast yard. The lead wires were cut to specific lengths depending on their location within the panel, labeled accordingly, and the ends were tind in the laboratory to streamline gage installation at the precast yard and connection at the construction site.

Figure 3.8 and Figure 3.9 depict installed gages just before casting. The vibrating wire gages were attached or "piggy-backed" on the instrumented rebar. Wooden spacers were used to ensure the gages did not touch. The zip ties holding the vibrating wire gages in place were purposely left loose to ensure the gages were not damaged. In Figure

3.8 installed thermocouple wires can also be seen. The thermocouples were attached to Fiber Reinforced bars to make sure they were not electrically shorted. To get a profile of temperatures, thermocouples were located at the top, middle, and bottom of the cross-section.   Figure 3.10 shows a broader view of instrumented rebar installed in the longitudinal and transverse directions. Strandmeters were installed in blockouts in the panels after they were transported and placed at the construction site. An installed strandmeter is shown in Figure 3.11. To isolate the strandmeters from the grout used to fill in the blockouts a PVC tube was secured around the gage. This is seen in Figure 3.12.
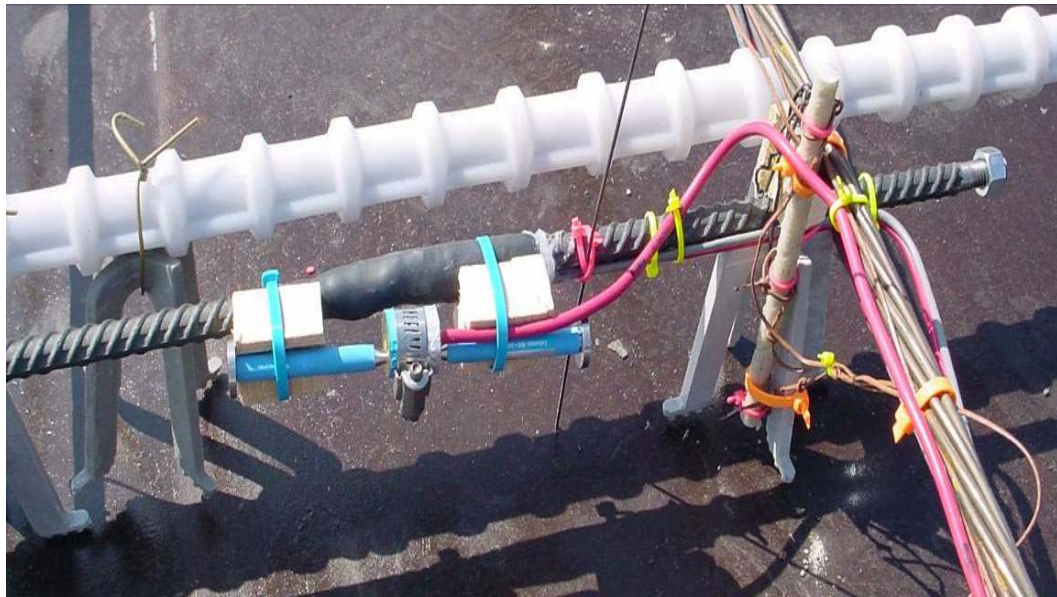
Figure 3.8 –   Picture of installed gages just before casting of concrete. A vibrating wire gage attached to a rebar can be seen along with thermocouples attached to FRP.
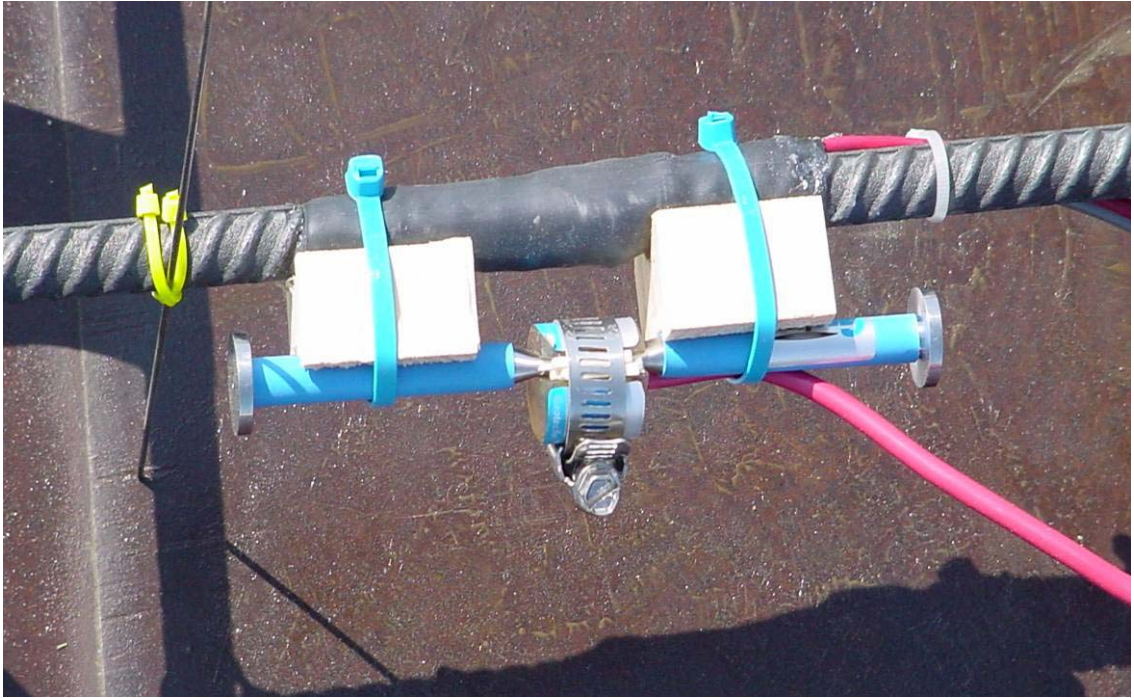
Figure 3.9 – Close-up view of vibrating wire gage attached to instrumented rebar. Zip ties were very loose to ensure the gage was not bent.
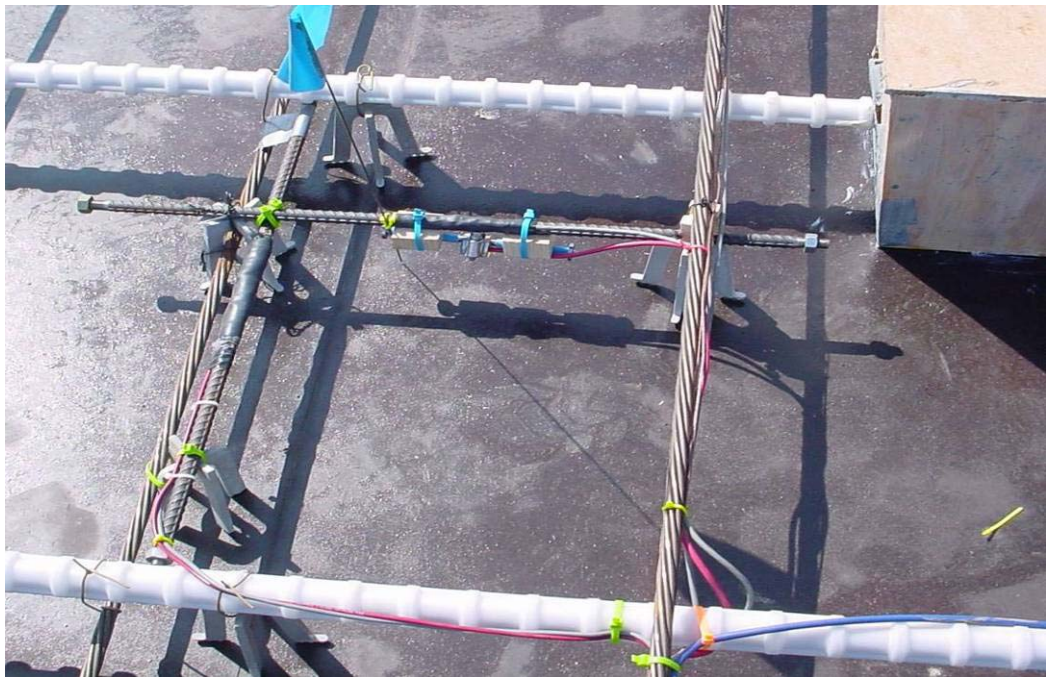
Figure 3.10 – Instrumented rebar installed longitudinal and transverse to the direction of traffic.
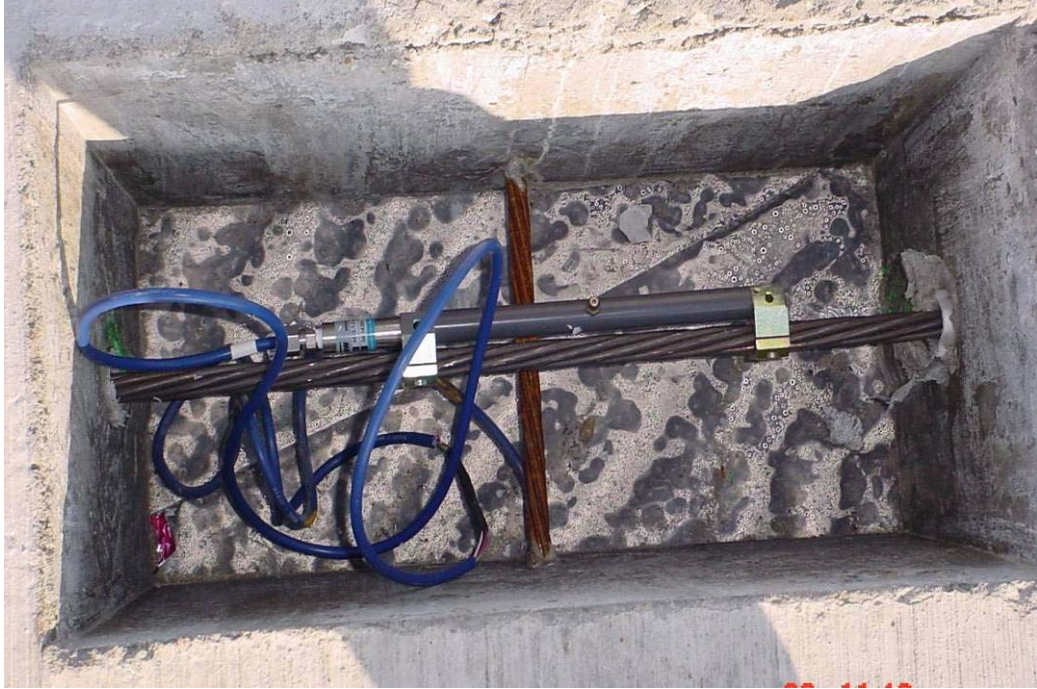
Figure 3.11 – Strandmeter installed in blockout around post-tensioning strand.
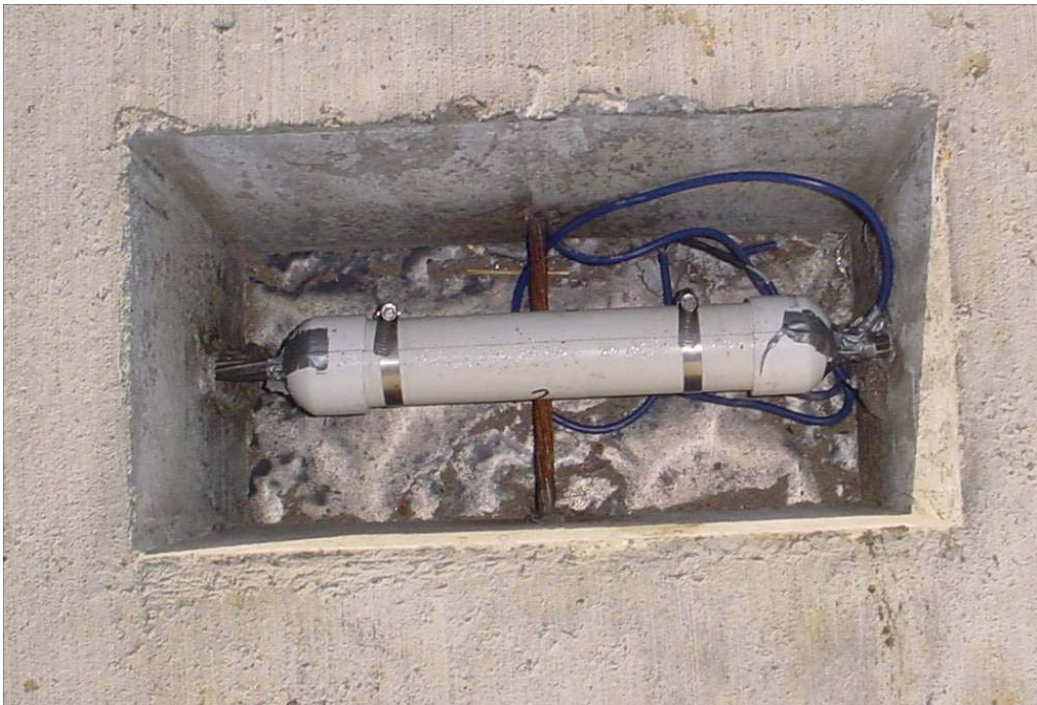
Figure 3.12 – Strandmeter encased in PVC tube to isolate it from grout.

3.1.3. DATA ACQUISITION SYSTEM

The many capabilities of the data acquisition system are briefly discussed in this section. Please refer to the companion thesis for an in-depth discussion involving the data acquisition system (Dailey 2006).

All instrumentation lead wires were run to blockouts cast in the outside shoulder of the precast panels. The junction boxes, shown in Figure 3.13, were fabricated at the University of Missouri – Columbia to accommodate quick connection, cold-junction compensation for thermocouples, and voltage step-down/regulation for the instrumented rebar. Multi-pair wires were run from the junction boxes to the data acquisition cabinet installed at the extents of the right of way for signal transmission. Figure 3.13 shows the signal cabinet and components of the main data acquisition system.

The cabinet is equipped with a 30 amp power supply and a DSL connection for remote communication. The Data acquisition system consists of a Campbell Scientific CR10X data logger, (3)-32 differential AM416 relay multiplexers, 110V AC to 12V DC power supply, two AVW1 vibrating wire interfaces, and an NL100 network link interface for remote communication. The remote communication feature allows the research team and other authorized personnel to monitor real time performance of the pavement system and download/upload new programs as appropriate.
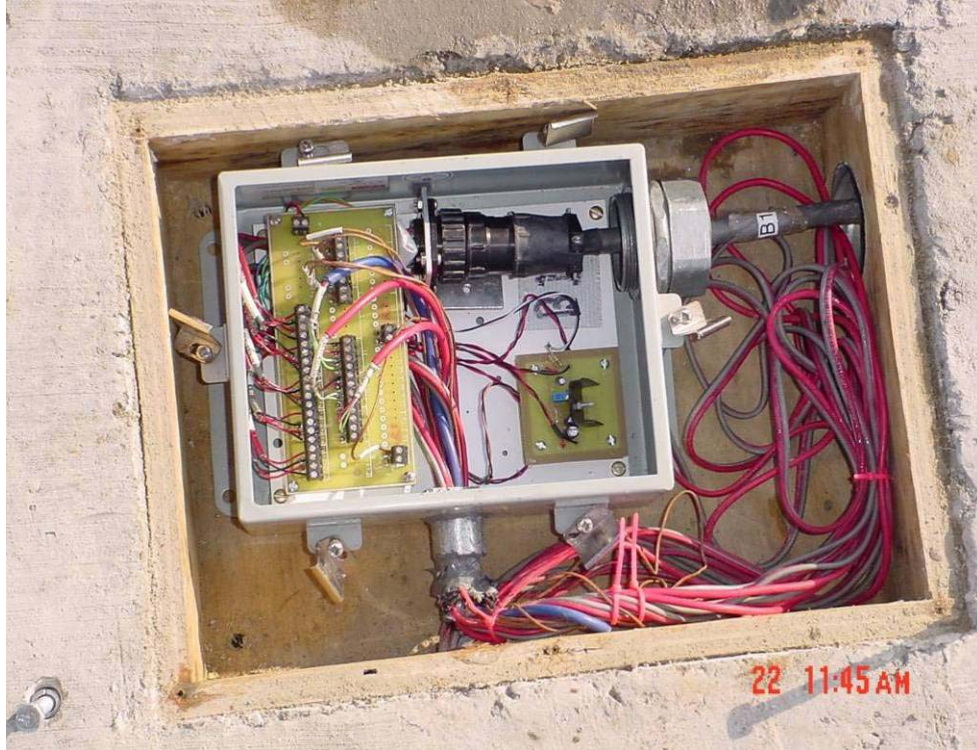
Figure 3.13 – Junction box installed in blockout cast in outside shoulder of precast pavement panels.

Figure 3.14 – Signal cabinet with main data-acquisition equipment installed at the edge of right of way.

3.2. LABORATORY STUDIES

3.2.1. GENERAL

A main focus of this thesis is to study the material properties in depth and understand how these properties will affect PPCP design. Details pertaining to all laboratory studies are discussed in detail, so the reader will have a good background on how characteristics of the materials were obtained.

Laboratory studies were conducted to determine important properties regarding the concrete mix design used in fabricating panels. All studies were performed at the University of Missouri-Columbia. Experimental specimens were taken during the casting of instrumented panel sets. Table 3.1 shows the date experimental specimens were cast along with the quantity and specimen dimensions/type. Typical cylinder casting performed at the precasting yard is seen in Figure 3.15. A total of (24) 6" diameter cylinders were cast to determine strength at various ages, (4) 4"diameter cylinders were made for chloride permeability tests, (6) prism molds were cast for freeze-thaw and flexure tests, and (5) creep and (5) shrinkage specimens were cast. It should be noted that the (5) creep specimens cast on October 12, 2005 were not used because of damage sustained from not removing gage spacer bars in a timely manner.

Table 3.1 –   Summary of experimental specimens cast for laboratory studies.

	Date Cast	6"X12" Cylinders	4"X8" Cylinders	3"X4"X16" Prisms	Creep Specimens	Shrinkage Specimens
Specimen Set 1	10/11/2005	6	0	0	0	0
Specimen Set 2	10/12/2005	6	0	6	5	5
Specimen Set 3	10/13/2005	6	0	0	0	0
Specimen Set 4	12/9/2005	6	4	0	5	0

Figure 3.15 – Strength and shrinkage molds cast during trips to precast yard.

3.2.2. COMPRESSION STRENGTH TESTS

The compressive strength of each specimen set was determined at 7, 28, and 56 days of moist curing. The tests were performed in accordance with ASTM C-39, "The Standard Test Method for Compressive Strength of Cylindrical Concrete Specimens" (ASTM 2005). The 6" x 12" cylindrical specimens were first capped to ensure parallel and smooth ends using Gilson Rediron 9000 sulfur mortar capping compound. This procedure was performed in accordance with ASTM C-617, "Standard Practice for Capping Cylindrical Concrete Specimen" (ASTM 1998) A Forney 600 kip capacity concrete compression testing machine pictured in Figure 3.16 was used for the actual compression tests. Specimens were loaded at a rate of 45-50 psi/s in accordance with ASTM C-39. The compressive force was measured on the hydraulic line with a pressure transducer. Three LVDT's evenly distributed around the specimen with an 8" gage length measured strain. Load output from the Forney and displacement output from the three LVDT's was recorded using a National Instruments data acquisition (DAQ) card and National Instruments LabVIEW.

Figure 3.16 – Compression test setup for capped 6" diameter cylinders using 3 LVDT's and a Forney Compression Machine.

3.2.3. CREEP AND SHRINKAGE TESTS

Specimens for creep and shrinkage were prepared in the exact same manner as the cylinders used the strength tests. The main differences between the creep and shrinkage tests are that shrinkage tests immediately begin after one day of curing and are not under any load, and the creep specimens were cured for 28 days and subjected to a sustained load. An overview of the specimen preparation process is reviewed in the following section followed by details of shrinkage and creep tests respectively.

3.2.3.1. SPECIMEN PREPARATION

Five creep and five shrinkage specimens were cast during instrumentation trips to the precasting yard. Only four of the five specimens cast were used in the actual tests. By sealing (100% relative humidity) two of the specimens and leaving two of the specimen's unsealed (50% relative humidity) comparisons are made at different values of relative humidity. A very specific process was used to prepare the specimens for the subsequent tests. This process is outlined below in detail and has been proven effective in previous research projects at the University of Missouri – Columbia (Earney 2006).

3.2.3.1.1. MOLD PREPARATION

Prior to casting, the 6" x 12" cylinder molds were prepared. The molds meet the requirements of ASTM C 470/C 470M-02a, "Specification for Molds for Forming Concrete Test Cylinders Vertically." Figure 3.17 is a photograph of a typical mold used. The molds contained three sets of equidistant holes to accommodate anchors for attaching extensometers. Temporary spacer bars to fix the distance between anchors were manufactured. The steel spacer bars measured 12" x 1" x 1/8" with two holes drilled 10" apart. Brass anchors on the interior of the mold were attached to the spacer bars with greased machine screws.

Figure 3.17 – **Interior and exterior view of cylinder molds used for creep and shrinkage. Brass anchors and spacer bars are seen (Earney 2006).**

3.2.3.1.2. CASTING AND CURING

All specimens were cast in accordance with ASTM C31/C31M-03A, "Standard Practice for Making and Curing Concrete Test Specimens in the Field." Five specimens used for shrinkage were cast October 12, 2005, and five specimens for creep were cast on December 9, 2005. Casting of the cylinders is seen in Figure 3.18. Both the creep and shrinkage specimens were steam cured with the precast panels to ensure representative samples.

The specimens used for shrinkage were immediately transported back to the laboratory the next day and the molds removed to begin testing. The creep specimens

were placed in a moist curing room until an age of 28 days. To accommodate free shrinkage the spacer bars in both specimen types were removed within 8 to 24 hours of casting.

Figure 3.18 – Creep and shrinkage cylinder casting during instrumentation trips to the precast yard.

3.2.3.1.3. CAPPING AND SEALING

Prior to capping and sealing all specimens were de-molded by drilling a small hole in the bottom of the mold and using compressed air to remove the plastic mold. Loose debris and moisture on the ends of the cylinders was removed by blowing compressed air over the specimens.

The four cylinders were capped in the same fashion as the compression specimens to ensure parallel ends. Two each of the capped creep and shrinkage specimens were sealed using aluminum foil tape. Studies done in the lab have proven the combination of sulfur mortar capping compound on either end and aluminum foil tape wrapped around specimen prevents over 99% of moisture losses. Figure 3.19 shows capped and sealed specimens ready for extensometer attachment.

Figure 3.19 – Picture of capped and sealed specimens used for creep and shrinkage studies (Earney 2006).

3.2.3.1.4. EXTENSOMETER ATTACHMENT

Brass anchor sets cast 120° apart around the circumference of the cylinders secured shrink wrapped studs to the specimens. The studs were screwed into the specimens after curing and upon completion of capping and sealing. The heat shrink was needed to electrically isolate the extensometers and provide a grip. Extensometers with a 10" gage length were then affixed between the three sets of studs. A close-up view of the

stud and extensometer connection is seen in Figure 3.20. A zip tie properly positioned was used to secure the extensometer to the stud. All extensometers were manufactured at the University of Missouri – Columbia and individually tested and calibrated (Earney).

Figure 3.20 – Close-up view of extensometer attachment to stud screwed into brass insert cast in concrete cylinder (Earney 2006).

3.2.3.2. CREEP SPECIMEN LOADING AND INSTALLATION

Four creep specimens were loaded into the creep frame shown in Figure 3.21 at an age of 28 days. Prior to loading the procedure outlined in the previous section regarding specimen preparation was followed. The capped specimens with attached extensometers were stacked in the creep frame. A hydraulic jack was then placed between two steel plates at the top of the frame and a load was applied. Nuts were tightened to secure the bottom plate and the jack was removed. The frame was located in a sealed chamber to hold the temperature and relative humidity constant. Details of this chamber are discussed further in the section on Test Control and Data Acquisition.

Figure 3.21 – Creep load frame with two sealed and unsealed specimens loaded in compression (Earney 2006).

3.2.3.2.1. DETAILS ON CREEP FRAMES

Creep frames are required to apply a constant load and measure the creep characteristics of concrete. Spring loaded creep frames designed and implemented on a previous research project at the University of Missouri – Columbia were used for this test (Earney). Springs apply constant load when compressed to prescribed levels, which is a very important characteristic for monitoring creep. The support structure of the frames consists of a tripod of steel bars that are perpendicular to the ground. At the top of the frame there are two steel plates. These plates are used to house a hydraulic jack that applies the stress to the concrete specimens. When the jack has compressed the cylinders

to a desired load, the nuts above the bottom steel plate are secured in place to retain the sustained compression load. A load cell under the bottom plate was used to monitor load for the duration of the experiment. The load cell was calibrated to measure the load of the jack by using strain gages that are glued to the inside of the cell. Below the load cell there is a small concrete stub cylinder used to distribute end restraint stresses. The stub cylinders also ensure that load is applied to the test cylinders through a "poisson ratio" compatible load pattern. Underneath the stub cylinder are the four test cylinders (two sealed and two unsealed). Between each cylinder is a pair of Teflon sheets to reduce friction between capped cylinders. The bottom of the creep frame includes another concrete stub cylinder. The cylinders rest on a circular steel plate that is rotationally unrestrained due to its spherical seating. The three springs at the bottom of the frame maintain the prescribed constant load applied via the hydraulic jack (Earney 2006).

3.2.3.3. SHRINKAGE SPECIMEN INSTALLATION

A total of four shrinkage specimens were monitored. Two were sealed and two were unsealed. After specimen preparation described above, the cylinders were placed in a hermetically sealed chamber and hooked up for monitoring. A sealed specimen placed the chamber with extensometers attached is shown in Figure 3.22. Monitoring began at an age of one day and continued until 83 days. The specimens were carefully situated in the sealed chamber such that they would not be disturbed.

Figure 3.22 – Sealed shrinkage specimen with three extensometers attached for measurement of shrinkage strains (Earney 2006).

3.2.3.4. TEST CONTROL AND DATA ACQUISITION

3.2.3.4.1. AUTOMATED TEMPERATURE AND HUMIDITY CONTROLLED CHAMBER

A hermetically sealed chamber constructed at the University of Missouri – Columbia maintained the creep and shrinkage specimens to a constant relative humidity of 50% and ambient temperature of 24° C. The atmosphere of the chamber was digitally controlled using a National Instruments LabVIEW program. The front panel displayed in Figure 3.23 shows a time history of relative humidity and temperature. Preset upper and lower limits of relative humidity and temperature were used to determine when devices needed to be activated to modify conditions within the chamber. The automated program could also be switched and controlled by the user.
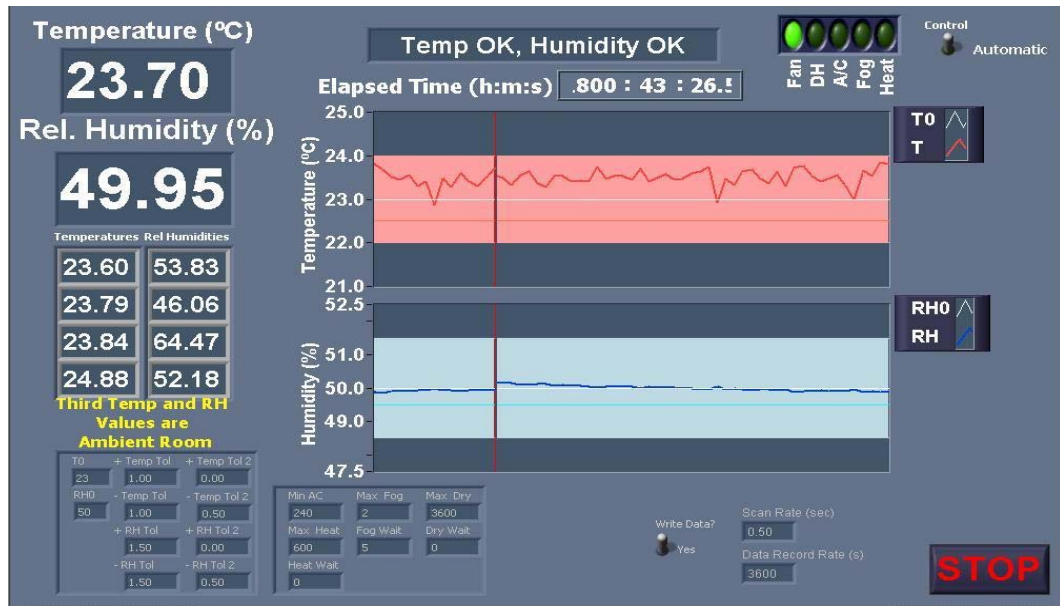
Figure 3.23 – Front panel view of LabVIEW control program for hermetically sealed chamber where creep and shrinkage specimens are located during testing (Earney 2006).

3.2.3.4.2. LABVIEW PROGRAMS FOR DATA ACQUISITION

Strain and load measurements were acquired via a National Instruments LabVIEW program. For each individual specimen the program recorded elapsed time, the strain in each of the three extensometers, and the output from the load cell for creep specimens. Data acquired during monitoring was saved to a file that could be copied into Microsoft Excel. In Excel calibration factors were applied and averaging was done to minimize the number of data points (Earney 2006).

3.2.4. CHLORIDE PENETRATION TESTS (RCPT)

All chloride penetration tests in this study were conducted according to ASTM C-1202 or AASHTO T-277, "The Standard Test Method for Electrical Indication of Concrete's Ability to Resist Chloride Ion Penetration" (ASTM 2005). All of the equipment and setup to complete this test was designed and constructed according to the standard.

3.2.4.1. TEST SETUP

The test setup shown in Figure 3.24 was constructed at the University of Missouri – Columbia for a previous project and is in accordance with the two standards mentioned above. The system is designed to test up to 12 specimens at any given time. Individual specimens are connected to a regulated 60 V DC power supply and current measuring system. The voltage regulators used are accurate to ±0.1V.

To obtain data, a computer automated data acquisition (DAQ) system was used, and consisted of a National Instruments DAQ card and National Instruments LabVIEW software. The LabVIEW program obtained data points of current and time every 5 seconds. The data points were averaged and written to a spreadsheet file every 10 minutes for the duration of the 6-hour test.

Upon completion of the 6-hour test the total charge passed (or area under the time-current plot) was calculated using the trapezoidal rule. Table 3.2 provides a basis for determining the ion penetrability of concrete specimens and was obtained from the ASTM standard.
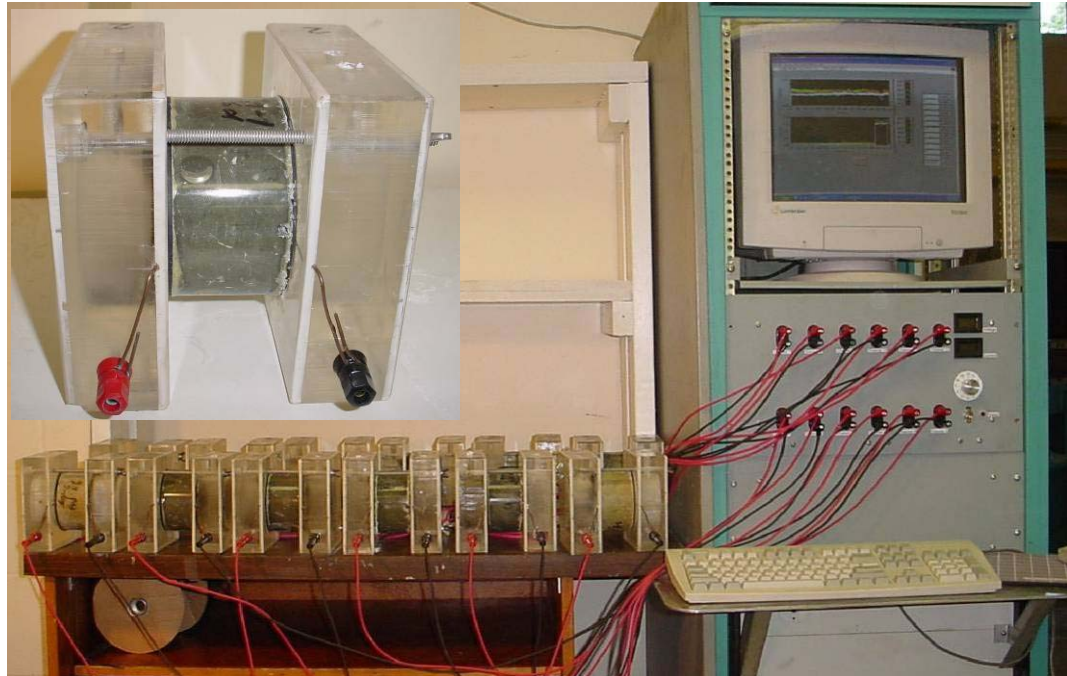
Figure 3.24 – Rapid chloride penetration test setup (Earney 2006).

Table 3.2 –   ASTM designation for chloride ion penetrability based on charge passed (ASTM 2005).

Charge Passed (Coulombs)	Chloride Ion Penetrability
>4,000	High
2,000-4,000	Moderate
1,000-2,000	Low
100-1,000	Very Low
<100	Negligible

3.2.4.2.   SPECIMEN CONDITIONING

Preparing specimens for the test was a multi-step process. Two days prior to the 6-hour chloride ion penetration test, 4" diameter cylinders were removed from the moist curing room, de-molded, and the sides were generously coated with a two-part epoxy from PolyCarb to seal them. The two part epoxy was allowed to cure overnight, and

three specimens were cut from each cylinder. A diagram of the specimen geometries and where the cylinder was cut is shown in Figure 3.25.

The next step in the specimen conditioning process involved de-airing. The specimens were placed in the conditioning chamber depicted in Figure 3.26 and vacuum desiccated for three hours. De-aired water was then drawn into the bucket until the specimens were completely submerged. Vacuuming continued for one-hour, and then air was allowed to reenter the chamber. The specimens continued soaking in the bucket for 18 ± 2 hours before the actual test commenced.
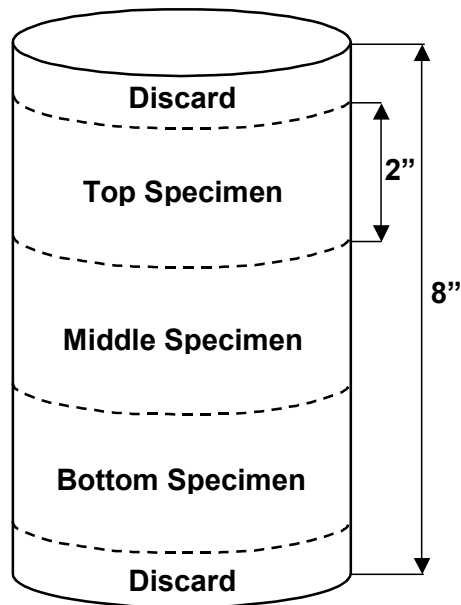
Figure 3.25 – Diagram of specimen slicing to be used for the rapid chloride penetration test

Figure 3.26 – Photograph of the rapid chloride penetration test specimen conditioning equipment

3.2.4.3.   PROCEDURE

The conditioned specimens were removed from the conditioning equipment and towel dried. The specimens were placed in the cells shown in Figure 3.24, and two rubber gaskets were placed on either end of the specimen before bolting the cells together. The side of the specimen hooked up to the positive terminal was filled with 0.3N NaOH, and the negative side was filled with 3.0% NaCl solution. The electrical leads were then plugged in after verifying the voltage across the leads was 60 V. The data acquisition discussed above was started and subsequent data was collected for the six hour test.

3.2.5.   FREEZE THAW

The freeze-thaw tests were conducted according to Procedure A of ASTM C-666, "The Standard Test Method for Resistance of Concrete to Rapid Freezing and Thawing" (ASTM 2003). ASTM C-215, "Standard Test Method for Fundamental Transverse, Longitudinal and Torsional Resonant Frequencies of Concrete Specimens," was used to determine the dynamic modulus of the concrete specimens (ASTM 2002). Four of the six prism specimens were subjected to the rapid freezing and thawing test.

3.2.5.1.   TEST SETUP

The freeze-thaw chamber at the University of Missouri – Columbia is capable of subjecting 18 prisms to approximately 10 freeze-thaw cycles every 24 hours. A single cooling unit freezes the specimens and strip heaters between the specimens thaw the concrete. The chamber is controlled by a concrete prism with two embedded thermocouples. One of the embedded thermocouples is connected to a chart recorder to monitor the number of cycles, and the other is connected to a control circuit that switches the heaters and cooling unit on and off. In Figure 3. freeze-thaw specimens are seen in the chamber. The specimens are placed in stainless steel containers allowing for a minimum of 1/8" of water to completely surround the concrete specimens.

Figure 3.27 – Overhead view of cabinet used to subject prisms to freeze-thaw cycles.

3.2.5.2.   PROCEDURE

The prism molds cast were steam cured with the pavement panels at the precasting yard, and then transported to the University of Missouri – Columbia and moist cured until an age of 28 days. The specimens were removed from the curing room and placed in the freeze-thaw chamber and brought to a temperature of 40^oF. Initial readings of weight and fundamental transverse frequency were then taken. After these initial readings the specimens were subjected to approximately 30 freeze-thaw cycles in between measurements of weight and fundamental transverse frequency. A total of 300 cycles is required to complete the test.

As mentioned earlier the fundamental transverse frequency of the concrete specimens was measured according ASTM C-215. The test-setup shown in Figure 3.28 was utilized to obtain transverse frequency values. An electromechanical driving unit oscillates the specimen at frequencies varied by the user. A lightweight pickup unit at the

opposite end of the specimen measures frequency. An oscilloscope on the control unit indicates when the end of the specimen and the pickup needle are in phase (the driving frequency is varied to accomplish this). Being in phase indicates the first fundamental transverse frequency.

The relative dynamic modulus of the specimens were then calculated and plotted against time to determine the damage done to the concrete from rapid freezing and thawing. The relative dynamic modulus is simply a ratio of the original dynamic modulus and the dynamic modulus at time t. A durability factor was also calculated. It is calculated by multiplying the relative dynamic modulus and the number of cycles at which the relative dynamic modulus reaches a specified minimum value for discontinuing the test and dividing by the specified number of cycles at which exposure is to be terminated.
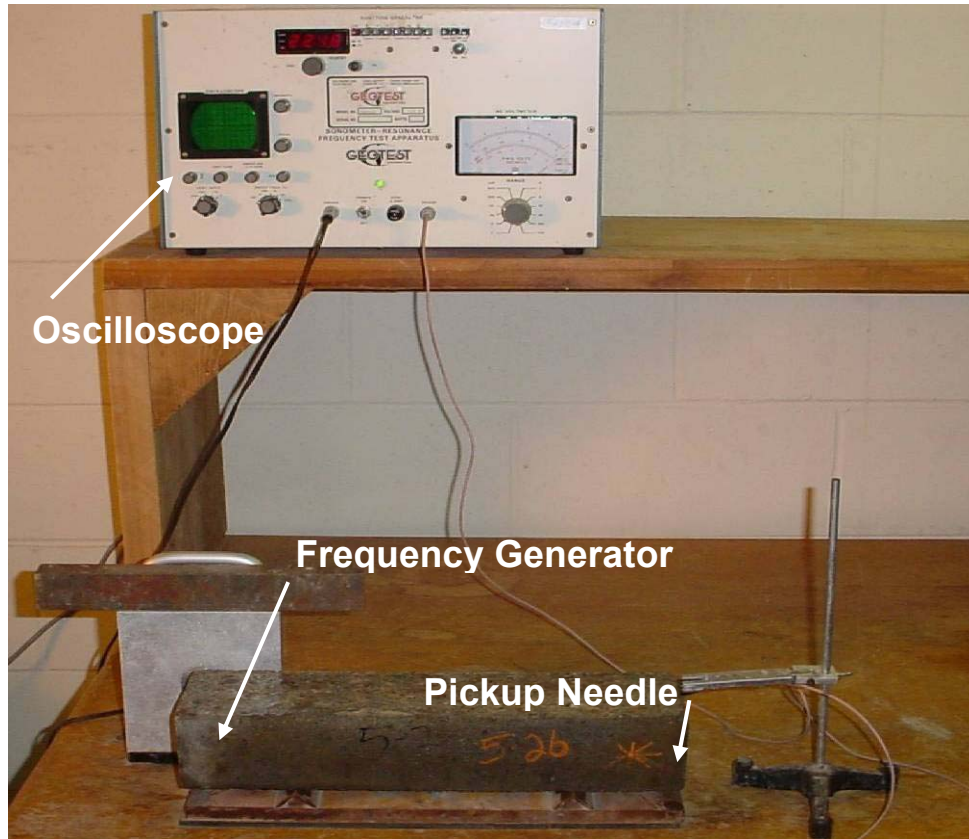
Figure 3.28 – Frequency generator and setup for measuring fundamental transverse frequency.

3.2.6. FLEXURE TESTS

Flexure tests were performed in accordance with ASTM C 78, "Standard Test Method for Flexural Strength of Concrete" (Using Simple Beam with Third-Point Loading)" (ASTM 2002).

3.2.6.1. TEST SETUP

The test setup used at the University of Missouri – Columbia is shown in Figure 3.29. The apparatus subjects concrete specimens to third point bending and measures gross and net deflections of the beam with two LVDT's. The LVDT on the bottom of the specimen measures the gross deflection, which takes into account both beam deflection and local crushing of the concrete at the supports. The LVDT labeled "Net" in Figure

3.30 only measures the deflection of the beam relative to the ends. An MTS machine with closed loop control and 110 kip capacity was used to deflect the beam. A computer based DAQ using a National Instruments DAQ card and LabVIEW program collected both deflection measurements from the LVDT's along with the applied load.

Figure 3.29 – Photograph of third point loading of concrete prism/beam.
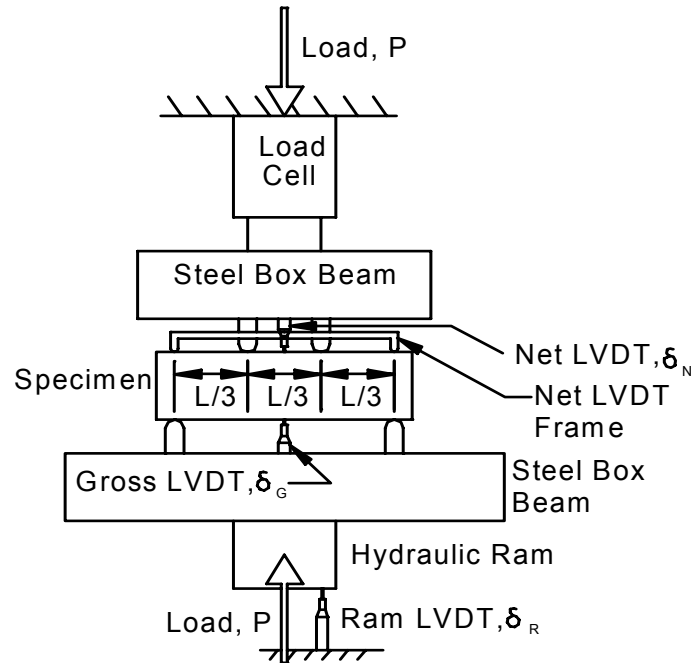
Figure 3.30 – Details of test setup used to test flexural strength of concrete specimens.

3.2.6.2. PROCEDURE

The prism molds were cast along with the precast panels at the precasting yard and allowed to steam cure with the panels. The molds were then transported back to the moist curing room at the University of Missouri – Columbia. When ready for testing the specimens were removed from the curing room and demolded. The specimens were placed sideways on the bottom box beam. The "Net LVDT Frame" depicted in Figure 3.30 was secured with plaster of paris on either end, and a small preload is applied to remove any slack in the testing apparatus. All DAQ channels were tested to ensure proper functionality, and finally the prism is loaded until failure. Values calculated at the conclusion the experiment include; the modulus of rupture (f_r), the Young's modulus (E_c), the total energy absorbed, and the fracture energy (G_f).

4. MATERIAL PROPERTIES AND THEORETICAL COMPARISONS

4.1. CONCRETE

4.1.1. MIX DESIGN

The nominal proportions of the PPCP mix designed and used by Concrete Products Incorporate are summarized in Table 4.1. The water content reported is the total water content including Saturated Surface Dry moisture present in the aggregates. The coarse and fine aggregate weights are for aggregates in a saturated surface dry (SSD) moisture state. The water – cementitious material ratio was 0.326. The mix was designed for a release strength of 3,500 psi (24 GPa) and 28 day strength of 5,500 psi (40 GPa) (500 psi (3.4GPa) higher than specified by MoDOT). The minimum specified air-entrainment was 5%, and the maximum specified slump was 6".

Type I Portland cement was used for the panels (Buzzi Unicem in Festus, Missouri). The fine aggregate was Crowley's Ridge Sand from Razor Rock in Harrisburg, AR, and the coarse aggregate was MoDOT #7 Salem Limestone from Vulcan Materials – Reed Quarry in Grand Rivers, KY. Admixtures used were manufactured by Degussa Admixtures, Inc. The admixtures include MB-AE 90, an air-entraining agent, Glenium 3000 NS, a full-range water-reducer, and Pozzolith 200 N, a water-reducer (Degussa 2006). The water was from the city of Memphis water supply.

Table 4.1 – Mix design of concrete used in precast pavement.

Constituent	Precast Pavement Mix /yd^{3*}
Cement	722 lb
Fine Aggregate	1162 lb
Coarse Aggregate	1766 lb
Water	28.25 gal
Water - Cement Ratio	0.326
Air Entrainment Admixture	MB AE 90 1 -3 oz
Full-Range Water-Reducer	Glenium 3000NS 4 - 8 oz / 100 lb Cement
Water Reducing Admixture	Pozzolith 200N 2 -5 oz / 100 lb Cement

* Unless specified otherwise

4.1.2. COMPRESSION TESTS

Compressive strength tests were performed on standard 6" diameter cylinders cast with each set of instrumented panels. Two of the six cylinders for each set of castings were tested at 7, 28 and 56 days respectively. Average results of strength and modulus of the specimens and comparisons to theoretical values are presented in Table 4.2. Modulus values were not determined at 7 days due to improperly functioning laboratory equipment. Concrete strength at an age of 7 days ranged from 5,210 psi (35.9 MPa) to 6,810 psi (46.9 MPa) with an average of 6,070 psi (41.9 MPa). At 28 days the strength ranged from 5,590 psi (38.5 MPa) to 8,700 psi (59.9 MPa) with an average of 7,190 psi (49.6 MPa), and at 56 days the strength range was 7,350 psi (50.7 MPa) to 9,960 psi

(68.7 MPa) with an average of 8,830 psi (60.9 MPa). Modulus values at 28 days ranged from 5.22 x 10^6 psi (36 GPa) to 6.32 x 10^6 psi (44 GPa) with an average of 5.69 x 10^6 psi (39 GPa) and at 56 days the range was 5.45 x 10^6 psi (38 GPa) to 7.06 x 10^6 psi (49 GPa) with an average of 6.26 x 10^6 psi (43 GPa). Average ultimate strain values at 28 days were 1,540 μstrain and at 56 days the average was 1,590 μstrain. The relatively high variation in compressive strength at various ages of the concrete may be attributed to varying amounts of admixtures contained in different castings. As expected cylinders for each panel casting tended to have similar compressive strengths, but cylinders from different mixes at the same age varied in properties as described.

Prediction models of strength and modulus developed by Branson et al were used for comparisons to theoretical values (Namaan 2004). Figure 4.1 shows the strength versus time comparisons for the model developed by Branson and results from laboratory studies. The model used to predict strength accurately reflects measured results up to 28 days. Beyond 28 days the model under-predicted strength and by an age of 56 days the difference was 15% less than actual values obtained during experimental observations. Predicted modulus values were about 35% lower than measured values. A major factor that is not accounted for in the prediction models is the lower than normal water to cement ratios used in the concrete mix design for the pavement.

Figure 4.2 shows representative stress versus compressive strain results for two sets of castings at ages of 28 and 56 days. The figure demonstrates the increase in stiffness and strength of the concrete between the ages of 28 and 56 days. Strength increased 23% and the modulus increased 10% between 28 and 56 days.

Table 4.2 – Experimental averages and predicted results of concrete strength and stiffness at 7, 28, and, 56 days.

Day	Experimental Strength		Predicted Strength		Experimental Modulus		Predicted Modulus	
	psi	MPa	psi	MPa	psi	GPa	psi	GPa
7	6,070	41.9	6,580	45.4				
28	7,190	49.6	7,290	50.3	5.69E+06	39.2	4.87E+06	33.6
56	8,830	60.9	7,430	51.2	6.26E+06	43.1	4.91E+06	33.9
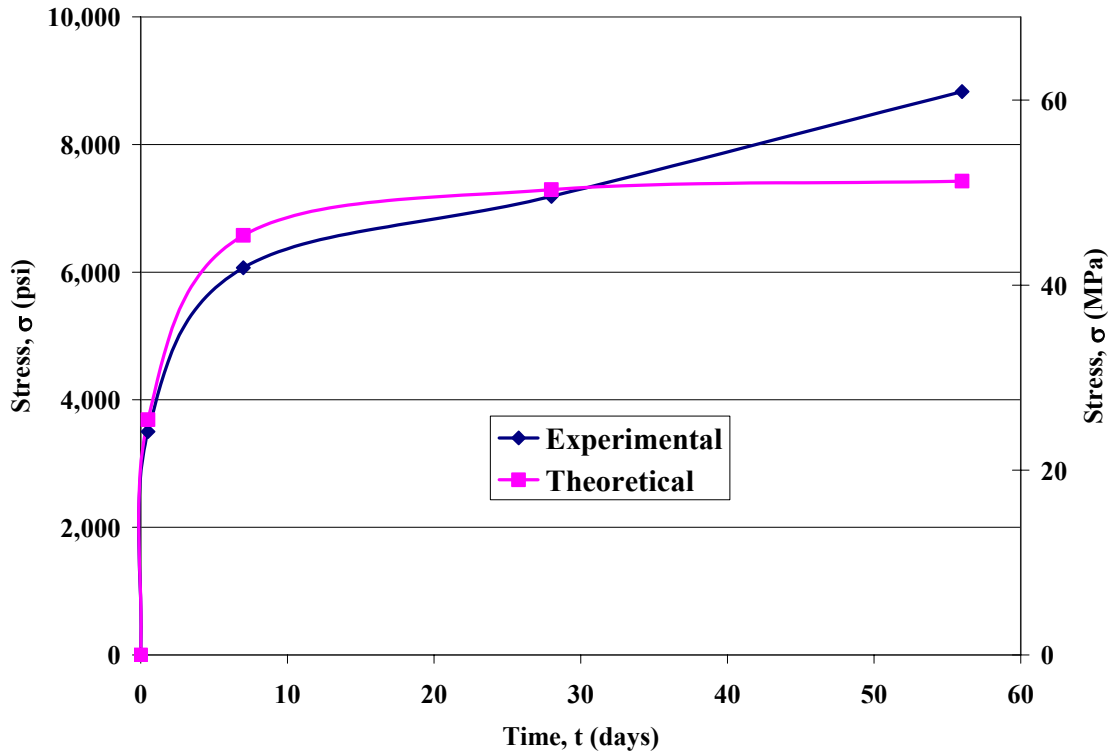
Figure 4.1 – Plot of experimental and theoretical strength versus concrete age.
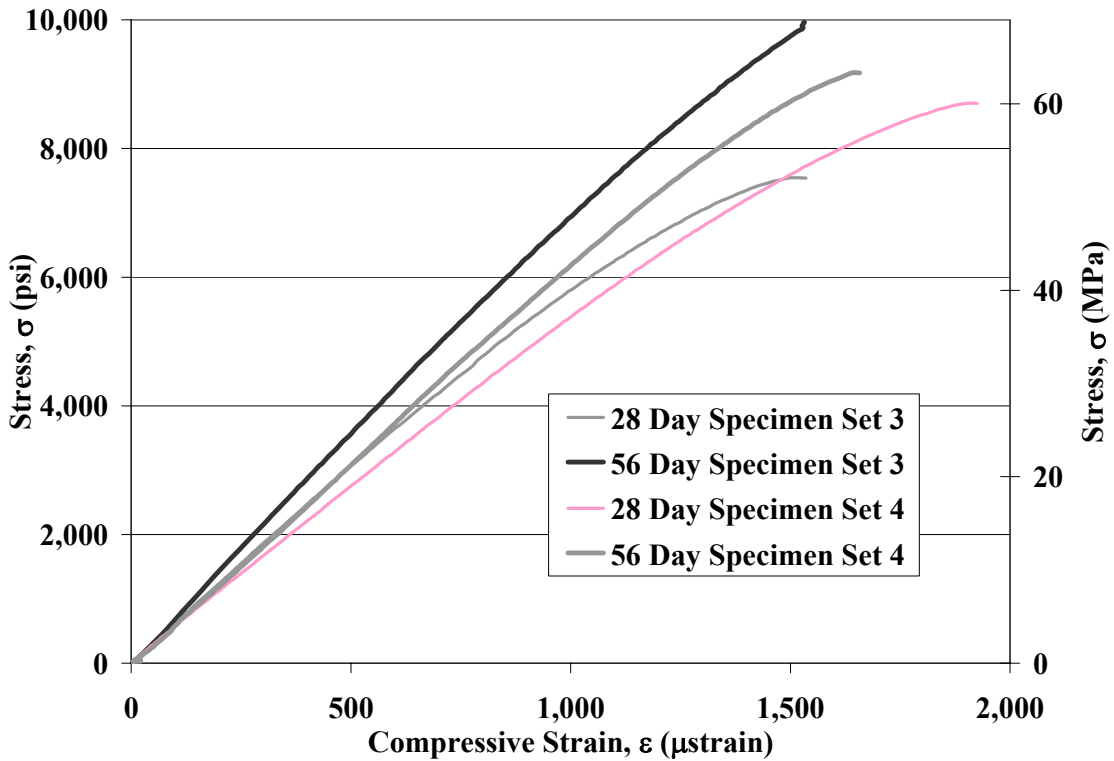
Figure 4.2 –   Stress versus compressive strain results from 28 and 56 day strength tests.

4.1.3.   SHRINKAGE RESULTS AND COMPARISON TO THEORETICAL VALUES

Four shrinkage specimens were monitored for 90 days. Two of the specimens were sealed and two were unsealed. Theoretical values were calculated using Equation 2.2 presented in Chapter 2. The various correction factors calculated according to ACI 209 for the sealed and unsealed specimens are presented in Appendix A.

Typical results from the shrinkage tests and comparisons to theoretical values for unsealed and sealed specimens are presented in Figure 4.3 and Figure 4.4 respectively. Figure 4.5 shows the average results for sealed and unsealed specimens along with comparisons to theoretical values. For theoretical models it is assumed that the sealed specimen is subjected to 100% relative humidity conditions and the unsealed specimen is subjected to 50% relative humidity.

As expected the sealed specimens exhibited lower shrinkage strains compared to the unsealed specimens. The sealed specimens exhibited 73% less shrinkage compared to the unsealed specimens. This difference implies that a large portion of the total shrinkage is due to drying shrinkage, which is a loss of moisture. The sealed specimens are assumed to be subjected 100% relative humidity. Therefore, the shrinkage observed in these specimens is mainly due to autogenous shrinkage, which is shrinkage associated with the hydration of cement particles. The spikes in strain values in Figure 4.3 and especially in Figure 4.4 can be attributed to activities associated with subsequent tests being run, and improperly functioning equipment used for temperature and humidity control. The door of the hermetically sealed chamber was opened and closed due to these activities resulting in temperature and humidity fluctuations.

The ACI prediction model for the unsealed specimen's under-estimated strain results by 37% at 90 days. Early-age shrinkage results from the laboratory tended to increase at a much faster rate compared to theoretical values. Beyond 10 days the change in magnitude of strains was similar for the laboratory results and the theoretical predictions.

The rapid increase in early age shrinkage may be due to factors such as autogenous shrinkage, and admixtures that the ACI model does not account for. The autogenous shrinkage is due to the low w/c ratio of the mix, which results in increased internal forces in the concrete matrix resulting in high early age shrinkage strains(Earney, Gopalaratnam et al. 2006). As stated earlier beyond 10 days the change in magnitude of the shrinkage strains is comparable between the model and measured results, therefore in Figure 4.3 and Figure 4.5 the theoretical values were adjusted by a magnitude of 250

microstrains beyond 10 days. Adjusting the prediction model demonstrates how well the model and measured results compare.

The prediction model for the sealed specimens tended to predict more accurately the results measured in the lab. The prediction model at 90 days was 20% less than the results from the laboratory. As seen in the unsealed specimens the early age shrinkage tended to be much higher in the laboratory as compared to the theoretical values.
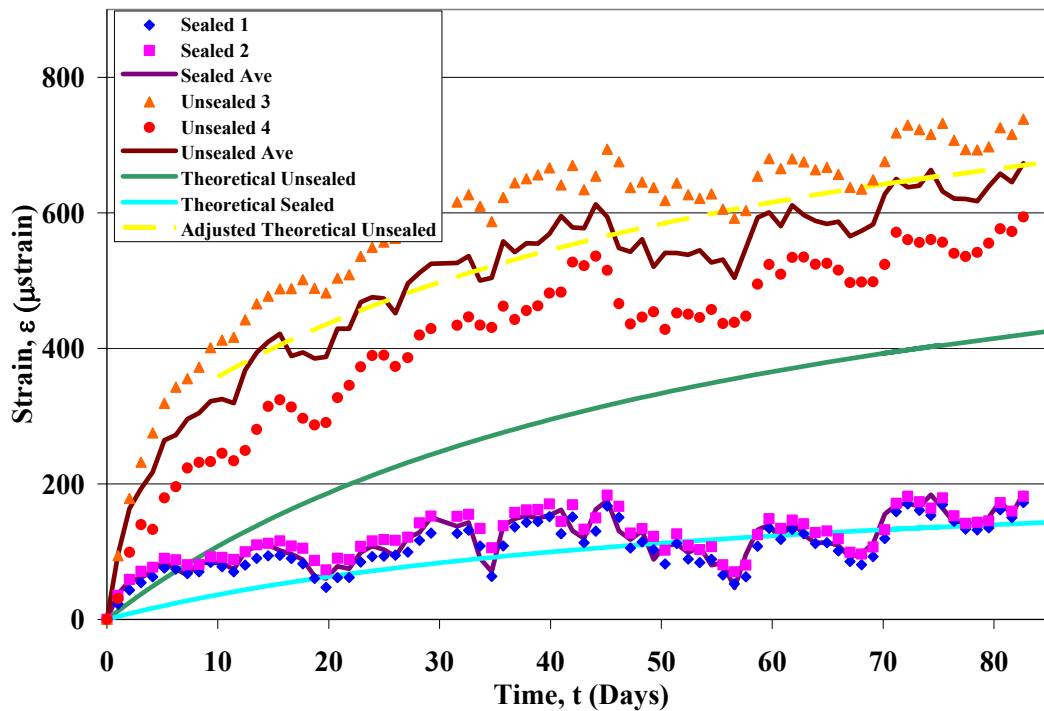
Figure 4.3 – **Unsealed shrinkage specimen results along with ACI 209 prediction of shrinkage.**
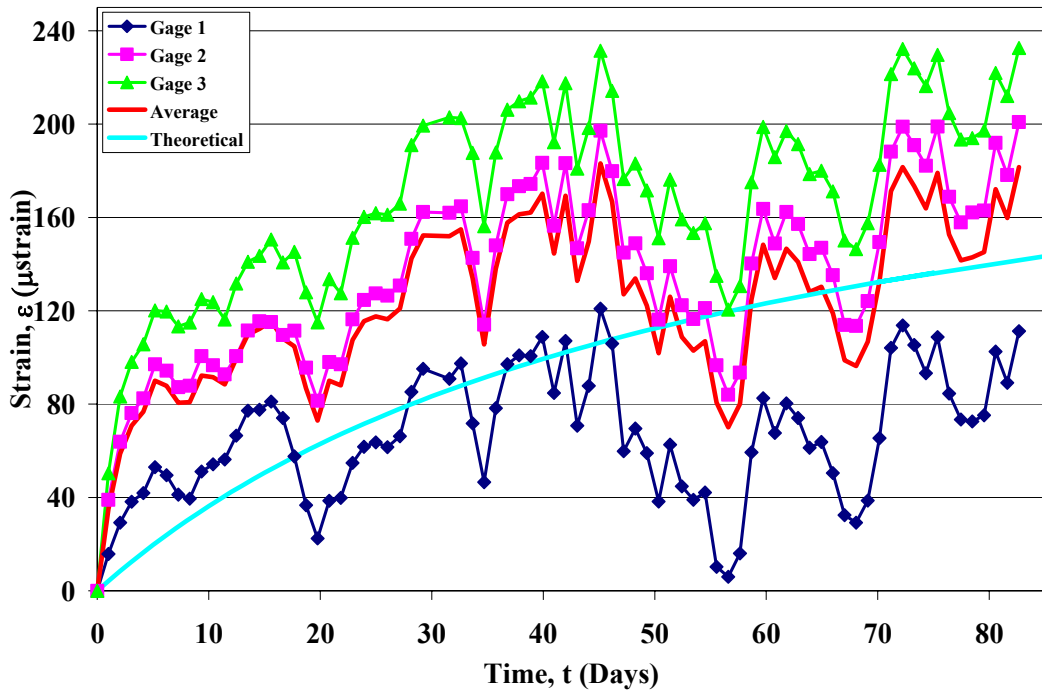
Figure 4.4 – Sealed shrinkage specimen and comparison to ACI 209 prediction of shrinkage.
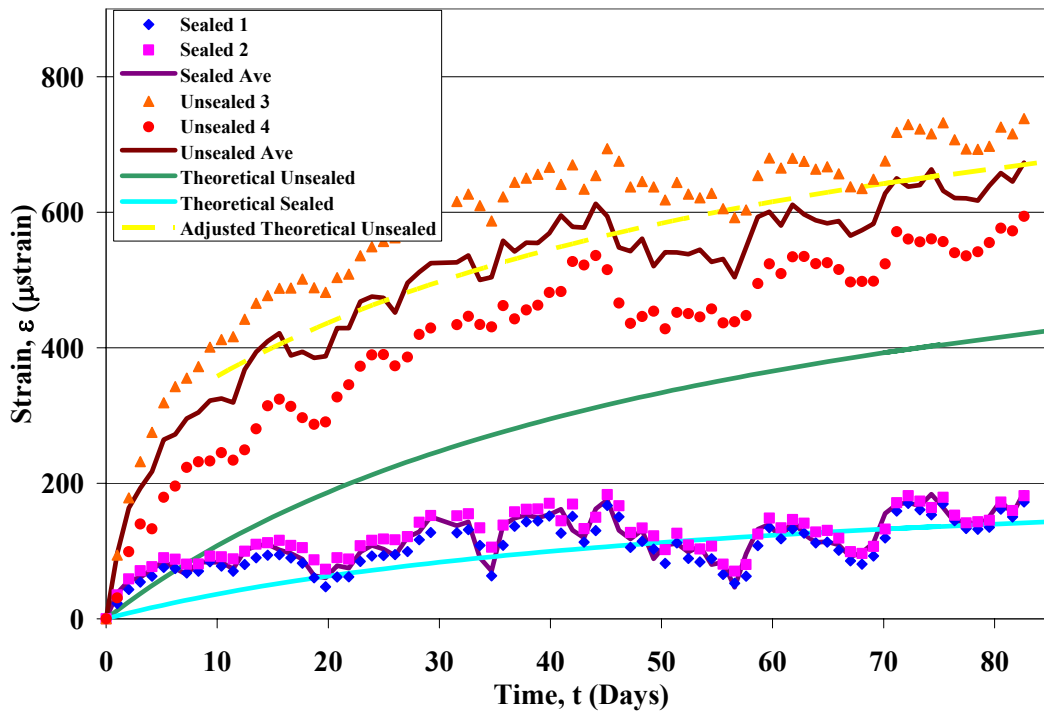
Figure 4.5 – Average values for two sealed and two unsealed shrinkage specimens and comparison with theoretical results.

4.1.4. CREEP RESULTS AND COMPARISONS TO THEORETICAL VALUES

Four creep specimens were monitored for 60 days after initial moist curing. Two of the specimens were sealed and two were unsealed. Theoretical values were calculated using Equations 2.3 and 2.4 presented in Chapter 2. The various correction factors calculated according to ACI 209 for the sealed and unsealed specimens are presented in Appendix B.

Theoretical predictions along with unsealed and sealed laboratory creep results are presented in Figure 4.6 and Figure 4.7 respectively. Average results from the creep specimens are shown in Figure 4.8. For theoretical models it assumed that the sealed specimen is subjected to 100% relative humidity conditions and the unsealed specimen is subjected to 50% relative humidity.

The initial elastic shortening of the cylinders (due to the 2,000 psi (14MPa) applied force) for both sealed and unsealed specimens averaged 350 μstrain. The inherent modulus from this load and resultant displacement was 5.62 x 10^6 psi (39 GPA). This modulus value is within 1.5% of the value calculated during the compressive strength tests.

The predicted creep strains from the ACI 209 model closely resembled observations made in the laboratory. The unsealed prediction model under-estimated measured creep strain by 10%, and the sealed prediction model under estimated creep strain values by 5%. Creep coefficients were also calculated based on theoretical and measured results. For comparative purposes the creep coefficients were calculated at 60 days of sustained loading, and only the unsealed specimen's creep strains were used. The

predicted creep coefficient was 1.66, and the measured creep coefficient was 1.82. This

represents a 9.5% difference between the predicted and measured creep coefficient.
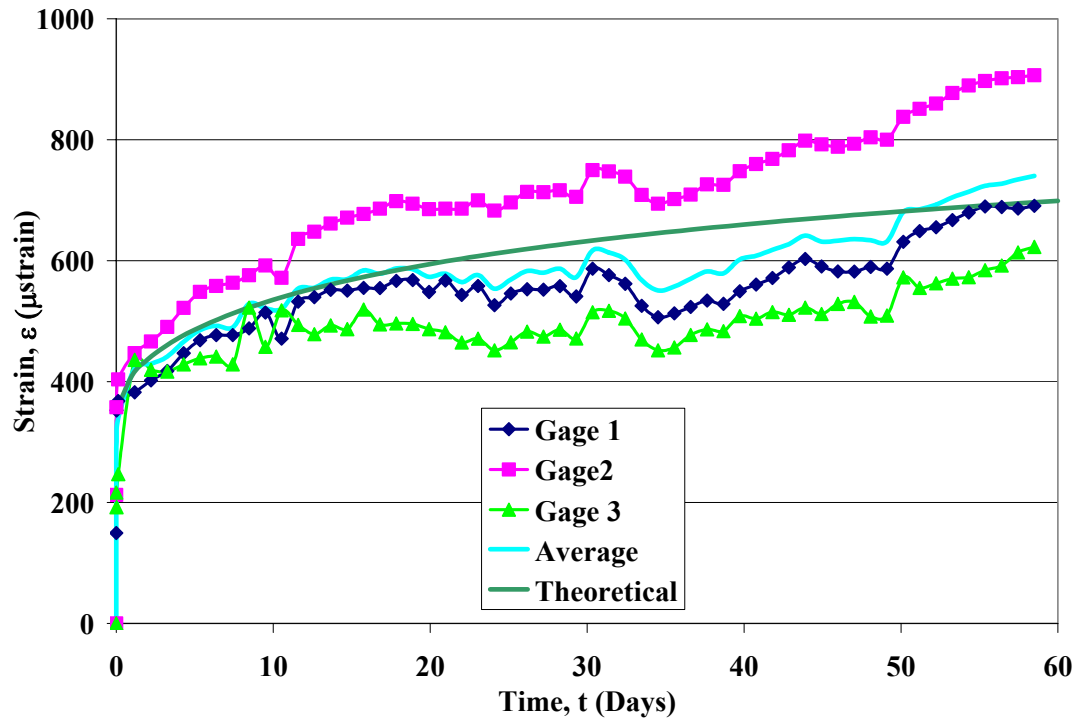
**Figure 4.6 –   Unsealed creep specimen and comparison to theoretical values
calculated using ACI 209.**
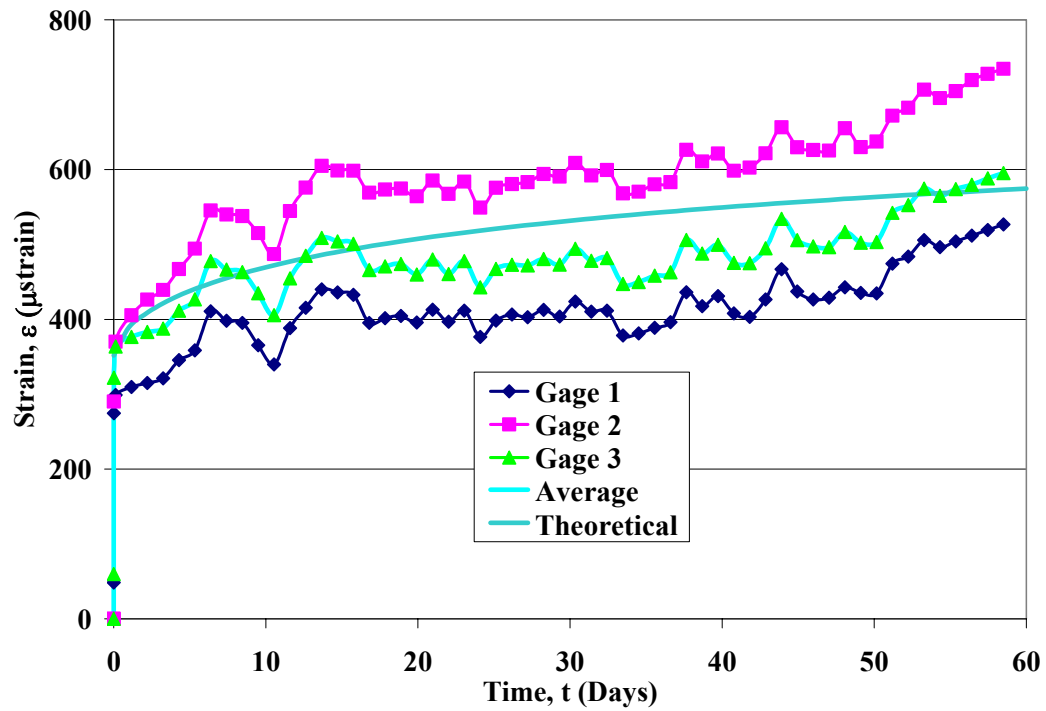
Figure 4.7 – Sealed creep specimen and comparison to theoretical values calculated using ACI 209.
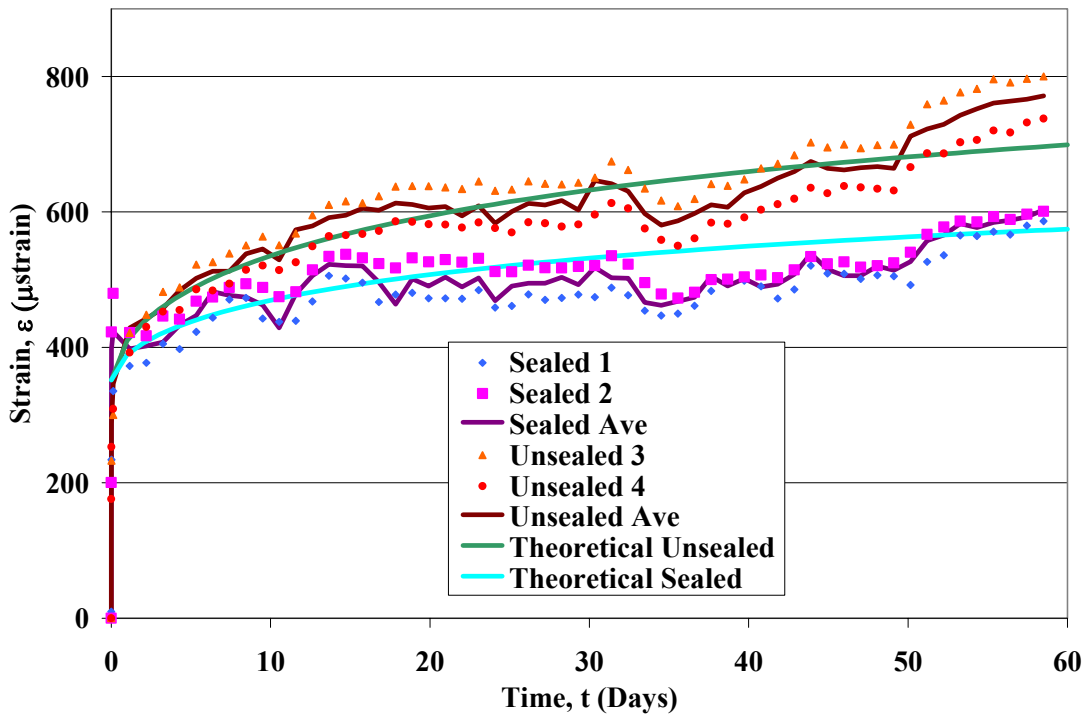
Figure 4.8 – Average creep values for two sealed and u two unsealed specimens along with comparison to ACI 209 models.

4.1.5. CHLORIDE PERMEABILITY

Results from the rapid chloride permeability tests (RCPT) are presented in Table 4.3. Initially, only baseline readings at an age of 28 days were planned. However, because of the relatively high permeability readings recorded in these tests more specimens were cored from 6" diameter cylinders to repeat the test at an age of 112 days. Nine specimens were initially tested, and only four additional specimens could be cored due to a limited number of remaining specimens for tests at 112 days.

Table 3.2 presented earlier gives a baseline for quantifying results from RCPT. The average charge passed in coulombs for the readings at 28 days was 4,000 which is high according to the guidelines set forth by ASTM. At 112 days the total charge passed decreased 22% to 3,150. This value is in the moderate range of chloride permeability according to ASTM standards. Literature reviewed also suggests looking at the first half-hour of the test and multiplying by twelve to obtain a more representative basis for comparison to other standard tests. Specimens tend to heat up as the test progresses which increases electron flow, thus resulting in over-estimation of chloride permeability (Hooton and Stanish 1997). From the data obtained the total charged passed based on the first half hour would be 3,160 coulombs and 2,430 coulombs for the 28 and 112 day tests respectively. These values represent more acceptable values according to the ASTM standard. In the literature review it was also discussed that the water to cement ratio plays a role on the influence of the accuracy of this test. The water cement ratios averaged around 0.33 for the pavement mix design, and it is stated in literature that the test is more accurate for values between 0.4 and 0.7 (Mindess, Young et al. 2003).

The baseline readings for chloride permeability tended to be higher than expected, and the pavement should be monitored for possible chloride ingress in the future. The results from chloride permeability tests on virgin specimens may be used as a basis for comparison of tests performed on the in-situ pavement in the future after deicing salts have been used under service conditions.

Table 4.3 – RCPT results for specimens tested at 28 days of moist curing and 112 days of moist curing.

Specimen	28 Day Charge (Coulombs)	112 Day Charge (Coulombs)
1	3,807	3,177
2	3,770	3,245
3	4,203	3,015
4	3,896	3,168
5	4,265	
6	4,082	
7	3,976	
8	4,179	
9	3,819	
Average	**4,000**	**3,150**

4.1.6. FREEZE THAW

The four prisms cast for freeze-thaw testing were subjected to a total of 315 cycles. Figure 4.9 shows the decrease in relative modulus with increased number of freeze-thaw cycles. No readings were taken between 250 and 315 cycles due to practical limitations as the researchers were installing instrumentation in panels at the precasting yard in Memphis, TN. The average total degradation in modulus was 3%. From these results it can be assumed the concrete mix is very durable when subjected to cycles of

freezing and thawing. This is a result of a proper air void system, sound aggregates, and a low water to binder ratio.

4.1.7. FLEXURE TESTS

A total of two prisms were tested in flexure at an age of 56 days. Figure 4.10 shows the load versus deflection response for the two prisms. The net and gross deflections are both plotted. The gross deflection for the two beams is five times greater than the net deflection, which is mainly due to local concrete crushing at the supports of the testing apparatus. The energy absorbed versus deflection is seen in Figure 4.11.

Results calculated are based on the net deflection values obtained during the experiments and are summarized in Table 4.4. The average modulus of elasticity from the flexural tests was 5.33 x 10^6 psi (37 GPa). This modulus is 15% lower than the average modulus obtained from the compressive strength tests. The average modulus of rupture for the two prisms was 872 psi (6.0 MPa) and the average fracture toughness for the concrete was 0.237 lb-in/in^2 (41.2 N-m/m^2). There was a significant variation in the results for the fracture toughness due to the limited number of prisms tested and the inherent scatter in this property.
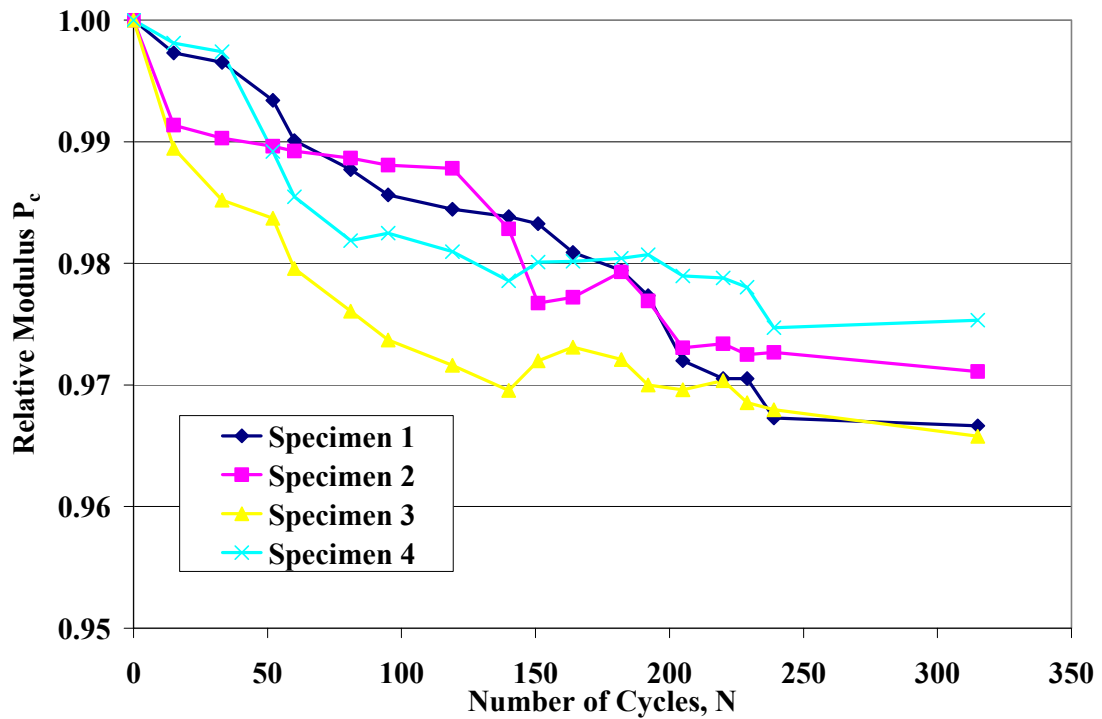
Figure 4.9 –   **Experimental results for freeze-thaw tests showing the degradation of modulus versus the number of cycles.**

Table 4.4 –   **Summary of results from flexural tests performed at 56 days.**

Specimen Number	Modulus of Elasticity, E_c psi (GPa)	Modulus of Rupture, R psi (MPa)	Fracture Toughness, G_f lb-in/in^2 (N-m/m^2)
1	5,550,000 (38.3)	798 (5.50)	0.211 (36.7)
2	5,110,000 (35.2)	946 (6.52	0.263 (45.8)
Average	5,330,000 (36.7)	872 (6.01)	0.237 (41.2)
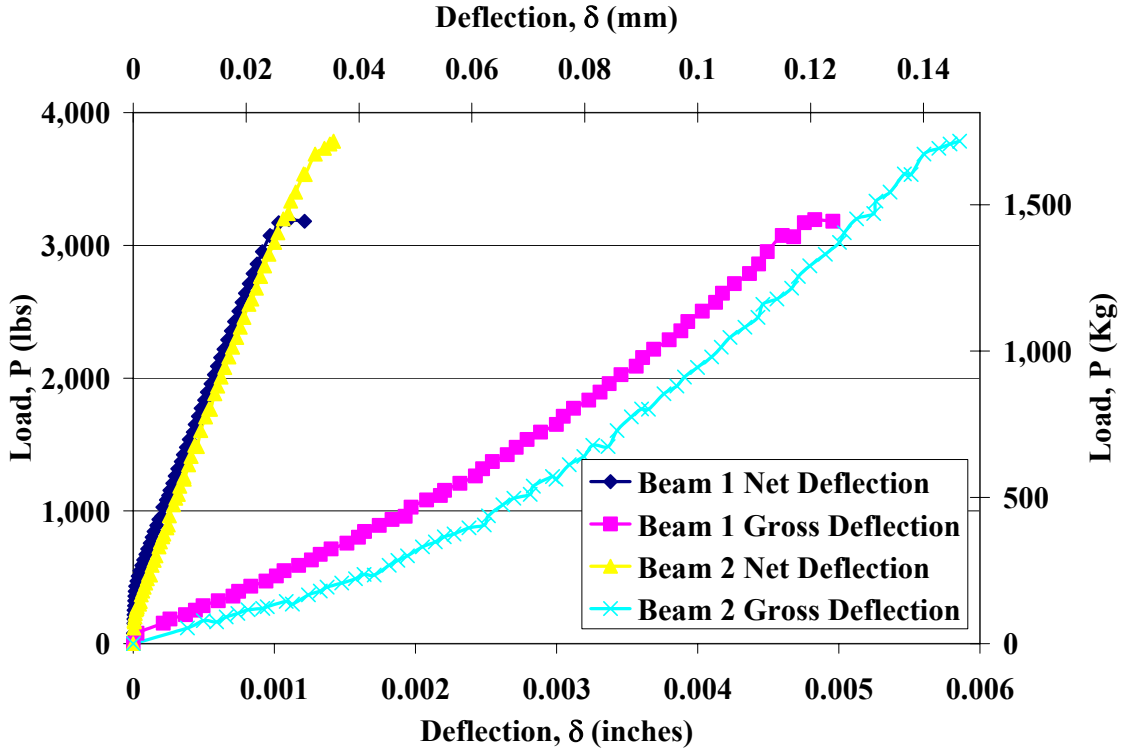
Figure 4.10 – Load versus deflection results for flexure tests of concrete prisms at an age of 56 days.
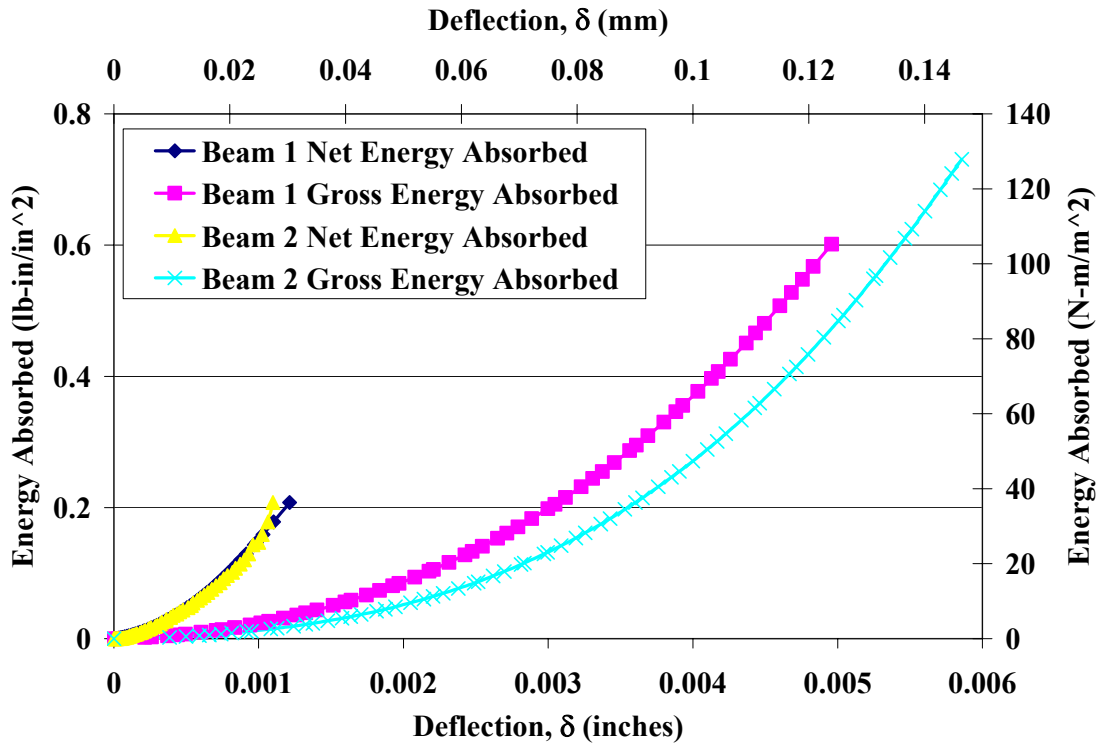
Figure 4.11 – Energy absorbed in concrete prisms during flexure tests.

5. TIME-STEP MODELS TO PREDICT PRESTRESS LOSSES

5.1. GENERAL INFORMATION

The purpose of estimating loss of pre-tension and post-tensioning in the precast pavement system was to compare the results with measured values in the field. From a design standpoint, accurately predicting the pre and post-tensioning losses results in increased design confidence. A lot of research has been done to investigate prestress losses in bridge girders and other types of prestressed systems, however little has been done with respect to pre and post-tensioned pavements mainly because it is a relatively new application of both pre-tensioning and post-tensioning. Estimating loss of prestress in the precast pavement system with the prediction models already developed will aid in future projects involving this type of system.

Stress loss in both the transverse and longitudinal direction was calculated up to the 45 year pavement design life. The time-steps when losses were calculated and subsequent effective prestress was updated were at ages of 1, 3, 7, 28, 56, 112, and 365 days and at 5, 10, 20, and 45 years. The application of post-tensioning occurred at 28 days. Thus, the time-steps preceding 28 days were not accounted for in the post-tensioning model. The time-steps increase in length as the concrete ages because many of the time dependent phenomena affecting prestress loss decrease in magnitude of change. Losses due to creep and shrinkage were individually calculated along with total stress loss. The total stress loss takes into account losses due to creep, shrinkage, elastic shortening, anchorage set, and friction. Only the results of the prediction models are

presented. For more detailed analysis refer Appendix B. The predicted results are also compared to current measurements from field instrumentation where applicable.

5.2. PRE-TENSION LOSSES (TRANSVERSE TO TRAFFIC)

The strands transverse to the direction of traffic were stressed before concrete placement. Therefore, the left-hand side of the flow chart in Figure 2.10 was followed to calculate the total pre-tension loss. Individual stress loss due to creep and shrinkage was calculated using a similar procedure for the calculation of total pre-tension loss. However, only losses due to creep or shrinkage were considered. The prestressing strands were cut after the concrete had steam cured for a period of twelve hours. Therefore, the time-step models estimate losses after one day. Figure 5.1 shows the losses estimated for creep, shrinkage, and total pre-tension loss versus time.

For the creep time-step model it was assumed that the initial effective pre-tension force was 189 kips. This takes into account estimations for elastic shortening of the strand. An initial average uniform force on the concrete was then calculated based on the number of strands, the concrete cross-sectional area, and the geometry of the cross-section. The creep loss was then determined for a given time-step based on the estimated creep strain over that particular time interval and modulus ratio. The creep loss from previous time-steps is subtracted from the current effective pres-tension force. After the final time-step, creep losses from all time intervals are summed to give the total loss due to creep.

Loss due to shrinkage was primarily based on the estimated shrinkage of the concrete. Based on the mix design and geometry of the pavement sections shrinkage

strains were estimated as a function of time. Loss due to shrinkage over all time intervals was added up to determine the total loss due to concrete shrinkage.

Pre-tensioning in the transverse direction was accomplished using half-inch diameter, uncoated, low relaxation seven-wire strands. The strands were stressed to 80% of ultimate. Estimated loss due to creep decreased the effective pre-tension force by 1.7%, and shrinkage losses accounted for an 8.7% decrease in effective force. The total estimated loss reduced the effective pre-tension force by 16%.
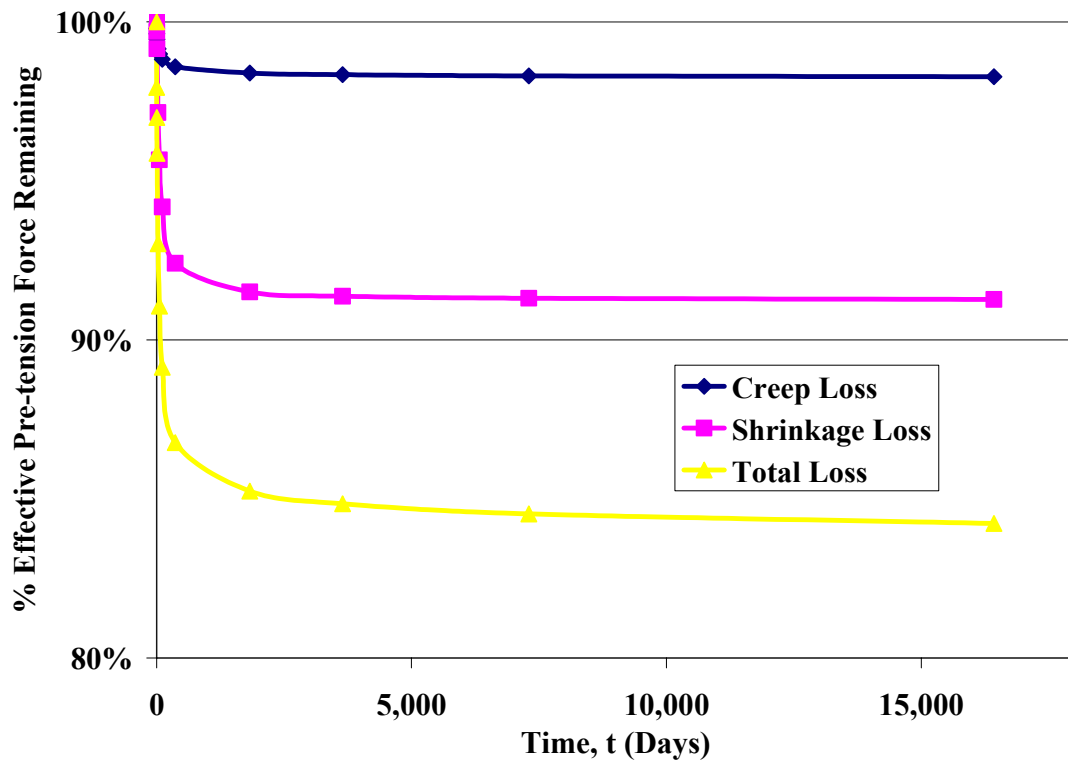
Figure 5.1 –   **Results from models used to calculate loss of pre-tension for strands transverse to the direction of traffic. Percentage loss is in relation to the effective pre-tension force applied (0.80f$_{pu}$).**

5.3.   POST-TENSION LOSSES (LONGITUDINAL TO TRAFFIC)

The model used for estimation of losses in strands longitudinal to the direction of traffic varied slightly from the model used to predict transverse pre-tension loss. The

post-tensioning models accounted for frictional losses due to wobble effects in the ducts. Also, it was assumed that the age of the panels at post-tensioning was 28 days. The outline of individual creep and shrinkage loss prediction presented in the previous section is the same method used for the post-tensioning strands. The total post-tensioning loss was calculated by following the right-hand side of Figure 2.10.

The strands used for post-tensioning were six-tenths inch diameter, uncoated, low relaxation seven wire strands. The post-tensioning strands were stressed to 80% of their ultimate capacity. Losses due to creep lowered effective post-tensioning by 0.5%, and shrinkage accounted for a 5.9% loss. Accounting for all factors contributing to post-tensioning loss, the effective post-tensioning force was decreased by 17%. Creep and shrinkage effects on post-tensioning were less substantial compared to their effects on pre-tensioning, because early age shrinkage does not contribute to losses and the concrete is much stronger and stiffer. Frictional losses accounted for 41% of the total post-tensioning loss, which resulted in similar losses in both the pre and post-tensioning forces. Environmental factors such as thermal expansion of the pavement are not accounted for in the model. However, readings taken from the strandmeters for comparison to prediction models were corrected for temperature variation from a baseline reading.
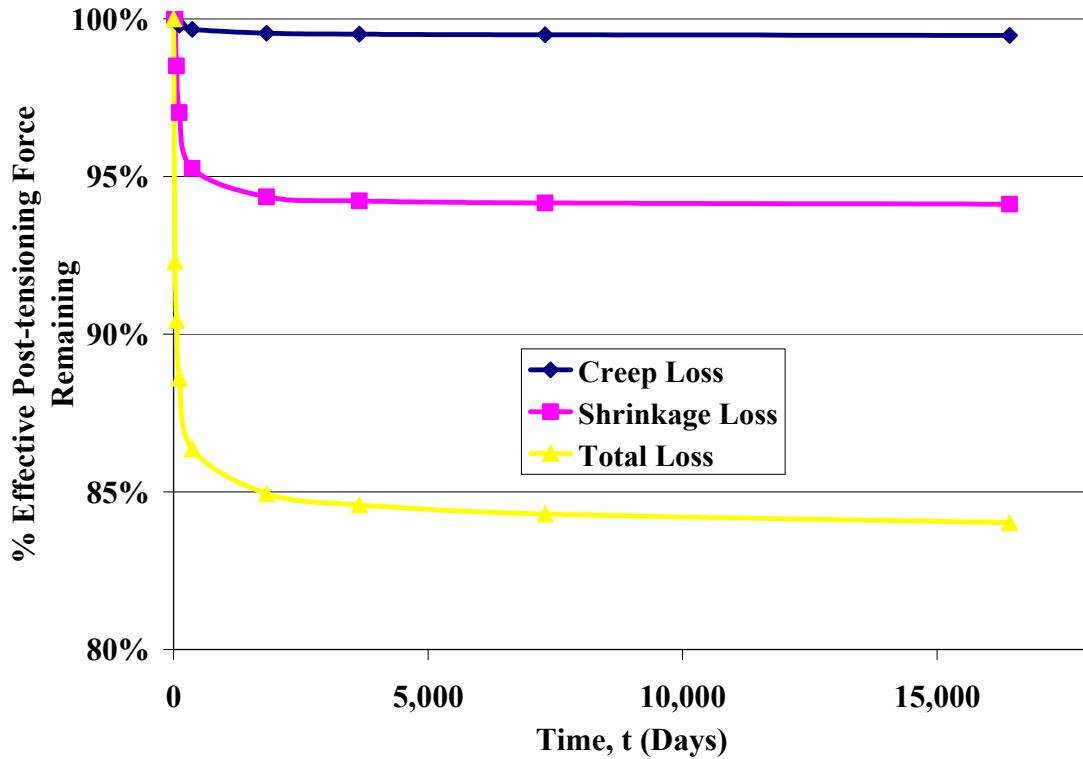
Figure 5.2 – **Results from models used to predict post-tensioning losses for strands longitudinal to the direction of traffic. Percentage loss is in relation to the effective post-tension force applied (0.80f$_{pu}$).**

5.4. ESTIMATED LOSSES COMPARED TO MEASURED VALUES

Due to instrumentation limitations only loss in post-tensioning stress is compared between theoretical and measured values. Strandmeters attached directly to the centerline post-tensioning strand are the main source of measured values. The strandmeters were located along the length of the strand and were monitored as the strand was stressed. This monitoring verified the applied force, and also showed frictional losses along the length of the strand. Subsequent in-service monitoring shows a decrease in effective force, which is compared to estimated total post-tensioning loss.

5.4.1. FRICTIONAL LOSSES DURING POST-TENSIONING

Figure 5.3 shows strain measurements taken during post-tensioning of the center-line strand. An overview of the instrumentation locations with respect to the active jacking end is depicted as well. The strandmeter labeled C1_S was in the middle of the section (between active and passive jacking ends), and B3_S was the furthest from the active jacking end. The strand was initially stressed from the side labeled active jacking end. However, after all post-tensioning strands were stressed from the active end they were jacked from the other end to minimize frictional losses. Due to logistical issues, measurement of this second jacking sequence was not monitored by the strandmeters.

Loss due to friction is seen as a function of distance from the active jacking end. The strands were stressed to 80% of ultimate, which is the assumed stress a small distance from the jack itself. The strain measured in strandmeter C1_S is 8.5% lower than the strain at the active jacking end. At strandmeter B3_S the measured strain is 21% less than the strain at the active jacking end. The trend of increasing frictional loss is expected, because as the distance from the active jacking end increases the strand is subjected to a build up frictional forces. Since the strand was subsequently jacked at the initial passive end frictional losses in B3_S are not compared with theoretical values. Frictional losses seen in B1_S are inconclusive, because as the strand was being tensioned the gage came into contact with the side of the blockout resulting in inaccurate measurements. Estimated frictional losses at the center of the section accounted for a 5.9% decrease in strain. The measured value does not take into account the second sequence of jacking; therefore, it is hard to directly compare the two results. However,

the results are very similar and may have been almost the same had the second sequence of jacking been monitored.
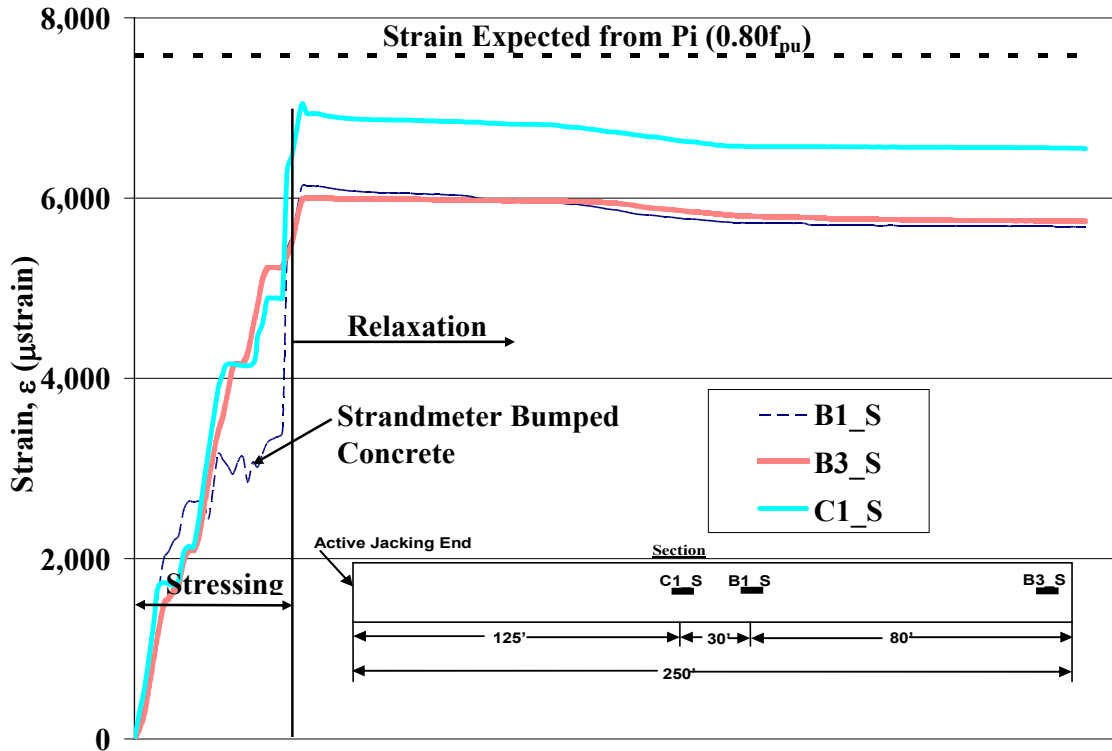
Figure 5.3 – **Strain measurements from strandmeters during post-tensioning of strand along crown of roadway.**

5.4.2. MEASURED RESULTS VS THEORETICAL TOTAL POST-TENSIONING LOSSES

The predicted remaining effective post-tensioning force is compared with measured values from strandmeters B3_S and C1_S in Figure 5.4 and Figure 5.5. The measured results cease at 270 days due to time constraints with regard to the publication of this thesis. It is planned to continue monitoring post-tension losses, and final results will be reported in future publications. A total of four strandmeters were installed along the length of the test section, however due to intermittent problems in data collection results from only two of the strandmeters is presented.

Careful determination of the measured losses was done to ensure everything was accounted for. Initial strandmeter frequency and temperature readings (or zero readings) were taken before and just after post-tensioning operations ceased. Subsequent readings of frequency and temperature were taken at 40, 60, 100, and 270 days after initial readings. The gages were isolated from the concrete by PVC tubing; therefore, it is assumed the gages are only monitoring strain in the post-tensioning strands. Temperature correction was then performed based on in-service data of temperature versus output from the strandmeters. A correction factor for temperature was developed from this data that has units of change in strandmeter output per degree Celsius. The correction factor is applied to readings by determining the variance between the initial temperature and the temperature of a subsequent reading and multiplying by the correction factor. Measured temperatures less than the zero reading temperature are increased and measured temperatures greater than the zero temperature reading are decreased by the temperature correction factor.

The predicted total loss in effective post-tensioning force at 270 days was 13.2% and 10.2% respectively for the two locations (B3_S and C1_S) instrumented along the strand. The difference in the predicted values is a result of the varying frictional forces that contribute to post-tensioning losses. B3_S was the furthest from the active jacking end and C1_S was the closest. The measured results from strandmeters B3_S and C1_S were 13.5% and 5.1% respectively. It is difficult to draw concise conclusions based on the comparisons between the measured results and predicted values. The loss in post-tensioning force measured by strandmeter B3_S closely followed the curve for predicted losses, and at 270 days the predicted value was within 2.3% of the measured value.

Based on the complex nature of predicting and measuring post-tensioning this difference is acceptable. However, strandmeter C1_S measured a loss in post-tensioning force of only 5.1%, which is less than half (50%) of the predicted loss from theoretical calculations and measured loss from strandmeter B3_S. The trend, as seen in Figure 5.4, is very similar for measured and theoretical values, but the magnitude of C1_S is less than the predicted and measured (strandmeter B3_S) results. It is important to note that during post-tensioning operations gage C1_S had to be moved because as the strand was stressed and subsequently elongated the gage came into contact with the concrete and had to be moved and reset. The resetting modified our zero reading, which may explain why the magnitude of post-tensioning loss is less than predicted.

Future monitoring of the pavement is recommended to draw solid conclusions regarding the applicability of using the time-step model for the prediction of post-tensioning losses in PPCP. If possible more data from improperly functioning gages at the time of publication should be collected and compared with the results presented in this thesis.
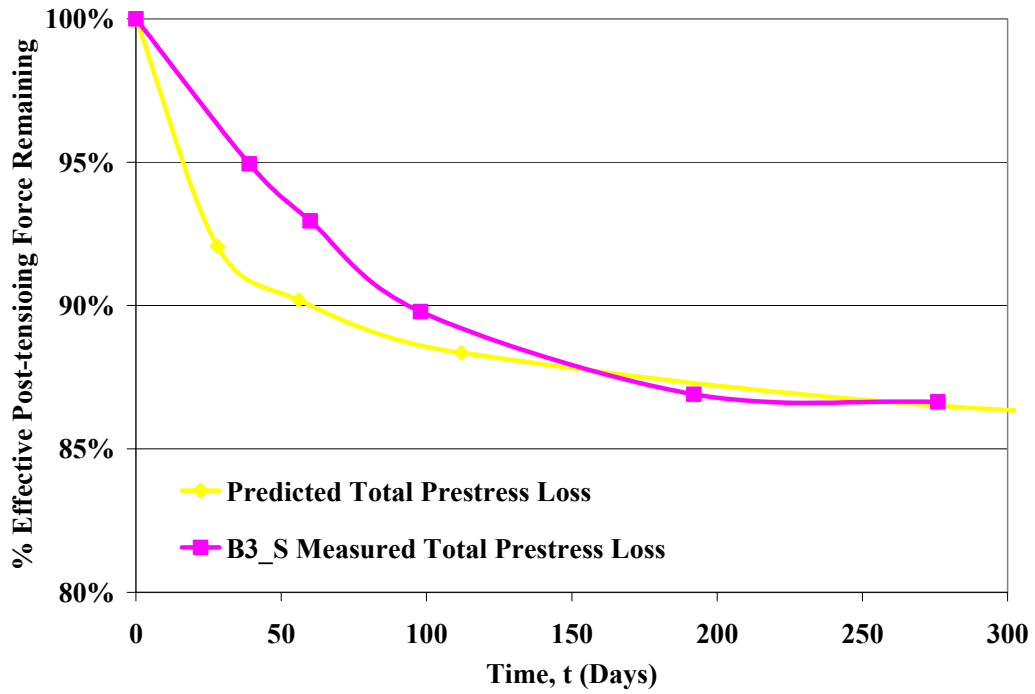
Figure 5.4 – Comparison of total predicted post-tensioning loss with measured results for strandmeter B3_S.
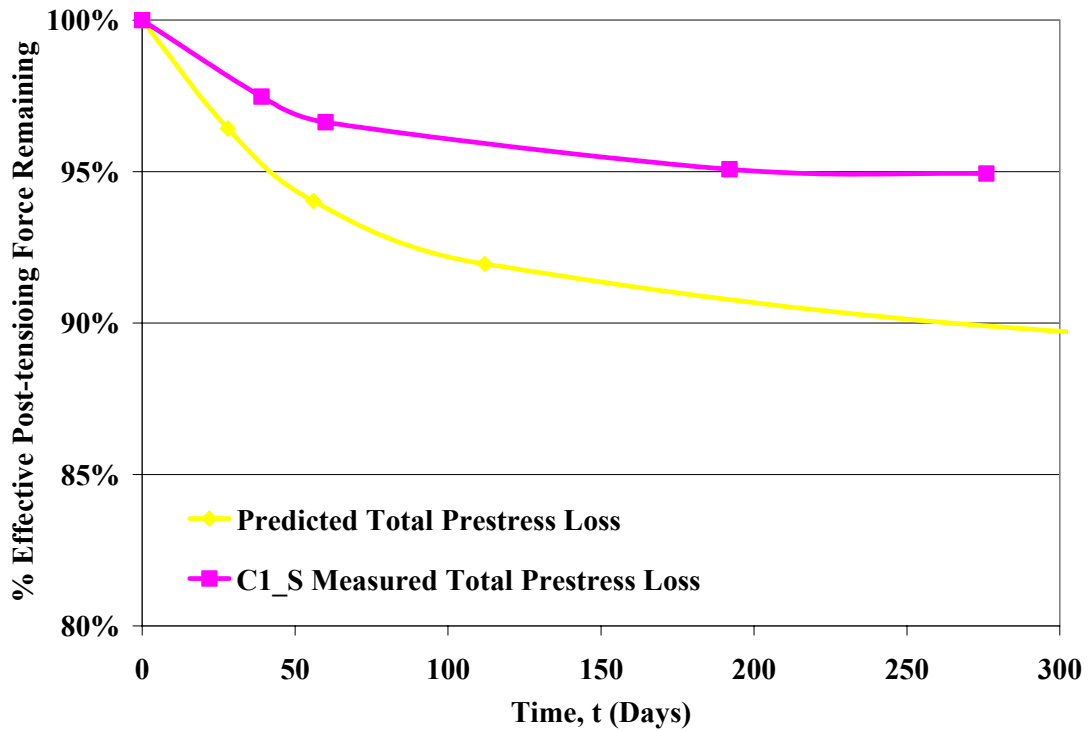
Figure 5.5 – Comparison of total predicted post-tensioning loss with measured results for strandmeter C1_S.

6. CONCLUSIONS AND RECOMMENDATIONS

6.1. SUMMARY OF THE INVESTIGATION

The use of PPCP proved to be an effective means of rehabilitating a distressed rigid pavement. The advantages of precasting and applying a pre-compressive force to the rigid pavement proved successful in the replacement of a 1,000 foot segment on the northbound lanes of I-57 near Charleston, MO. Precasting minimized construction time in the field by eliminating the need to wait for the concrete to cure. Also, the panels were cured in a controlled environment, mitigating the effects of climate changes and reducing residual stresses due to restrained shrinkage that would normally occur in a cast-in place pavement. The pre-compressive force economized the use of concrete by improving the overall tensile capacity of the system. Concretes weak tensile strength results in a typical pavement thickness that approaches one foot. By confining the concrete using pre and post-tensioning, the pavement thickness can be decreased by nearly a third, to and average of 8". The main advantage of PPCP, although not directly tested in this investigation, involves rapid deployment during off-peak traffic periods. This project further demonstrated the viability of PPCP, which will enable future pilot projects to be constructed under stricter time constraints with little tolerance for lane closures during peak traffic times.

- Material tests were successfully performed and correlated well to prediction models. Material properties quantified included:
  - Compressive strength and elastic modulus at 7, 28 and 56 day
  - Unrestrained shrinkage

- Unrestrained creep

- Chloride permeability at 28 and 112 days

- Freeze-thaw durability

- Flexure tests to determine the modulus of rupture and fracture toughness.

The material tests were performed in accordance with relevant standards, and provided important characteristics of the concrete that aided in the evaluation of the overall performance of the pavement system. Theoretical prediction models successfully verified the validity of our laboratory studies.

- Models predicting the total loss of stress or applied force in the pre and post-tensioning strands for the 45 year design life of the pavement were successfully developed. Individual models for losses due to creep and shrinkage were carried out, along with a time-step model predicting coupled losses due to creep, shrinkage, strand relaxation, anchorage set, elastic shortening, and frictional losses. Separate calculations were performed for the transverse and longitudinal strands. The model for total post-tensioning loss was then compared to measured losses from strandmeters installed on a single post-tensioning strand. To date the model developed compares readily with the measured total post-tension loss.

A thesis by Cody L. Dailey entitled, "Instrumentation and Early Performance of an Innovative Prestressed Precast Roadway System" (Dailey 2006) rigorously discusses the instrumentation program, curing and hydration of the precast panels, and in-service performance of the pavement. A future thesis will present long-term analysis of the precast pavement system.

6.2. SUMMARY OF LABORATORY RESULTS

Properties of the concrete used for PPCP are summarized in Table 6.1. Overall, the results from the laboratory were soundly predicted by theoretical models. The unrestrained creep and shrinkage models under-predicted strain measurements, however adjusting the shrinkage models to account for autogeneous shrinkage effects shows that beyond an age of 10 days the predicted curve follows the measured results very closely.

Table 6.1 – Summary of material properties from experimental investigations of concrete used for precast panels.

Tests Performed	Parameter	Experimental Result
Results from Compressive Strength Laboratory Studies (ASTM C 39)	28 Day Strength, f'_c psi (MPa)	7,190 (49.6)
	28 Day Ultimate Strain, ε_{ult} in/in	0.00154
	28 Day Modulus of Elasticity, E_c psi (MPa)	5.69×10^6 (3.92×10^4)
	56 Day Strength, f'_c psi (MPa)	8,830 (60.9)
	56 Day Ultimate Strain, ε_{ult} in/in	0.00159
	56 Day Modulus of Elasticity, E_c psi (GPa)	6.26×10^6 (4.31)
Results from Flexural Laboratory Studies (ASTM C 78)	Modulus of Rupture, f_r psi (MPa)	872 (6.01)
	Fracture Toughness, G_f lb-in/in^2 (N-m/m^2)	0.237 (41.2)
Results from Freeze-Thaw Laboratory Studies (ASTM C 666 Procedure A)	Durability Factor, DF	97%
Results from Chloride Permeability Laboratory Studies (ASTM C 1202)	28 Day Charge Passed, Q_s Coulombs	3,999
	112 Day Charge Passed, Q_s Coulombs	3,151

6.3. RECOMMENDATIONS FOR FURTHER RESEARCH

Future monitoring of post-tensioning losses is imperative to ensure the mathematical models developed to predict these losses are accurate. A main purpose of investigating the loss of pre-tension and post-tensioning was to verify design assumptions and give future practitioners confidence in some of the assumptions they will make. The losses were computed up to the pavement design life of 45 years. Monitoring the losses over this entire time period is not practical, however since over 80% of the post-tensioning losses will occur during the first year, monitoring losses during this time is vital for comparison to the theoretical prediction. Beyond this time, the rate of loss will decrease dramatically and will not be as important to verify. It is recommended at a minimum to monitor the pavement for post-tensioning loss over the first year. Monitoring of the pavement beyond the trial year of service could be beneficial, but is not necessary.

In-situ chloride permeability tests should also be done after the pavement has been subjected to deicing salts to determine the rate of chloride ingress in the field. These results can then be compared to baseline readings taken on virgin specimens.

7. REFERENCES

ACI (1997). Prediction of Creep, Shrinkage, and Temperature Effects in Concrete Structures**:** 47.

ACPA (2004). Concrete Types, American Concrete Pavement Association. **2004**.

ASTM (1998). Standard Practice for Capping Cylindrical Concrete Specimens, ASTM**:** 5.

ASTM (2002). Standard Test Method for Flexural Strength of Concrete (Using Simple Beam with Third-Point Loading, ASTM**:** 3.

ASTM (2002). Standard Test Method for Fundamental Transverse, Longitudinal, and Torsional Resonant Frequencies of Concrete Specimens, ASTM**:** 7.

ASTM (2003). Standard Test Method for Resistance of Concrete to Rapid Freezing and Thawing, ASTM**:** 6.

ASTM (2005). Standard Test Method for Compressive Strength of Cylindrical Concrete Specimens, ASTM**:** 7.

ASTM (2005). Standard Test Method for Electrical Indication of Concrete's Ability to Resist Chloride Ion Penetration, ASTM**:** 6.

Bazant, Z. P. and F. H. Wittmann (1982). <u>Creep and Shrinkage in Concrete Structures</u>, John Wiley and Sons.

Dailey, C. (2006). Instrumentation and Early Performance of an Innovative Prestressed Precast Pavement System. <u>Civil and Environmental Engineering</u>. Columbia, University of Columbia - Missouri.

Degussa (2006). Degussa Admixtures. **2006**.

Earney, T. P. (2006). Creep and Shrinkage Studies of High Performance Concrete. <u>Civil and Environmental Engineering</u>. Columbia, University of Columbia - Missouri.

Earney, T. P., V. Gopalaratnam, et al. (2006). <u>Understanding Early-Age Shrinkage of High-Performance Concrete for Bridge Deck Applications</u>. Transportation Scholars Conference, Iowa State University, MTC.

Eatherton, M. (1999). Instrumentation and Monitoring of High Performance Concrete Prestressed Girders. <u>Civil Engineering</u>. Columbia, University of Missouri**:** 223.

Gopalaratnam, V. S., J. Donahue, et al. (2006). <u>Precast Prestressed Panels for Rapid Full-Depth Pavement Repair</u>. ASCE Structures Congress 2006, Saint Louis, MO.

Hooton, R. D. and K. D. Stanish (1997). Testing the Chloride Penetration Resistance of Concrete: A Literature Review. Toronto, University of Toronto31.

Kropp, J. and H. K. Hilsdorf (1995). Performance Criteria for Concrete Durability. Great Britain, RILEM**:** 327.

Merritt, D. K. (2001). <u>Feasibility of Precast Prestressed Concrete Pavements</u>. 7th International Conference on Concrete Pavements.

Merrrit, D. K., B. F. McCullough, et al. (2000). The Feasibility of Using Precast Concrete Panels to Expedite Highway Pavement Construction. Austin, TX.

Mindess, S., J. F. Young, et al. (2003). <u>Concrete</u>. Upper Saddle River, NJ, Prentice Hall.

Muench, S. T. (2004). Pavement Facts. **2004**.

Namaan, A. (2004). <u>Prestressed Concrete Analysis and Design</u>. Ann Arbor, MI, Techno Press 3000.

Pigeon, M. and R. Pleau (1995). <u>Durability of Concrete in Cold Climates</u>. Bury St. Edmunds.

Tyson, S. and D. K. Merritt (2006). Concrete Pavement Technology Update, FHWA. **2006**.

Tyson, S. S. and D. K. Merritt (2005). Pushing the Boundaries, Federal Highway Administration. **2006**.

APPENDIX A – CREEP AND SHRINKAGE CORRECTION FACTORS

Table A1 – **Correction factors for the prediction of unsealed concrete shrinkage specimens. For the prediction of sealed shrinkage values the relative humidity was adjusted to 100%.**

Factor	Description	Value Used	Result
$\gamma_1 =$	Correction for variation in relative humidity (%)	50%	0.89
$\gamma_2 =$	Correction for size and shape (mm)	153	1.00
$\gamma_3 =$	Correction for concrete slump (mm)	153	1.14
$\gamma_4 =$	Correction for fine aggregate ratio (%)	40%	0.85
$\gamma_5 =$	Correction for air content (%)	7%	1.01
$\gamma_6 =$	Correction for cement content (kg/m^3)	428	1.01
$\gamma_7 =$	Correction for initial moist curing	--	1.20

Table A2 – **Correction factors for the prediction of unsealed concrete creep specimens. For the prediction of sealed creep values the relative humidity was adjusted to 100%**

Factor	Description	Value Used	Result
$\gamma_1 =$	Correction for loading age (days)	28	0.83
$\gamma_2 =$	Correction for variation in relative humidity (%)	50%	0.94
$\gamma_3 =$	Correction for size and shape (mm)	153	1.00
$\gamma_4 =$	Correction for concrete slump (mm)	50.4	0.95
$\gamma_5 =$	Correction for fine aggregate content (%)	40%	0.98
$\gamma_6 =$	Correction for air content (%)	7%	1.09

APPENDIX B – TIME-STEP MODELS (ADAPTED FROM NAAMAN)

Table B3 –   Calculation of creep loss over time for prestressing strands.

	Days							Years			
	1	3	7	28	56	112	365	5	10	20	45
Moduli Ratio n_{pi} or n_p	8.23	8.23	8.23	5.86	5.86	5.86	5.86	5.86	5.86	5.86	5.86
$f_p(t_i)$, ksi	189	189	189	188	188	187	187	186	186	186	186
$f_{cgp}(t_i)$, ksi	0.23	0.23	0.23	0.22	0.22	0.22	0.22	0.22	0.22	0.22	0.22
$\Delta f_{pC}(t_i,t_j)$, ksi	0.45	0.35	0.40	0.63	0.36	0.35	0.51	0.43	0.11	0.08	0.06
$f_p(t_j)$, ksi	189	189	188	188	187	187	186	186	186	186	186
$\Sigma\Delta f_{sC}(t_i,t_j)$, ksi	0.45	0.80	1.20	1.83	2.19	2.54	3.05	3.48	3.59	3.67	3.72
% Total Creep	12%	21%	32%	49%	59%	68%	82%	93%	96%	98%	100%
% Creep Left	88%	79%	68%	51%	41%	32%	18%	7%	4%	2%	0%

Table B4 –   Calculation of shrinkage loss over time for prestressing strands.

	Days							Years			
	1	3	7	28	56	112	365	5	10	20	45
$f_p(t_i)$, ksi	--	189	188	187	183	180	176	173	171	170	170
$\Delta f_{ps}(t_i,t_j)$, ksi	0.00	0.65	1.18	4.32	3.22	3.20	3.82	1.96	0.28	0.14	0.08
$f_p(t_j)$, ksi	189	188	187	183	180	176	173	171	170	170	170
$\Sigma\Delta f_{ps}(t_i,t_j)$, ksi	0.00	0.65	1.83	6.15	9.37	12.57	16.39	18.35	18.63	18.77	18.85
% Total Shrinkage	0%	3%	10%	33%	50%	67%	87%	97%	99%	100%	100%
% Shrinkage Left	100%	97%	90%	67%	50%	33%	13%	3%	1%	0%	0%

Table B5 –   Calculation of total loss for prestressing strands.

	Days							Years				Total Loss
	1	3	7	28	56	112	365	5	10	20	45	
Moduli Ratio n_{pi} or n_p	8.23	8.23	8.23	5.86	5.86	5.86	5.86	5.86	5.86	5.86	5.86	
$f_{ps}(t_i)$, ksi	213	209	206	204	198	194	190	184	181	180	180	
$f_{cgp}(t_i)$, ksi	--	0.25	0.25	0.24	0.24	0.23	0.23	0.22	0.22	0.22	0.21	
Δf_{pC} (t_i,t_j), ksi	--	0.39	0.44	0.69	0.38	0.36	0.51	0.43	0.11	0.07	0.06	3.43
Δf_{pS} (t_i,t_j), ksi	--	0.65	1.18	4.32	3.22	3.20	3.82	1.96	0.28	0.14	0.08	18.85
Δf_{pR} (t_i,t_j), ksi	2.40	0.77	0.57	0.89	0.39	0.36	0.56	0.67	0.27	0.26	0.30	7.44
Δf_{pES} (t_i,t_j), ksi	2.05	--	--	--	--	--	--	--	--	--	--	2.05
Δf_{pT} (t_i,t_j), ksi	4.45	2.05	2.43	6.14	4.23	4.15	5.12	3.28	0.87	0.69	0.65	34.07
f_{ps} (t_j), ksi	209	206	204	198	194	190	184	181	180	180	179	
$\Sigma\Delta f_{pT}(t_i,t_j)$, psi	4.5	6.5	8.9	15.1	19.3	23.5	28.6	31.9	32.7	33.4	34.1	
$\Sigma\Delta f_{pT}(t_i,t_j)/\Delta f_{pt}$ (%)	13%	19%	26%	44%	57%	69%	84%	94%	96%	98%	100%	
$f_{ps}(t_j)/f_{pu}$	77%	76%	76%	73%	72%	70%	68%	67%	67%	67%	66%	

Table B6 –   Calculation of creep loss for post-tensioning strands.

	Days				Years			
	28	56	112	365	5	10	20	45
Moduli Ratio n_{pi} or n_p	5.86	5.86	5.86	5.86	5.86	5.86	5.86	5.86
$f_p(t_i)$, ksi	--	189	189	189	188	188	188	188
$f_{cgp}(t_i)$, ksi	--	0.19	0.19	0.19	0.19	0.19	0.19	0.19
Δf_{pC} (t_i,t_j), ksi	0.00	0.21	0.21	0.30	0.26	0.07	0.05	0.04
$f_p(t_j)$, ksi	189	189	189	188	188	188	188	188
$\Sigma\Delta f_{sC}(t_i,t_j)$, ksi	0.00	0.21	0.42	0.73	0.99	1.05	1.10	1.13
% Total Creep	0%	19%	37%	64%	87%	93%	97%	100%
% Creep Left	100%	81%	63%	36%	13%	7%	3%	0%

Table B7 – Calculation of shrinkage loss for post-tensioning strands.

	Days				Years			
	28	56	112	365	5	10	20	45
$f_p(t_i)$, ksi		189	186	183	179	177	177	176
Δf_{ps} (t_i,t_j), ksi	0.00	3.22	3.20	3.82	1.96	0.28	0.14	0.08
$f_p(t_j)$, ksi	189	186	183	179	177	177	176	176
$\Sigma\Delta f_{ps}(t_i,t_j)$, ksi	0.00	3.22	6.42	10.24	12.20	12.47	12.62	12.70
% Total Shrinkage	0%	25%	51%	81%	96%	98%	99%	100%
% Shrinkage Left	100%	75%	49%	19%	4%	2%	1%	0%

Table B8 – Calculation of total loss for post-tensioning strands.

	Days				Years				Total Loss
	28	56	112	365	5	10	20	45	
Moduli Ratio n_{pi} or n_p	5.86	5.86	5.86	5.86	5.86	5.86	5.86	5.86	
$f_{ps}(t_i)$, ksi	216	199	195	191	186	183	182	181	
Δf_{pF}	12.71	--	--	--	--	--	--	--	
$f_{cgp}(t_i)$, ksi	0.21	0.20	0.19	0.19	0.19	0.18	0.18	0.18	
Δf_{pC} (t_i,t_j), ksi	--	0.23	0.22	0.31	0.26	0.06	0.04	0.03	1.1
Δf_{pS} (t_i,t_j), ksi	--	3.22	3.20	3.82	1.96	0.28	0.14	0.08	12.7
Δf_{pR} (t_i,t_j), ksi	3.62	0.40	0.37	0.58	0.70	0.28	0.27	0.31	6.5
Δf_{pES} (t_i,t_j), ksi	0.31	--	--	--	--	--	--	--	0.3
Δf_{pT} (t_i,t_j), ksi	17.13	4.04	3.98	4.89	3.10	0.80	0.64	0.61	35.2
f_{ps} (t_j), ksi	199	195	191	186	183	182	181	181	
$\Sigma\Delta f_{pT}(t_i,t_j)$, psi	17	21	25	30	33	34	35	35	
$\Sigma\Delta f_{pT}(t_i,t_j)/\Delta f_{pt}$ (%)	49%	60%	71%	85%	94%	96%	98%	100%	
$f_{ps}(t_j)/f_{pu}$	74%	72%	71%	69%	68%	67%	67%	67%	